SOUTHAMPTON UNIVERSITY

FACULTY OF SCIENCE

PHYSICS

DOCTOR OF PHILOSOPHY

# A High Precision Length Measuring Interferometer System for use in the Free Atmosphere

By M. J. Downs C.Phys M.Inst.P

For: A.C.D
K.L.D
K.S.D
A.L.D

Sans Lesquelles Rien

# A HIGH PRECISION LENGTH MEASURING INTERFEROMETER SYSTEM FOR USE IN THE FREE ATMOSPHERE

by

M J Downs

Division of Mechanical and Optical Metrology
National Physical Laboratory
Teddington, Middlesex, England

ABSTRACT

The International standard of length is realised through interferometry and in order to identify the limitations to the accuracy and resolution achievable by interferometric techniques in this application, a high precision length measuring system for use in the free atmosphere has been developed. The apparatus, including a Helium-Neon laser reversible fringe counting length interferometer and interference refractometer, is fully described, together with the instrumentation and techniques developed to achieve the optimum performance from this equipment.

The results of the research have identified all of the fundamental limitations in the physics in this application, and the lengths of optical scales have been measured in the free atmosphere to an absolute accuracy of better than 1 part in $10^7$ with a resolution of 0.02 μm. A major achievement of the research has been the development of a refractometer and cell capable of measuring the refractive index of the atmosphere in a typical laboratory environment to an accuracy of 1 part in $10^8$. This instrument has enabled a significant error in the water term in the Edlen's equation of up to 1.3 parts in $10^7$ to be identified, Edlen's formula being the most widely used method for correcting optical length measuring systems for atmospheric variations by calculating a refractive index value from measurements of pressure, temperature and humidity.

By accurately measuring the required atmospheric parameters and employing the modified Edlen's equation, the refractive index of the atmosphere can be calculated to an absolute accuracy of ±3 parts in $10^8$. The interference refractometer and cell further improve this accuracy to ±1 part in $10^8$, an order of magnitude more precise than the values

currently achieved by compensation techniques in length measuring systems.

All the results and recommendations in this thesis are directly applicable to precision length measuring interferometers and atmospheric refractometers enabling the ultimate accuracy and precision to be achieved from these systems.

C O N T E N T S

**APPENDICES**

# CHAPTER I

## 1.1 INTRODUCTION

Optical interferometry has been increasingly applied to precision length measurement since Michelson (1852-1931) determined the number of wavelengths of the cadmium line which were equivalent to the length of the standard metre bar, and over the years improvements in optics and electronics have resulted in the development of a number of instruments suitable for use in a wide variety of length measuring applications. The precision and accuracy achievable by interferometric measurement were endorsed by the definition in 1960 of the primary standard of length (the metre) in terms of the wavelength of an optical radiation of Krypton 86, and the development of frequency stabilised lasers with their narrow bandwidths, coherence and brightness led to the redefinition of this metre at the Conference Generale des Poids et Mesures in 1983 as the length travelled by light in free space during

$\left( \frac{1}{299792458} \right)$ second.

This standard is only realisable through interferometry [Rowley, 1972], which will continue to play an essential role in all precision length measurement.

The most commonly used interferometric length measuring systems currently employed are based on the Michelson interferometer and use bi-directional fringe counting techniques to automatically correct for vibration and retraced motion, ensuring that the fringe count truly represents the displacement of the moving reflector.

These instruments measure length in terms of wavelength of the radiation from the light source, the most widely employed source being a helium-neon laser. The frequency of a typical frequency stabilised helium-neon laser can be calibrated and maintained to a few parts in $10^8$ over the lifetime of the laser. This would readily satisfy the accuracy required for precision length measurement; however invariably these interferometers are used for measurement in the free atmosphere and to realise the full potential accuracy of these systems not only must they be carefully aligned but the wavelength of the radiation must be

corrected for variations in the refractive index of the air.

The interferometric length measurement system developed in this thesis uses a bi-directional fringe counting interferometer in conjunction with an interference gas refractometer to enable the length of optical scales to be measured with an absolute accuracy of 1 part in $10^7$ in the free atmosphere and with a resolution of 0.02 μm.

## 1.2 OBJECTIVES

The objectives of the research in this thesis were to develop a helium-neon interferometer length measuring system and to identify the limitations to both the accuracy and resolution achievable in precision length measurement by these systems, in particular when they are used for measurement applications in the free atmosphere. The completed apparatus comprised a Helium Neon laser reversible fringe counting length measuring interferometer, an interference refractometer, an optical system for precision positional setting on the boundaries of the object being measured, and a stepping motor driven specimen stage. The completed system will then be used to check measurements taken on similar interferometer systems at the National Physical Laboratory Teddington, used in a controlled environment for disseminating the international standard of length.

A second objective was to investigate the correctness of the universally used equation due to Edlen by comparison of refractive index values calculated from this equation with those obtained directly with an instrument constructed to give the highest possible accuracy. This was done by using suitable sensors to measure the atmospheric pressure, temperature and humidity which are the parameters used in the Edlen equation. Using these sensors, a study was carried out of the variations of these parameters throughout a typical laboratory environment. The information obtained from this study provided an indication of the significance these parameters play in the physics of interferometric measurement. The development of the complete length measuring apparatus involved the following investigations:

(a) The configuration and tracking of the length measuring interferometer system, so that the errors arising from both the optical and mechanical alignment were at a minimum.

(b) A study of the variation in the atmospheric refractive index in a typical laboratory environment by measuring the parameters of pressure, temperature and humidity throughout the laboratory and using Edlen's equation (Appendix I).

(c) A comparison of air refractive index values measured by the refractometer with those calculated using Edlen's equation.

(d) To investigate the highest positional setting accuracy achievable in practice on the markings on a typical optical scale, a major limiting factor in the resolution achievable by length measuring systems in this particular application.

The results of the research are intended to cover all the major aspects of the physics of interferometry when applied to the precision measurement of length, enabling the ultimate performance to be achieved from these systems in terms of absolute accuracy and resolution by identifying the limitations imposed by the physics and making recommendations on both the design and use of these instruments.

# CHAPTER II

## THEORY AND DESIGN

### 2.1 Principles

Interferometers are widely used for precision length calibration by measuring the displacement of a reflector in terms of the wavelength of light.

When these systems are used in the free atmosphere they measure displacements in terms of the wavelength in air rather than the vacuum wavelength of the radiation concerned, and it is common practice to make the appropriate corrections for changes in the refractive index of the air using Edlen's equation which involves measuring the parameters such as pressure, temperature and humidity. This technique, however, is expensive and has been shown to be in error due to the instability of the sensors and variations in the composition of the atmosphere and, in addition, it is difficult to maintain the calibration of the sensors to the required accuracy.

The interference refractometer and gas cell used in the length system described were developed to provide a direct measurement for the refractive index of the atmosphere, using this instrument and the appropriate measurement technique, the only calibration required to achieve and maintain an accurate value for the refractive index of the atmosphere is the relatively crude one of the length of the gas cell employed in the refractometer.

Experience has shown that the laser frequency, once calibrated, is unlikely to change by more than 2 parts in $10^8$ over the lifetime of the tube. The technique of using an interference refractometer with an accuracy of ±1 part in $10^8$ in conjunction with a length measuring interferometer enabled the absolute accuracy of the complete measuring system to be maintained to better than 1 part in $10^7$.

The performance of any length measuring system can of course be monitored by the periodic measurement of a calibrated standard, and the optical scale described in this thesis would be suited for this purpose.

## 2.2 Theory

The general equation for two-beam interferometry is:

$$a^2 = a_1^2 + a_2^2 + 2a_1a_2\cos 2\pi \left[ \left[ f_2 - f_1 \right] t + \frac{(p_1 - p_2)}{\lambda_1} + p_2 \left[ \frac{1}{\lambda_1} - \frac{1}{\lambda_2} \right] \right] .$$

where a is the amplitude
f is the frequency
p is the optical path
$\lambda$ is the wavelength

In single frequency interferometry $f_1 = f_2 = f$ and $\lambda_1 = \lambda_2 = \lambda$.

Then the general equation reduces to

$$I = a_1^2 + a_2^2 + 2a_1a_1\cos \left[ \frac{2\pi(p_1 - p_2)}{\lambda} \right]$$

As $p_1$ or $p_2$ changes, the output intensity varies between $(a_1 + a_2)^2$ and $(a_1 - a_2)^2$, the signal varying sinusoidally with path difference. The resulting number of fringes is counted and the change in $p_1$ or $p_2$ calculated from the wavelength. [Downs and Raine 1979].

On the other hand in dual frequency interferometry when $f_1 \neq f_2$ $(\lambda_2 \neq \lambda_1)$.

The two-frequency beam laser beam is split into the components of $f_1$ and $f_2$ by the polarising beam splitter. These are incident on the reference and probe corner-cube reflectors, respectively. The reflected beams interfere at the beam splitter, so that the beat signal from $(f_1 - f_2)$ is generated. If the probe corner-cube reflector approaches the beam splitter at a velocity of v, the frequency of $f_1$ shifts by $\Delta f = 2vf_1/c$ because of the Doppler effect (where c is the speed of light). Subtracting the reference beat signal from $(f_1 - f_2 + \Delta f)$, the frequency $\Delta f$ due to the Doppler effect is finally obtained and counted. From this count, the length under test is determined from the relationship $2vtf_1/c = 2d\lambda_1$, where the reflector moves over the length d for the time t.

Interferometers employing fringe counting are not suited to all length measurement applications as they require a moving carriage and impose the condition that the light beam cannot be interrupted during the

measurement, and some applications are more suited to the method of excess fractions. This technique requires the use of a multiple wavelength source and a system for scanning the interference fringes to obtain fringe fractions at the various wavelengths employed. [Tilford 1977, Matsumoto 1984, Lyubomudrov *et al* 1984].

Consider two beam interference with wavelengths $\lambda_1$ and $\lambda_2$, the following equation applies:

$$2D = (m_1 + \phi_1)\,\lambda_1 = (m_2 + \phi_2)\,\lambda_2 \qquad \ldots\ldots (2)$$

where $D$ is the length under test, $m_1$ and $m_2$ are the integer numbers of the interference orders, and $\phi_1$ and $\phi_2$ are the fractions of the interference orders. The beat frequency $f_3 = f_1 - f_2$ where $f_1$ and $f_2$ are the two frequencies employed. Using

$$f_1 = \frac{c}{\lambda_1},$$

$f_2 = \frac{c}{\lambda_2}$ and $f_3 = \frac{c}{\lambda_3}$ where $c$ = the speed of light

The synthetic wavelength $\lambda_3 = \frac{\lambda_1\lambda_2}{\lambda_1-\lambda_2}$.

In this technique only $\phi_1$ and $\phi_2$ are measured by scanning a few fringes and applying a phasemeter. If a rough value of $D$ is known to an accuracy of

$$\frac{\pm\,\lambda_1\lambda_2}{4(\lambda_1-\lambda_2)}\,.$$

by another method, then $m_1$ and $m_2$ can be uniquely determined. The value of $D$ is then determined using equation (2). If a light source with several wavelengths is used, $D$ can be uniquely determined, even when the accuracy with which $D$ is known beforehand is poor. However it should be appreciated that the application of this technique over larger ranges requires either the use of an extremely accurate measurement of the fringe fraction which will be limited by the quality of the components in the optical system, or the application of an increasing number of wavelengths from the source.

As lasers have improved in their capabilities and techniques for frequency measurement developed, another method for length measurement has emerged; that of scanning frequency interferometry. With this

technique the radiation source is not frequency stabilised but is scanned between two known frequency points and any fringes or fractions of fringes occurring during the scan are counted and measured, the length is then calculated from the fringe count and the two known frequencies. The technique is effectively a hybrid of fringe counting and multiple wavelength interferometry.

The interferometric measuring technique chosen for both length measuring interferometer and the interference refractometer in this thesis employs a Helium-Neon laser ($\lambda$ 633 nm) and reversible fringe counting, the length interferometer requiring the laser to be frequency stabilised.

This method was chosen as extremely practical and relatively inexpensive instruments could be readily developed to meet the performance required from the complete length measuring system.

## 2.3 Optical design of length measuring interferometer

The optical configuration of the original Michelson interferometer, on which most length measuring interferometer systems are based, is shown in Figure 1. The interferometer has been made easier to align and insensitive to tilt of the reflecting units by replacing the original plane mirrors with cube corner retro-reflectors as shown in the Figure. This has the advantages of preventing problems from light being reflected back into the cavity when a laser source is employed and also of making the second interferogram produced by the interferometer more accessible. The measurement direction of this system is along a line through the apex of the corner cube retro-reflector, and the tolerance to the alignment of this direction through the point in the system satisfying the Abbe measurement principle, and along the tracking direction of the sample stage is described in Section 3.1. The coefficients for the interfering intensities of the two beams are shown for each of the interferograms and polarising beamsplitters have been incorporated to separate two orthogonally polarised components from each of the interferograms, making four electrical signals available from the two optical outputs of the interferometer.

To obtain optimum performance from single frequency length measuring interferometers, the bi-directional fringe counting electronics require two signals with constant dc levels and sinusoidal components related to the optical path difference in the interferometer, that are in phase

quadrature. Normally in unmodulated dc coupled interferometer systems (the dc coupling being required to achieve *zero count* rate), any fringe contrast variations cause the mean dc level of the path length signals to change as shown in Figure 2(a), and indeed if the contrast falls below a certain level see Figure 2(b), the counter electronics will fail to count. The interferometer system built was based on a design developed at the National Physical Laboratory by [Downs and Raine 1979] and in this interferometer the required counting signals are obtained by viewing the two interferograms produced by a Michelson interferometer in orthogonal polarisations, and then subjecting 3 of the 4 signals available to an electronic subtraction process. By this means it is possible to generate two sinusoidal optical path difference signals $90^{o}$ out of phase, with an average signal level of 0 volts and free of dc components unrelated to the optical path difference. For this to be achieved several conditions must be fulfilled. The ratios of the sinusoidal amplitude and the average signal level must be the same for the 3 selected signals, so that after suitable amplification and appropriate subtraction only the sinusoidal signal related to the optical path difference remains. Also, if for example the signals (1), (2) and (3) as shown in Figure 1 are selected, then signals (1) and (2) should be in antiphase and ideally separated in phase by $\pm 90^{o}$ from signal (3) (see Figure 3). A dielectric beamsplitter will provide the required antiphase relationship between signals (1) and (2), while an appropriately orientated $\lambda/8$ plate in one arm of the interferometer will secure the correct phase for signal (3). It can also be shown that the signal ratios previously described can be obtained from an all dielectric thin film beamsplitter design that equalises the beamsplitter transmittance and reflectance for one state of polarisation; this can be achieved more readily for the S polarisation and therefore signals (1), (2) and (3) are used.

Three signals like those shown in Figure 3 can then be produced. Electronic subtraction of the appropriate pairs of these signals (ie (3)-(1) and (3)-(2)) as shown in the Figure then gives two outputs in phase quadrature with zero average levels, which are consequently free of components unrelated to the optical path difference; although their amplitudes are dependent on the light source intensity and fringe contrast, the positions at which the signals cross the zero voltage level have a fixed relationship to the optical path difference and are unaffected by the presence of dc components in the original

interferogram signals.

An interferometer based on the system described was constructed with two major modifications (Figure 4), a dual plate beamsplitter and an additional reflector to enable the interferograms to be examined remotely from the interferometer. A Spectra-Physics 117 frequency stabilised helium neon laser (output 1.0 mW) was used as a radiation source together with United Detector Technology silicon photodiodes with a frequency response of 1 MHz. However, it is worth noting that this interferometer will function with any source of radiation provided that the measurement range is within the coherence length of the source. Narrow-band interference filters and high quality Kasemann Ks-MIK grade sheet polarisers with an extinction ratio of 1 part in $10^6$ (King *et al* 1971), and about 5 mm in diameter were cemented together and placed immediately in front of the detectors eliminating problems from extraneous light. A polarising beamsplitter designed by Downs and McGivern (1983) was used to separate the two orthogonally polarised interferograms, while the sheet polarisers effectively rejected any unwanted leakage from the polarising beamsplitter. This particular beamsplitter design uses the phase inversion of the reflected parallel polarised component at the Brewster angle to achieve an extinction ratio for the device of 1000:1.

In theory if the two corner cubes are in identical orientations in the arms of the interferometer their depolarisation effects are cancelled out; in practice these effects are almost totally eliminated by metalising the total internally reflecting surfaces and, although it is still preferable for the corner cubes to be in the same orientation, the angular tolerance to this is extremely low. The corner cubes were aluminised so that their polarising properties were acceptable [Peck 1962] and the remaining optical surfaces, with the exception of the beam splitter interface, were anti-reflection coated a double passed 3/8 $\lambda$ mica waveplate provided the phase shift. The additional thickness (ie compared to a 1/8 plate) made the device more robust and allowed, by tilting, phase errors in the plate and phase differences arising from the beamsplitter to be corrected more readily (Appendix II). One of the axes of the waveplate needs to be aligned with the plane of incidence of the beamsplitter to an accuracy of a few degrees. Unmounted mica phase plates were employed as they were significantly cheaper than both quartz phase plates and glass mounted mica. However, the surfaces need to be anti-reflection coated to less than 0.2% to avoid the problems due to

multiple reflections and the coherence of the radiation source (Holmes, Sept 1964. Jerrard, March 1962).

The details of the thin film coatings used in the length interferometer are given below:

The length interferometer beamsplitter coating specification was for an all electric 50% reflectance 50% transmittance coating for the S polarisation component. (Wavelength 633 nm at a $45^{o}$ angle of incidence). These requirements were met by a $\lambda/4$ thick Zirconium Dioxide film (n = 1.95).

The polarising beamsplitters were made to a design by Downs and McGivern (NPL Report 1983) with an extinction ratio approaching 1000 to 1.

The corner-cube retroreflectors were aluminised to minimise their depolarisation effects.

The anti-reflection coatings applied to all normal incidence surfaces were standard 2-layer V-coatings.

The anti-reflection coating on the rear surface of the beamsplitter plate was a 3-layer design by Downs involving neodymium and magnesium fluoride films. The reflectances for both P and S components are less than 0.25% at $45^{o}$ angle of incidence.

## 2.4 Mechanical Design of the length measuring interferometer system

Interferometer measurement and calibration techniques are widely used in machine tools [Wuerz *et al* 1983, Baldwin *et al* 1983]. The schematic layout of the components of the length measuring interferometer system in this thesis is shown in Figure 5. The optical scale being measured was placed on the Unimatics stepping motor driven positioning stage shown in Figure 6. This stage provided a total range of movement of 150 mm in 1 micron steps and a range of switches could be selected to address the position of the scale within 1 micron of any required point within its range of travel. A substrate holder capable of moving the scale over a limited range of movement with extremely fine control using differential screw adjusters, shown in Figure 7 was mounted on the

positioning stage, together with a corner cube retroreflector. The optical setting head incorporating an inverting eyepiece, television camera and fibre optic illumination system, shown in Figure 8, was mounted above the specimen with the focal point of the 0.5 numerical aperture 50x magnification telephoto microscope objective arranged to be intersected by the measurement direction of the interferometer system (a line through the apex of the corner cube retroreflector and parallel to the laser beam). An intensity profile obtained from the television camera was displayed on the monitor as shown in Figure 9.

The optical setting head was mounted over the specimen on the bridge structure shown to provide the high mechanical stability required, and this structure was then enclosed with aluminium sheeting to provide a relatively stable temperature enclosure for the interferometer path and measurement area. This enclosure also minimises the problems caused by air turbulence or inhomogeneity of the air in the optical measuring path. These variations in the atmosphere not only result in noise in the system due to changes in optical path, but also from fluctuations in the wavefront causing the contrast in the interferometer to vary. When these systems are used over ranges of 30 metres or more atmospheric variations in the optical path can cause up to 1 fringe of tilt across the wavefront of the light beam causing a complete loss of contrast in an interferometer and total failure of a single frequency system.

The unwanted effects of heating from the laser were minimised by thermally isolating the laser tube using Nylatron V-blocks and mounting it outside the measurement enclosure. Heating effects from the illumination required for the optical setting heat were eliminated by the use of an optical fibre allowing the 100 watt quartz halogen light source to be remote from the system.

## 2.5 Radiation source and frequency calibration

Frequency stabilised helium-neon laser sources are now readily available commercially - their intense collimated beams being ideally suited to laser interferometry and their narrow bandwidths providing, in theory, an interferometric measurement range of hundreds of metres. In practice however, the inhomogeneity of the media in the optical paths traversed by the two beams restricts this measurement range.

The helium-neon laser does however have three main limitations when used

in interferometric applications; the possibility of multiple modes of oscillation, frequency instability and sensitivity to optical back coupling into the cavity. [Duardo *et al* 1976].

By careful optical design, helium-neon lasers can be restricted to axial modes and off-axis modes prevented. The axial modes have a frequency spacing of $\frac{c}{2L}$ (where $c$ is the speed of light and $L$ is the cavity length) and the number of modes can be directly controlled by the separation of the laser mirrors. By making the mirror spacing sufficiently short for example, the axial mode spacing is made larger than the Doppler width of the transition, shown in Figure 10a, and only a single axial mode is then emitted.

The general shape and width of the emission spectrum at 632.8 nm is determined by the Doppler effect caused by thermal motion of the neon atoms in the high temperature plasma discharge. This shape is Gaussian and the intensity of the profile is given by:-

$$I(\omega) = I_o \, EXP \frac{-Mc^2\omega^2}{2RT\omega_o^2}$$

where $I_o$ is the intensity at line centre, $c$ is the speed of light, $M$ is the molecular weight, $R$ is the universal gas constant, $T$ is the absolute temperature and $\omega$ is the frequency deviation from the line centre, frequency $\omega_o$. For the 632.8 nm line, the line-width (frequency separation of points where amplitude is 1/2 maximum) is approximately 1500 MHz (or 0.002 nm in wavelength terms). In practice this would be dependent upon the laser threshold level.

The 3 main types of frequency stabilised laser commercially available are shown schematically in Figure 10. The Lamb dip [Javan and Szoke 1983] and Zeeman split types [Baer *et al* 1980, and Takasaki *et al* 1980] shown in Figure 10(a) and Figure 10(b) respectively, use short tubes supporting only a single frequency, and the two mode type shown in Figure 10(c) employs a tube length capable of supporting two axial modes.

The frequency stabilisation of all these lasers is achieved by maintaining a constant distance between the mirrors employed for the cavity, automatically correcting for any thermal expansion changes that may occur. The mirrors may be separated from the discharge tube or, as is now more usual, form an integral part of the tube providing a durable

permanently aligned structure. In the case of the mirrors separated from the discharge tube, their positions may be readily controlled using piezo-electric devices. When the mirrors are an integral part of the tube, a number of techniques are employed for cavity length control and these include the mechanical stretching of the tube with piezo-electric devices and several thermal techniques including the following:-

(1) Using a fan for controlled cooling of the tube.
(2) Heaters to regulate the tube length by thermal expansion.
(3) Varying the electrical power in the discharge to control the expansion of the tube.

All these techniques normally involve small acceptable variations in the output power of the laser.

## CAVITY LENGTH SERVO-SYSTEMS

### Lamb dip

At the centre of the Doppler profile less power is obtainable within approximately one natural line width of the Doppler line centre than is possible towards the edges of the line as shown in Figure 10(a). This effect was first described by Lamb and more recently by Javan and Szoke.

By examining the power output of the cavity and applying a small length modulation the laser can be frequency locked to the "Lamb dip". In practice the Lamb dip in the visible Helium Neon laser is about 200 MHz wide and 5 to 10% deep. A commercial example of this type of laser is the Spectra Physics 119 model.

Measurements at the International Bureau of Weights and Measures (BIPM Baer *et al* 1980) show the stabilised vacuum wavelength of a new Lamb dip laser device to be 632.991410 nm, drifting to 632.991430 nm 3 years later near the end of the plasma tube life. (ISOTOPE NEON-20)

### Zeeman Split

Zeeman split lasers use either axial or transverse magnetic fields to split the emission into two polarised components. In the case of the axial field (shown in Figure 10(b)) these components are orthogonal circularly polarised components, the Doppler profile of each being

frequency shifted. The components have equal intensities only when they are symmetrically disposed about the central frequency of the laser and by using a polarising beam splitter and photodetectors to measure their relative-amplitudes, a servo signal can be obtained to control the cavity length.

The two components from such a Zeeman split laser, due to refractive index differences, have slightly different optical frequencies shown in Figure 10(b) and are ideally suited as sources for the dual frequency heterodyne interferometer systems previously described.

A commercially available example of this type of laser is produced by Hewlett Packard in America.

Two-mode

The "two-mode" method of stabilisation [Balhorn *et al* 1972, Bennett *et al* 1970 and Ciddor *et al* 1983] is shown schematically in Figure 10(c). The relative intensity of adjacent, linear, orthogonally-polarised modes is measured. The cavity length is then controlled to maintain a fixed intensity ratio between the two modes. The control system is continuous and there is no frequency modulation of the laser output. One or both of the modes can then be selected using a polariser or polarising beam splitter. It is worth noting that in practice the two frequencies sit approximately $\pm$250MHz ($\pm$5 parts in $10^7$) on either side of the laser frequency at the centre of the Doppler profile. All three types of frequency stabilised laser sources described have long term frequency stabilities of better than a few parts in $10^8$ and, when calibrated, can be used in precision length measurement applications requiring an absolute accuracy of 1 part in $10^7$. A frequency calibration curve shown in Figure 11 was produced by the wavelength standards group at the NPL for the two-mode 117 Spectra Physics laser used as a radiation source for the length interferometer. This curve was obtained by beating the laser with an absorption stabilised Helium-Neon laser specifically developed as a wavelength standard. The saturated absorption iodine stabilised Helium-Neon laser used for this calibration employed an inter-cavity iodine cell, the frequency stability and reproducibility of this type of laser being better than 1 part in $10^{10}$ [Wallard, 1973].

In order to calibrate the frequency to 1 part in $10^8$ it is essential to

measure 'two-mode' stabilised radiation sources, as variations in the constituents of the gas and the pressure can cause significant variations in the laser frequency. However, in practice, measurements have shown that once the frequency has been calibrated for a typical laser, it will not vary by more than 1 part in $10^8$ over a period of a year.

It is vitally important that no light is reflected back into the laser cavity as reflections of the order of 0.01% of the original laser intensity can severely disturb the frequency stabilisation of the laser and can even prevent the stabilisation mechanism from functioning. Some manufacturers deal with this problem, not only by antireflection coating the outer surface of the ouput mirror but also by wedging the mirror approximately $1.5^{\circ}$, accepting the slight deviation of the output beam this causes.

The orientation of the plane of polarisation of the laser beam was controlled by rotating a $\lambda/2$ mica phase retardation plate, slightly inclined to the beam to prevent stray light being reflected back into the cavity, rather than rotating the laser tube itself.

The laser was mounted in Nylatron V-blocks both to thermally isolate the tube from the system and to allow the frequency stabilising system to function correctly. Vertical and horizontal micrometer adjusters were fitted at the front and rear of the tube in order to control both the position and direction of the laser beam.

## 2.6 Fringe counting and fractioning techniques

Analog Devices integrated circuits were used throughout the electronics and were chosen for their frequency responses (at least 1 MHz was required for the length interferometer) and low dc drift characteristics. A unimetrics bi-directional electronic counter with a maximum count rate of 1 MHz was arranged to display a count every time one of the signals crossed the zero voltage level and thus each count represented a movement of the retro-reflector by one-eighth of a wavelength (ie approximately 0.08 μm). It was also possible to arrange for one count to correspond to a displacement of one-quarter or one-half of a wavelength. This was achieved by the selection of the appropriate counter input logic by a switch on the unit.

The United Detector Technology silicon photo-diodes used in the length measuring interferometer were run in a voltage biased mode, minimising the effect of their internal capacitance and allowing a frequency response of 1 MHz (retro-reflector velocity of 0.3 metres/sec) to be achieved from the circuit shown in Figure 12.

The two counting signals from these electronics, each VARYING sinusoidally with path difference and in phase quadrature with one another, were fed to both the inputs of the electronic fringe counter and to the Y-axis and timebase of the oscilloscope. The Lissajous figure obtain in this way (ideally a circle) was used to continuously check the performance of the interferometer system and by attaching the grid shown in Figure 13 to the face of the oscilloscope display, a sensitivity of better than 0.01 μm was achieved ($\lambda/80$). One complete revolution of the Lissajous figure being equivalent to 0.32 μm displacement of the retro reflector ($\lambda/2$).

An electronic unit capable of reading the fringe fraction into an IEEE interface was also developed in collaboration with FT Technologies Ltd (Teddington, Middlesex).

The electronic circuitry was based on an arc tangent function block manufactured by Analog Devices (Molesey, Surrey) and is capable of measuring to a precision of 0.001 of a fringe at a frequency of 100 Hz.

The fringe fraction provided electronically by this unit was used to check the value obtained visually by displaying the signals as a Lissajous's figure on the oscilloscope. It is also possible to fringe fraction by digitising the counting signals and analysing them on a computer. This technique [Heydemann, 1981] would have had the advantage that the quality of both the sine and cosine counting signals can be examined and corrections made for any imperfections, enabling an extremely accurate fringe fraction to be made. However, this approach is really only required when an absolute accuracy of 0.001 of a fringe is needed and would have taken considerable time to effect.

An accuracy of better than one hundredth of a fringe was readily obtained visually from the oscilloscope display and this was confirmed by the values obtained electronically by the FT Technologies unit.

## 2.7 Optical Setting Microscope

In order to achieve precision length measurements on optical scales up to 150mm long with an absolute accuracy of 1 part in $10^7$ it was necessary to develop a position location technique capable of setting on a feature on a scale to 0.01 μm. The optical system devised involved the use of a low cost inverting eyepiece in conjunction with a television camera. This system was further improved by the use of a television scanning system enabling photo-electric setting to be achieved. The inverting eyepiece produces two images of any line in the field of view of the microscope. These images are related in that they are inversions of each other projected through the centre of the eyepiece. Thus as a line is moved away from the centre of the field of view its two images separate and conversely as the object is brought closer the images move together as shown in Figure 14. By setting at the point where the 50% intensity levels of each of the images coincide (Figure 14(d)) a uniform illumination ocurs across the two images of the edge of a line. With lines produced in 1000Å thick chromium using photo lithographic techniques this 'edge setting' method enables an edge setting accuracy of 0.01 μm to be readily achieved. This setting accuracy is essential for the achievement of precision length measurements on optical scales. The ease of setting was then improved using the television scanning technique shown in Figure 9. The image intensity profile of the line on a scale is extracted from the TV line scan and displayed on the monitor. The intensity information required is achieved by aligning the length of the line being examined parallel to the scanning direction on the TV tube.

The intensity profile across the line is then generated by examining a suitable sample length of each of the TV scan lines using a sample and hold technique. The system has the advantage that the sample length can be chosen to integrate out any irregularities in either the specimen or the camera tube. Although the resolution is limited to the line spacing and camera type, the technique of setting at the overlapping 50% intensity points in the two images of an edge is almost completely insensitive to these parameters. The method is not dependent on the linearity or uniformity of the camera tube; nor, as the position is located using the inverting optics in the eyepiece rather than the position of the TV scan line, is the technique dependent upon the stability of the raster scan of the camera tube.

The achievement of accurate feature position location when measuring the lengths of scales necessitates the use of reasonably high magnification in the optical system, in order to increase the sensitivity to setting on the intensity profile of the diffraction broadened image of the feature. The choice of setting is further complicated by the 'ringing' effects that occur with the typically partially coherent illumination found in microscopes. [King *et al* 1981, Martin 1966]. Theoretical curves for a diffraction broadened edge with incoherent and coherent illumination as shown below;

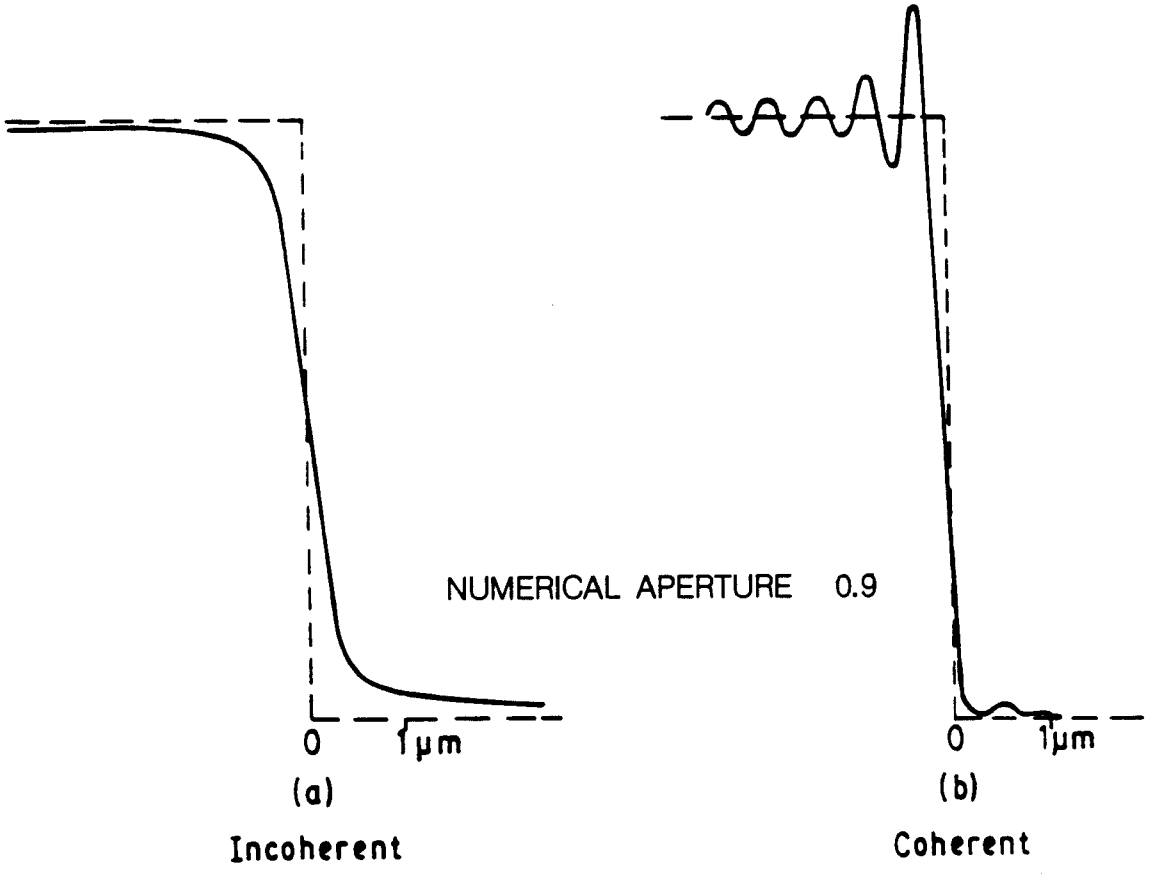


The 50x magnification telephoto microscope objective employed for the optical setting system had a numerical aperture of 0.5 and a working distance of 12.5 mm. When used for setting on features in reflected light the contrast ratio was measured to be approximately 12:1 rather than the near infinite contrast ratio with transmitted illumination. In reflected light the edge setting criteria is extremely close to that for incoherent light making the 50% setting technique extremely insensitive to focus as shown in Figure 15. This was confirmed in practice and although focus would not have been a problem with the distance between two points, the system would be quite capable of measuring the distance between several points on the scale without incurring any length errors

due to variations in the focus causing an optical offset from the true edge position.

## 2.8 Design of Interference Refractometer

As previously described interferometer systems measure length in terms of the wavelength of the radiation from the light source, which for frequency stabilised Helium-Neon lasers can be maintained to a few parts in $10^8$ over a period of a year. When these systems are used for measurement applications in the free atmosphere, the wavelength of the radiation depends upon the refractive index of the air; which varies with temperature, pressure, humidity and gas content. In order to make accurate interferometric measurements it is essential to correct the wavelength used in the calculation of the linear measurement, for variations in these parameters. The sensitivity of the refractive index or the air to these parameters is shown in Appendix I.

A number of techniques are currently used to minimise the problems caused by the media in which these interferometer are measuring and these include:

(1) Measurement in an atmosphere of helium

(2) Measurement in a vacuum

(3) Using suitable sensors and electronics to measure the various parameters involved and to calculate corrections for the atmospheric variations

The approach taken in this thesis is to use an interference refractometer to provide directly an extremely accurate measurement of the refractive index of the atmosphere and to use this to maintain the accuracy of the length measuring interferometer.

In order to realise the high measurement sensitivity of which this type of refractometer is capable, a common-path optical configuration was employed for the interferometer, involving a double passed Jamin beam splitter and cat's eye retroflector, shown in Figures 16 and 17. This interferometer has the advantages of being insensitive to mechanical vibration and does not require the laser source to be frequency stabilised. The interferometer provides two optical outputs, one derived

from two interfering beams and the second from a single beam. Two photo detectors are used to examine orthogonally polarised components of the interference output and a third detector to examine the non-interfering output. The three electrical signals are then subjected to an electronic subtraction process shown in Figure 18, similar to that used in the length measuring interferometer. The two electronic counting signals produced by this technique maintain the performance of the instrument even in the presence of variations in the fringe contrast and fluctuations in the light source intensity. The low frequency circuit used in the refractometer is shown in Figure 19.

The refractometer beamsplitter coating was a 42Å thick aluminium film (+ 30Å of oxide), providing a match between the intensities of the two orthogonally polarised interferograms. All the aluminium reflectors used at non-normal incidence were coated with magnesium fluoride to minimise the depolarisation effects (Figure 20).

Normally the refractometer measures the refractive index of the atmosphere by evacuating the air from both compartments of the cell and then admitting a sample of the atmosphere to be measured into one of these compartments, whilst counting the fringes produced in the system. However, the poor thermal control of the measurement environment used for the research work in this thesis made it necessary to employ a single compartment cell as described in Chapter 3.5. Direct comparison of different types of air refractometers existing in Europe [Schellekens *et al* 1986] ha previously indicated that in a closely controlled environment a measurement accuracy of parts in $10^8$ can be achieved from these instruments, and one of the objectives of this work was to achieve the optimum performance in a typical metrology environment.

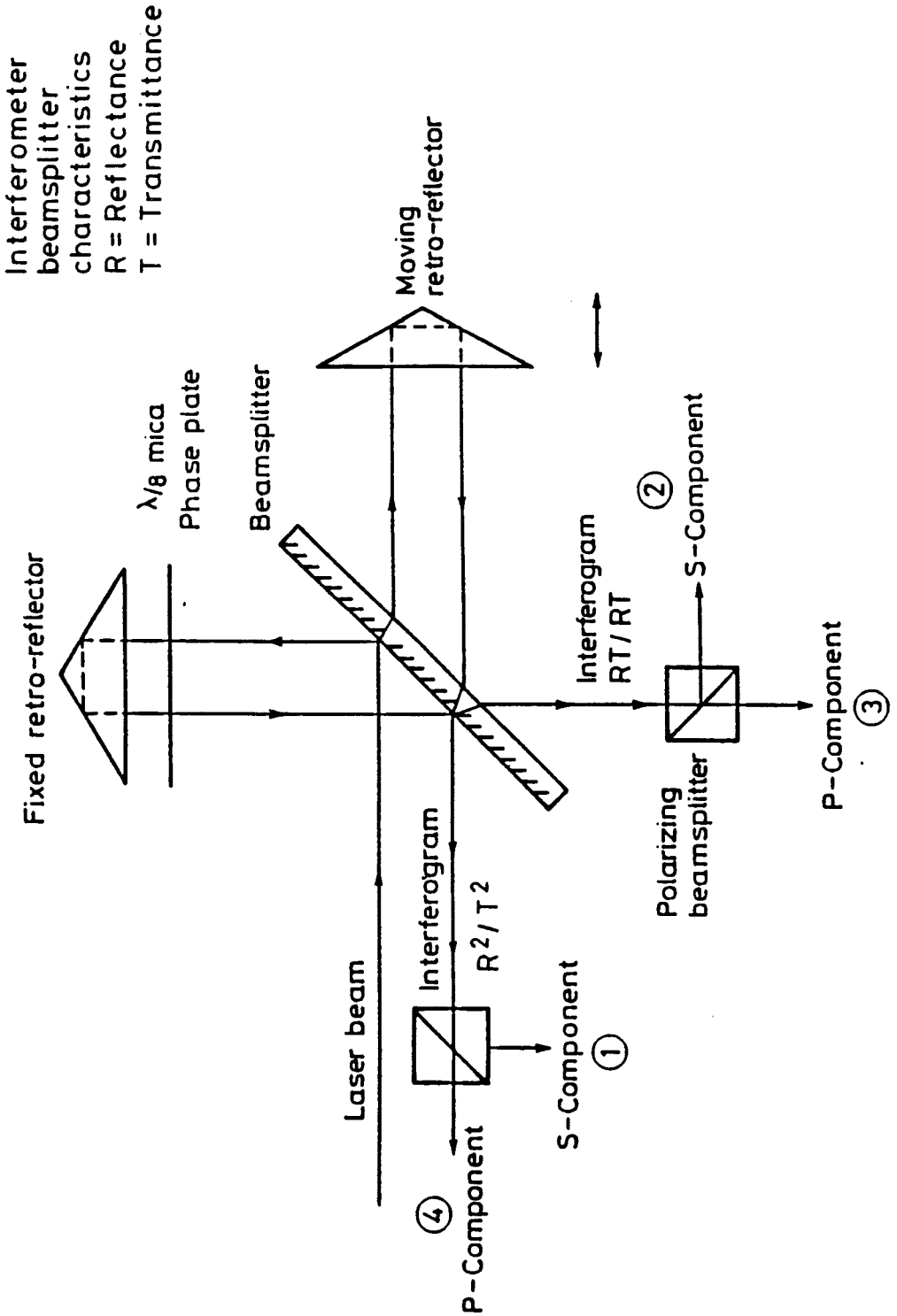


LENGTH INTERFEROMETER
(CH 2 FIG 1)

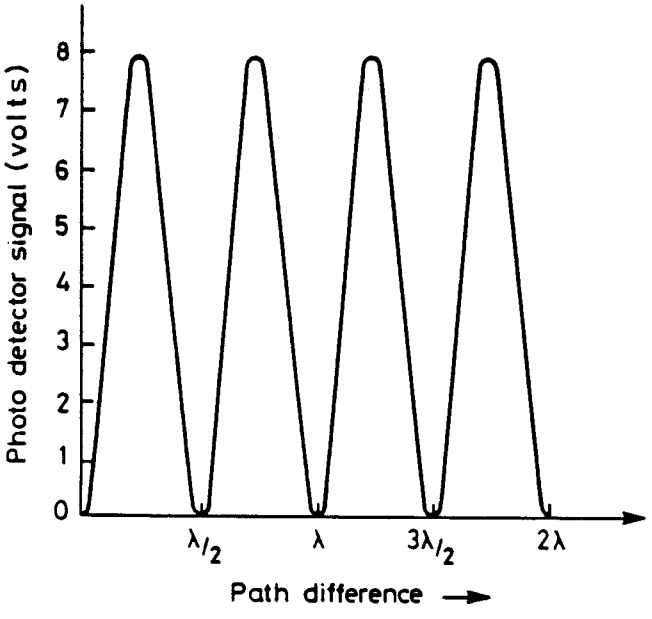


(a) Optimum contrast

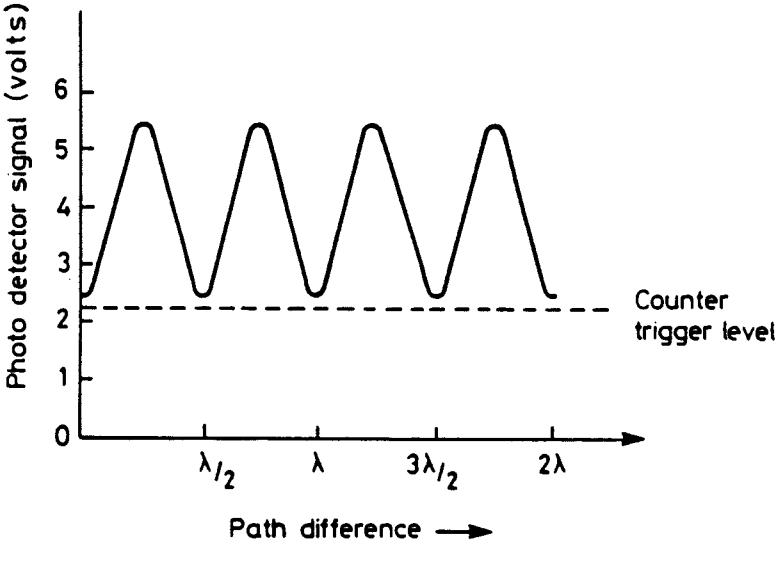


(b) Reduced contrast

PHOTO DETECTOR SIGNALS
(CH 2 FIG 2)

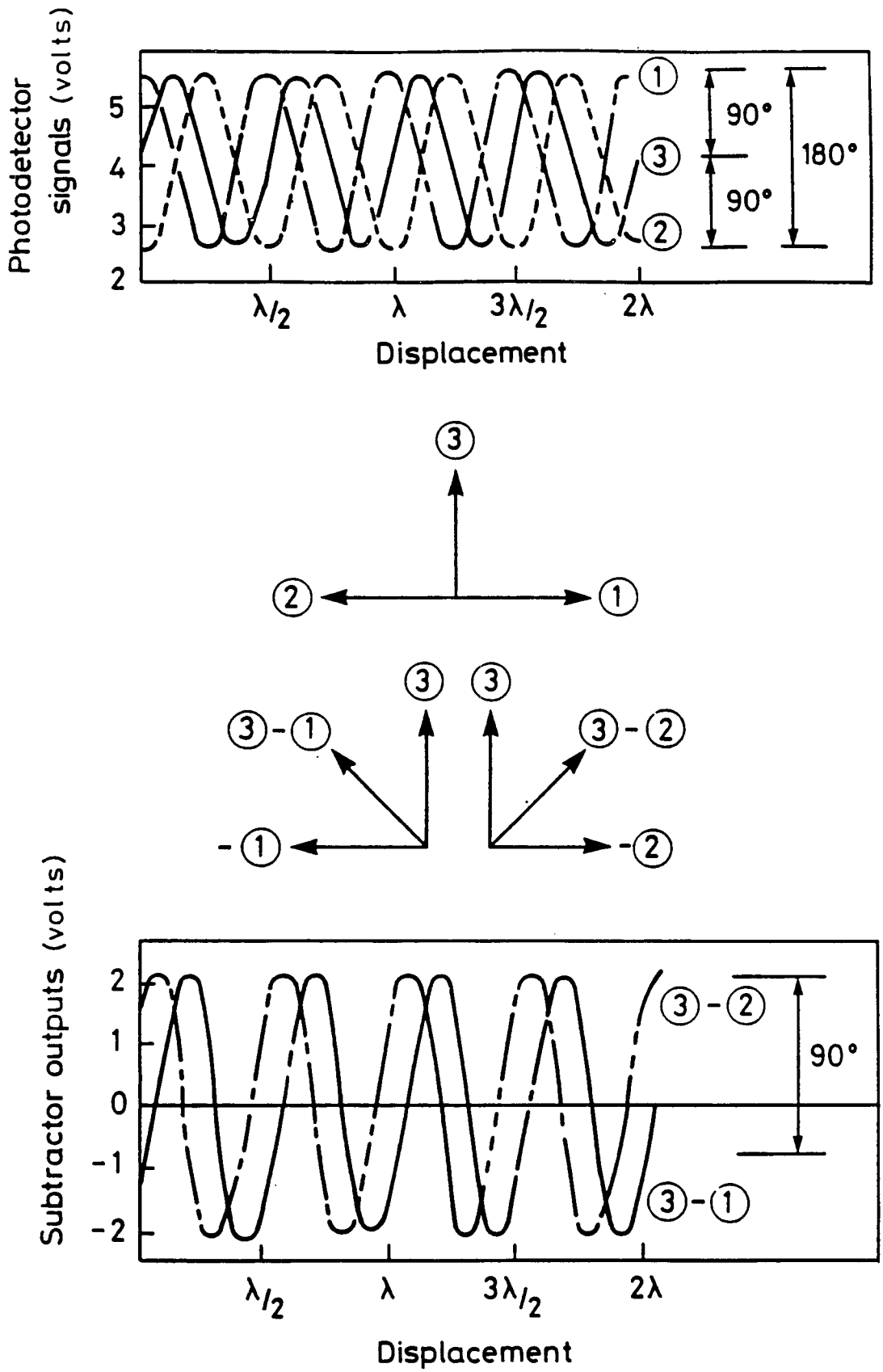


LENGTH INTERFEROMETER
(CH 2 FIG 3)

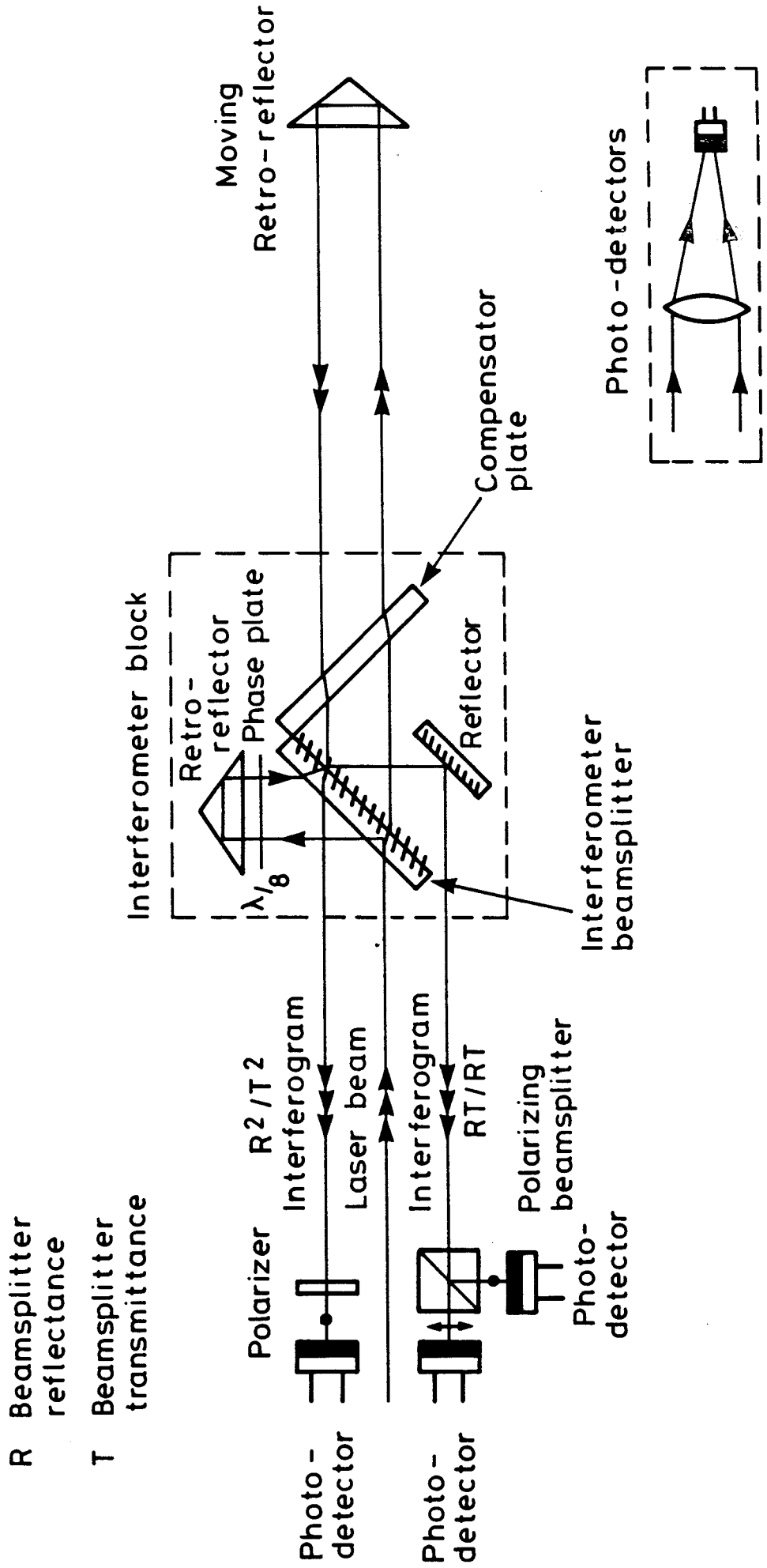


Length measuring interferometer
(CH2 FIG 4)

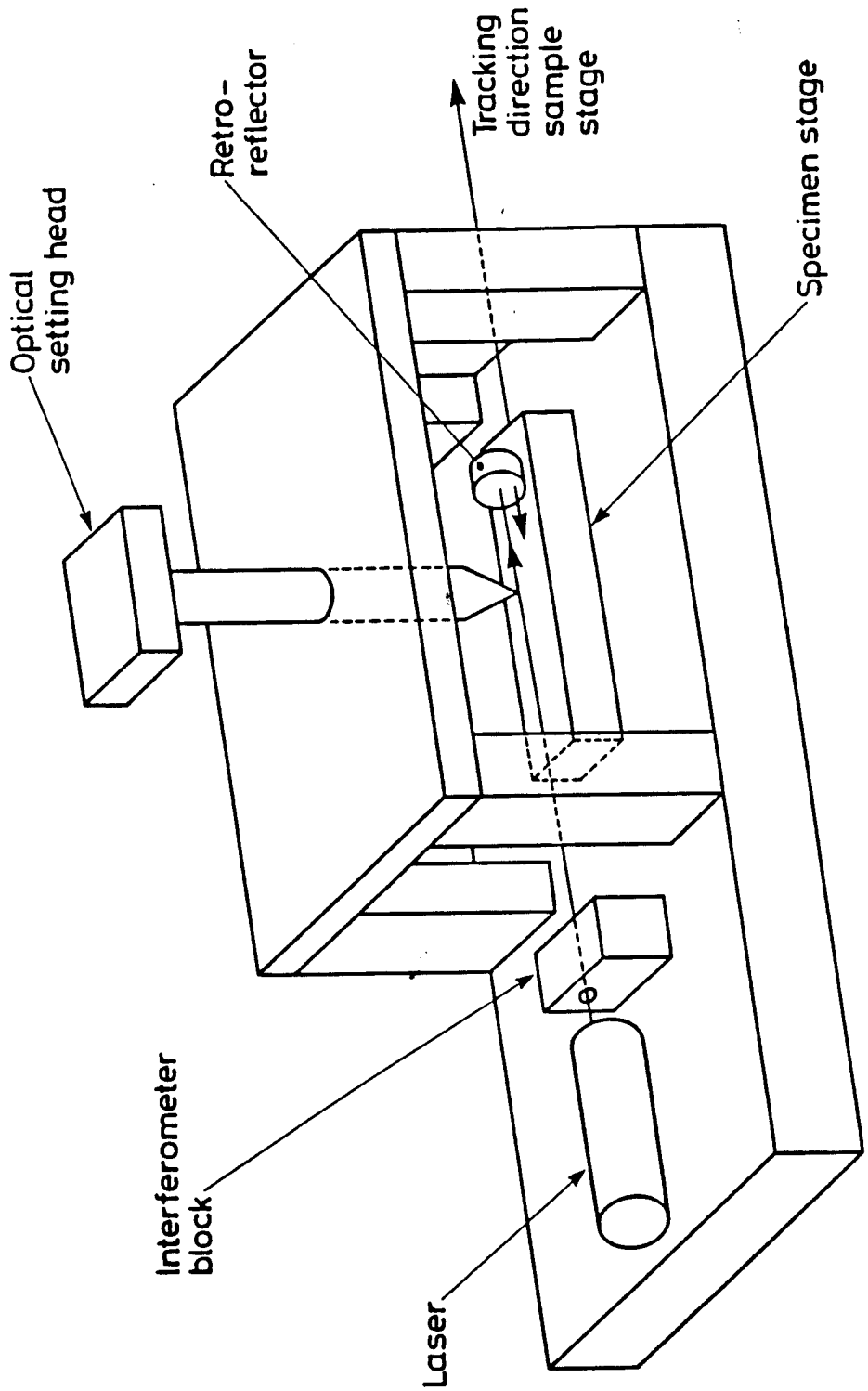


Schematic diagram of length measuring interferometer system
(CH 2 FIG 5)

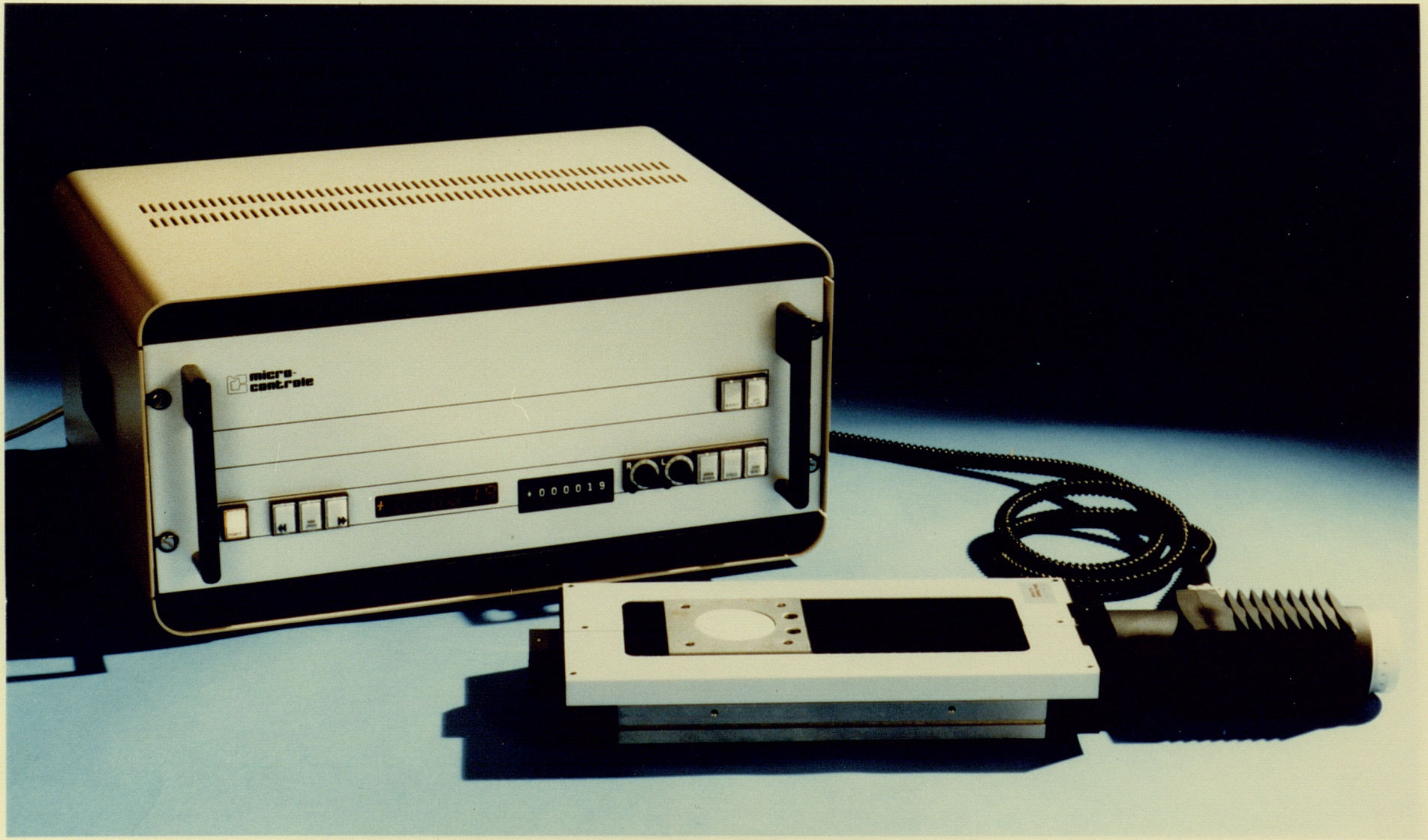


SCANNING STAGE
(CH2 FIG 6)

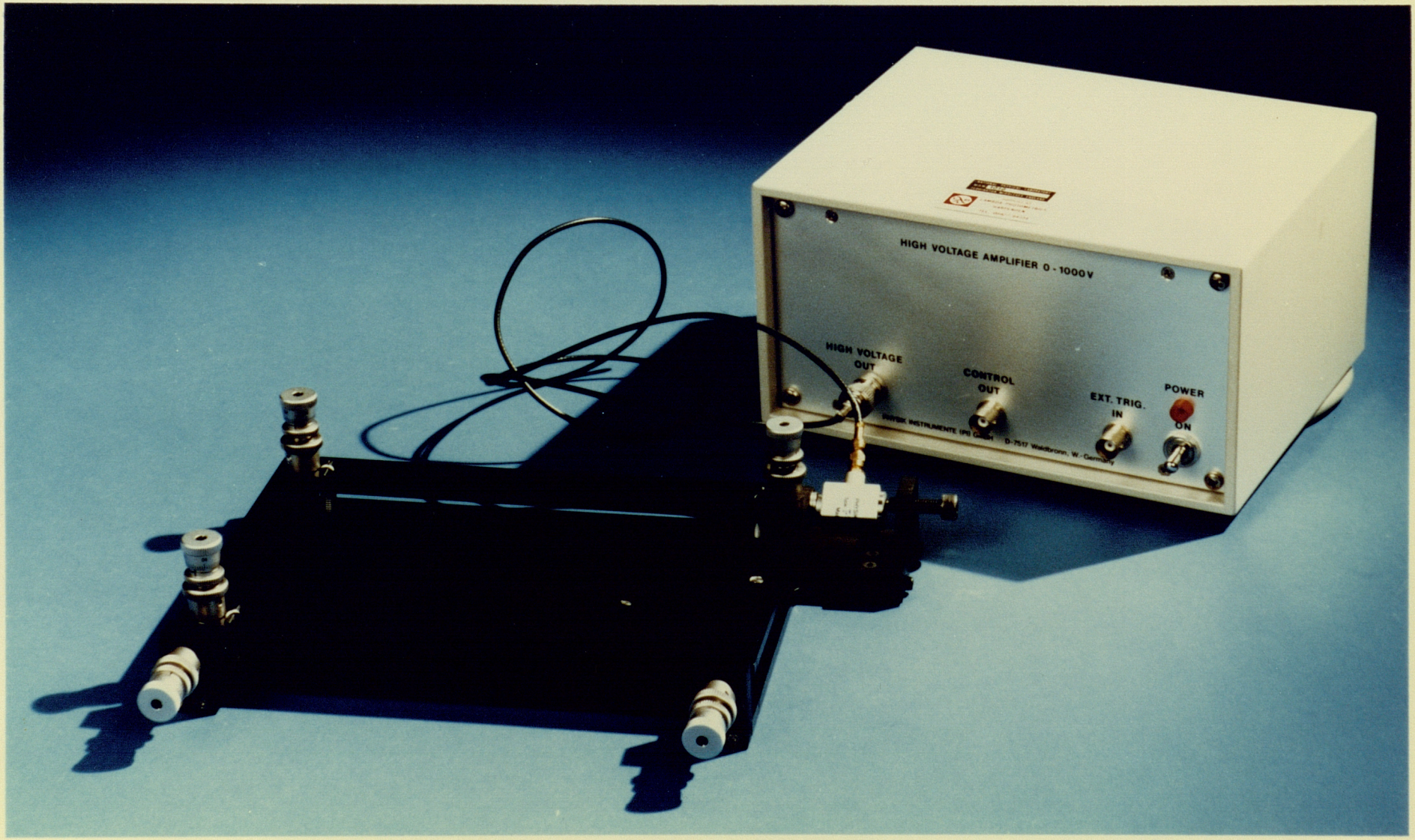


SUBSTRATE POSITIONING STAGE

(CH2 FIG 7)

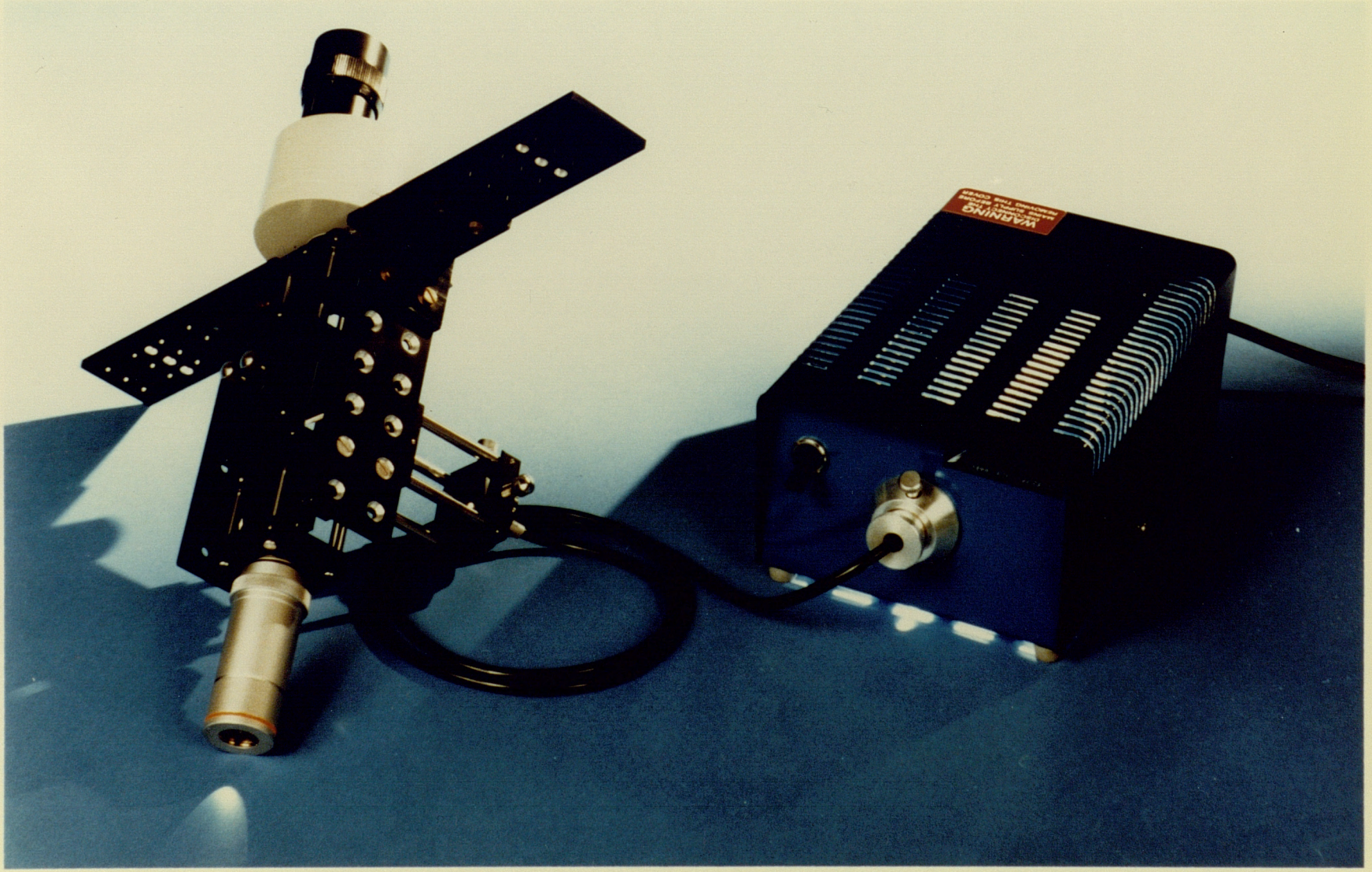


OPTICAL SETTING HEAD
(CH2 FIG 8)

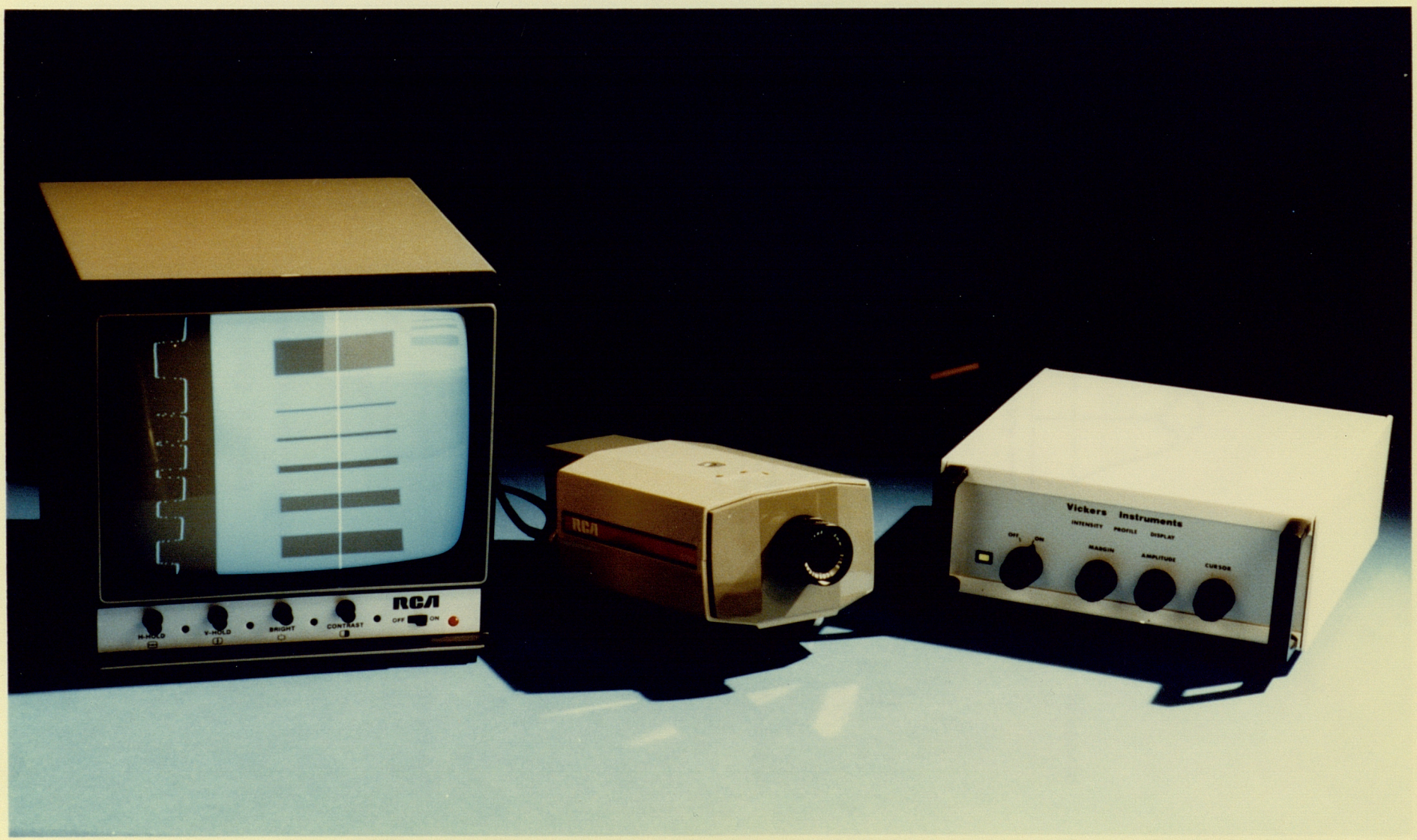


INTENSITY PROFILING SYSTEM
(CH2 FIG 9)

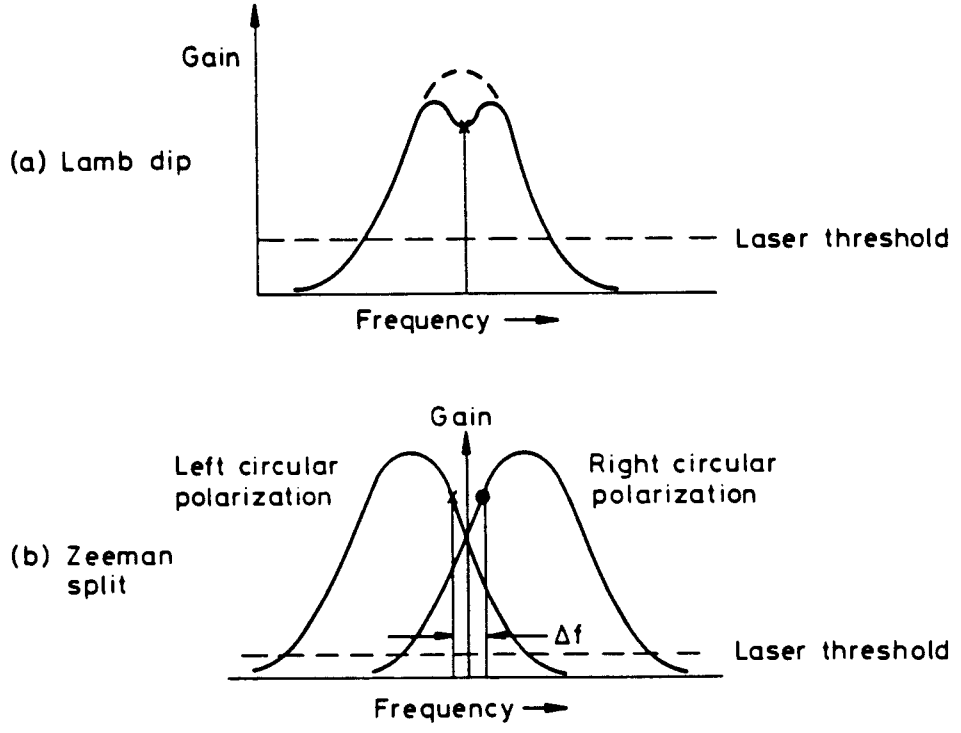


Laser doppler profiles

(CH2 FIG 10)

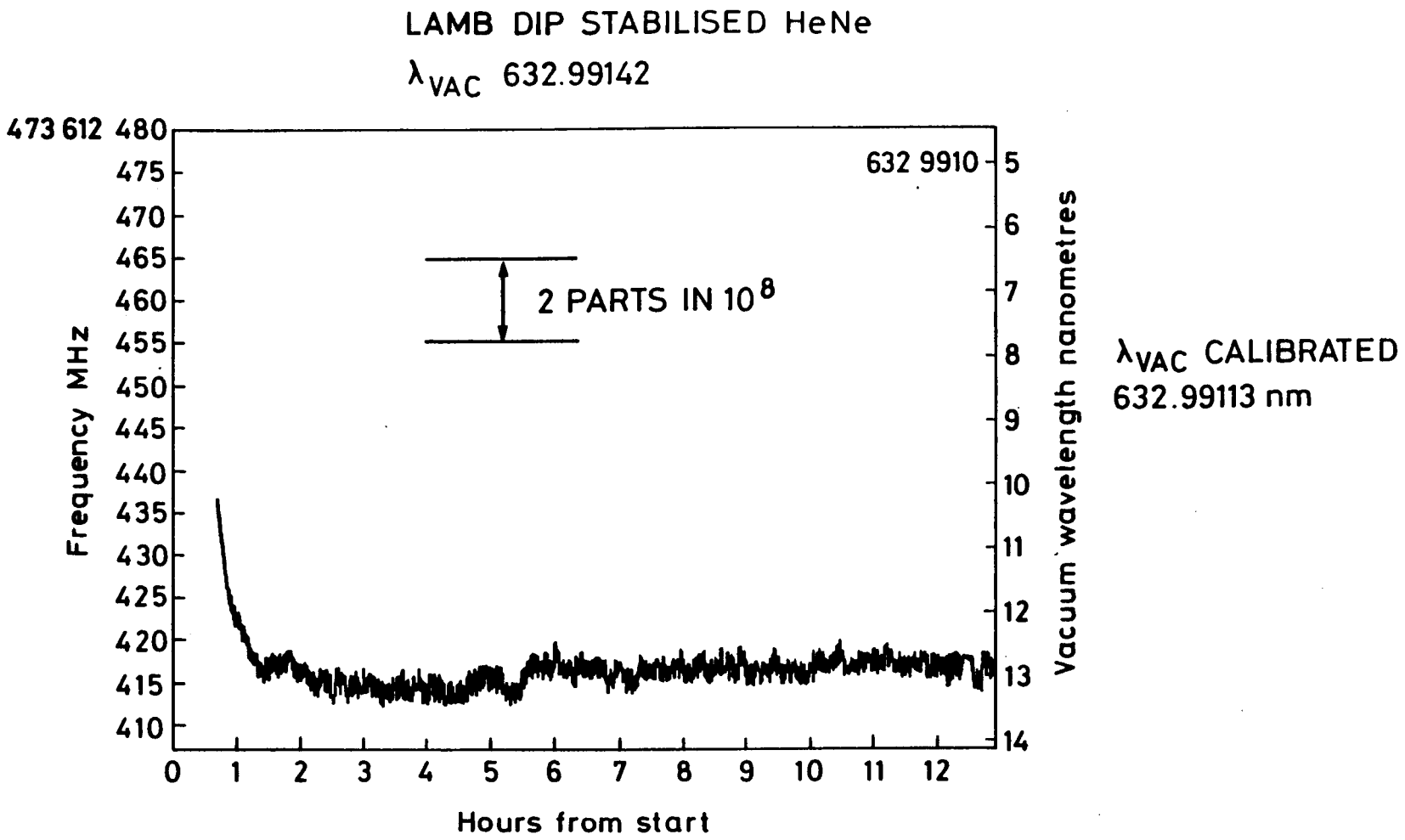


Laser frequency calibration curve

SPECTRA PHYSICS

117

(CH2 FIG 11)

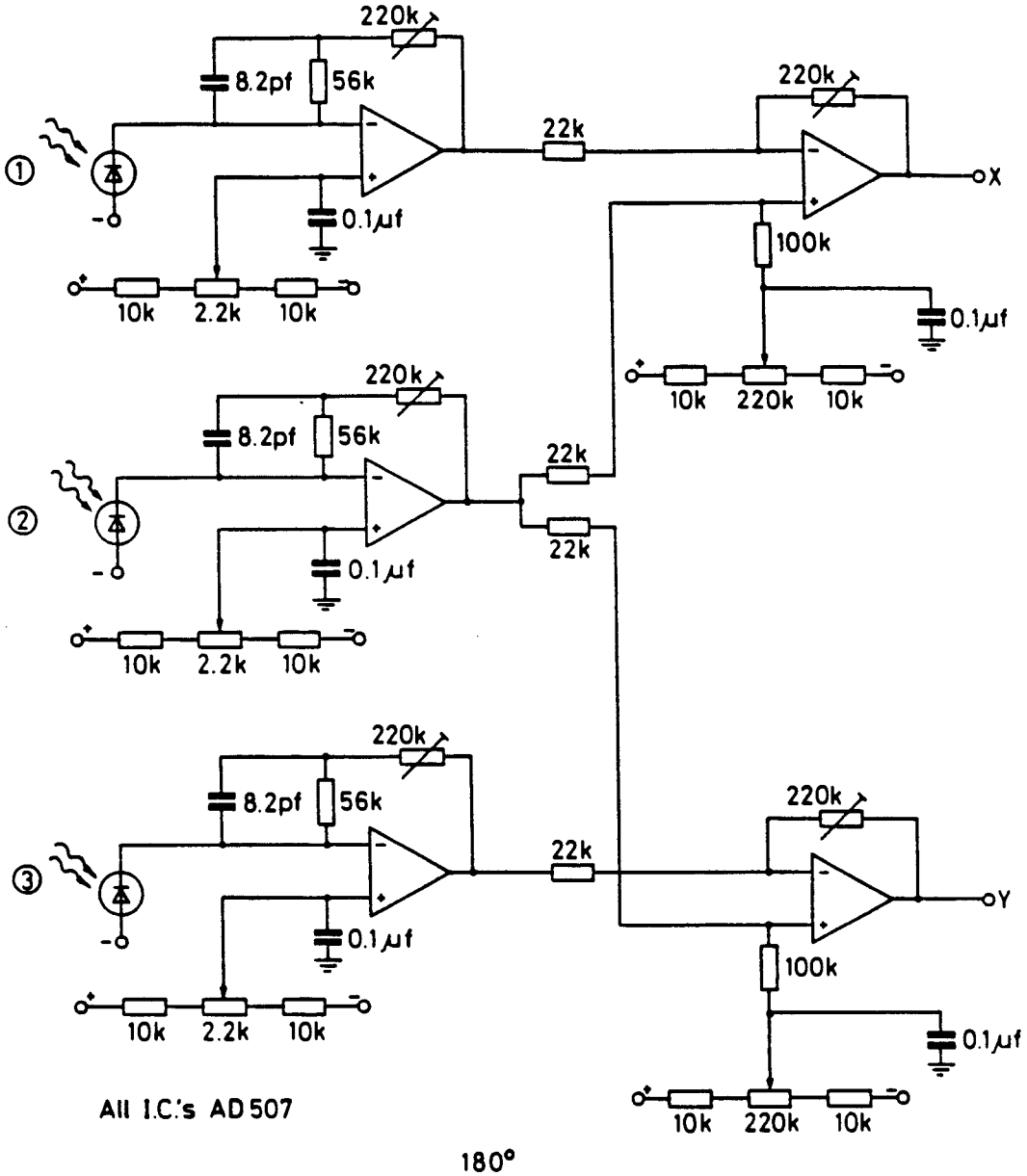


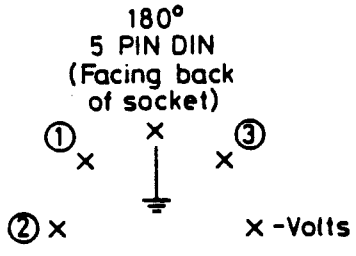


1MHz Interferometer electronics
(CH 2 FIG 12)

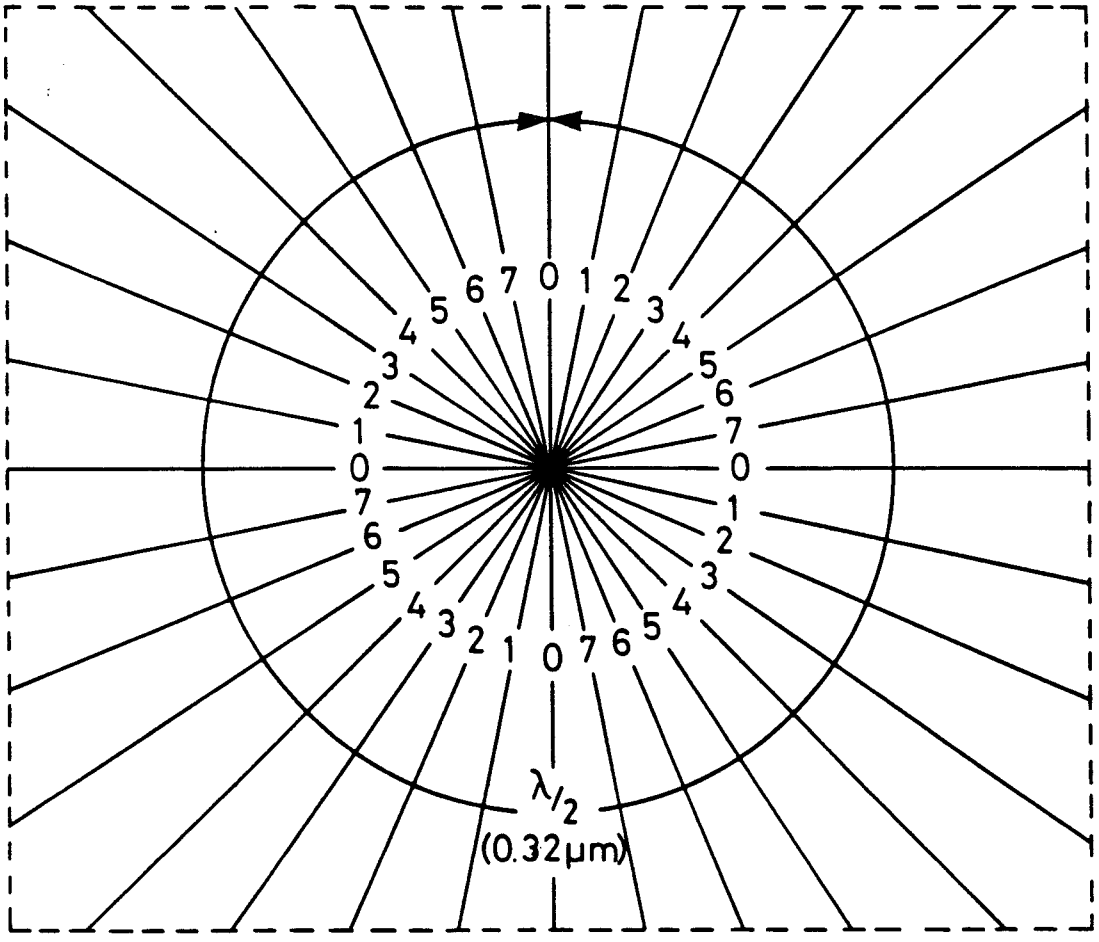


Fringe fractioning
length measuring
interferometer
(CH 2 FIG 13)

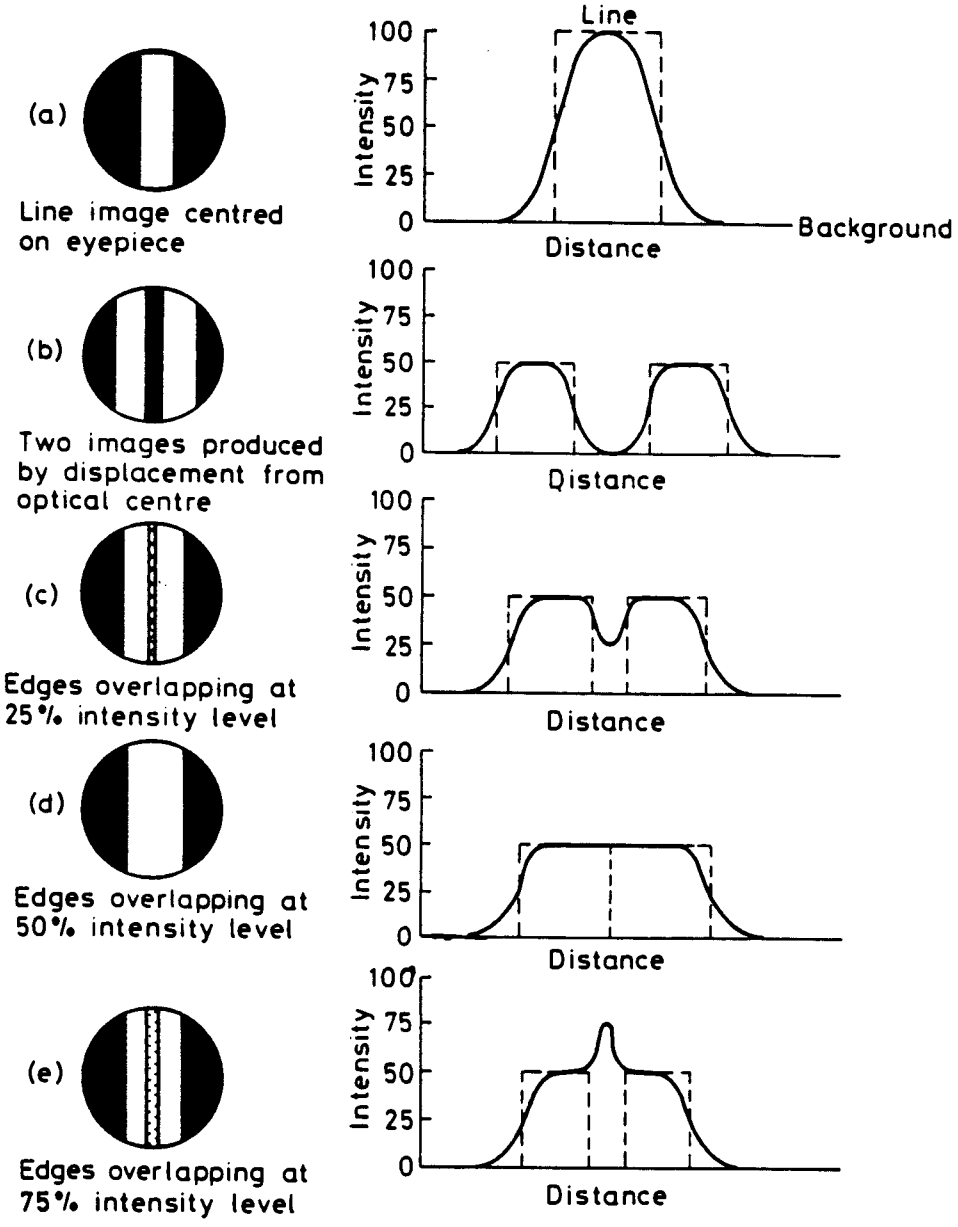


Line edge location with an image splitting and inverting eyepiece

(CH2 FIG 14)

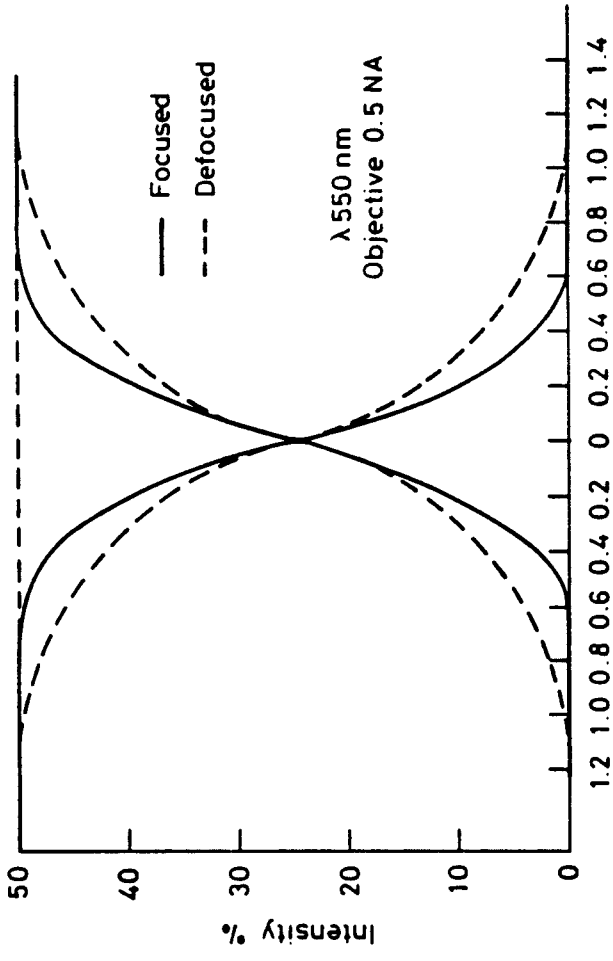


Superimposed edge intensity profiles (CH2 FIG 15)

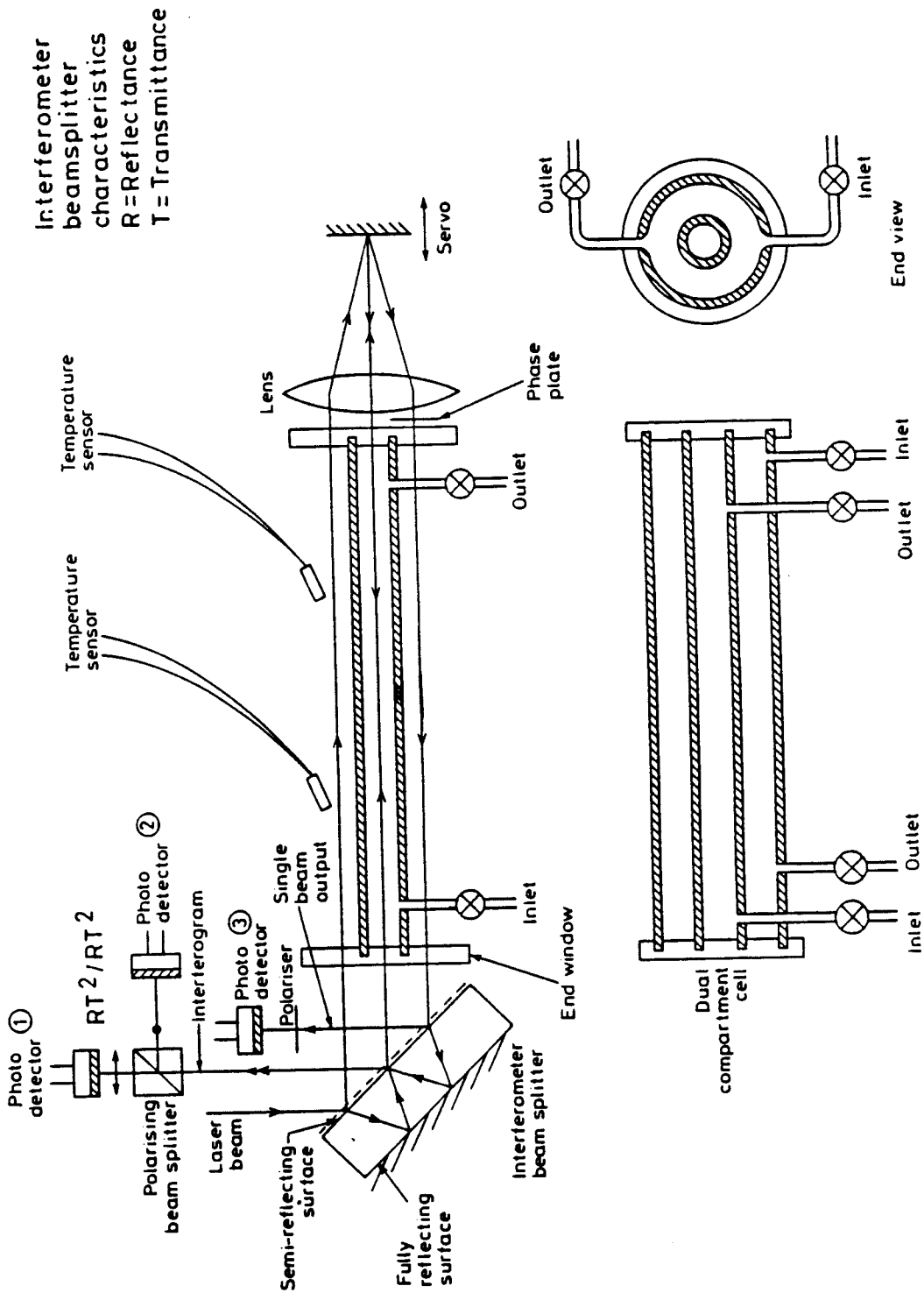


Refractometer optical configuration
(CH2 FIG 16)

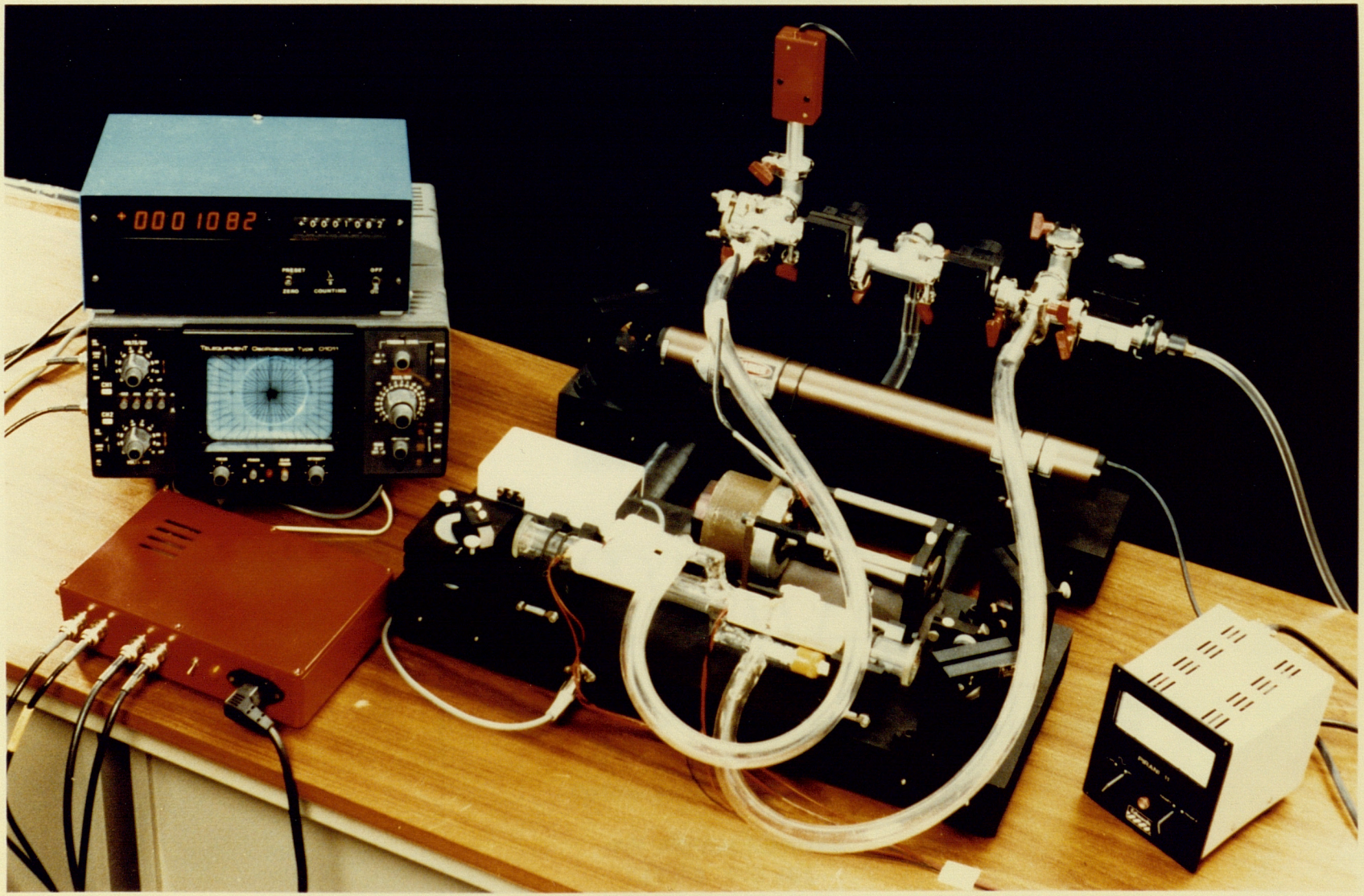


AIR REFRACTOMETER

(CH2 FIG 17)

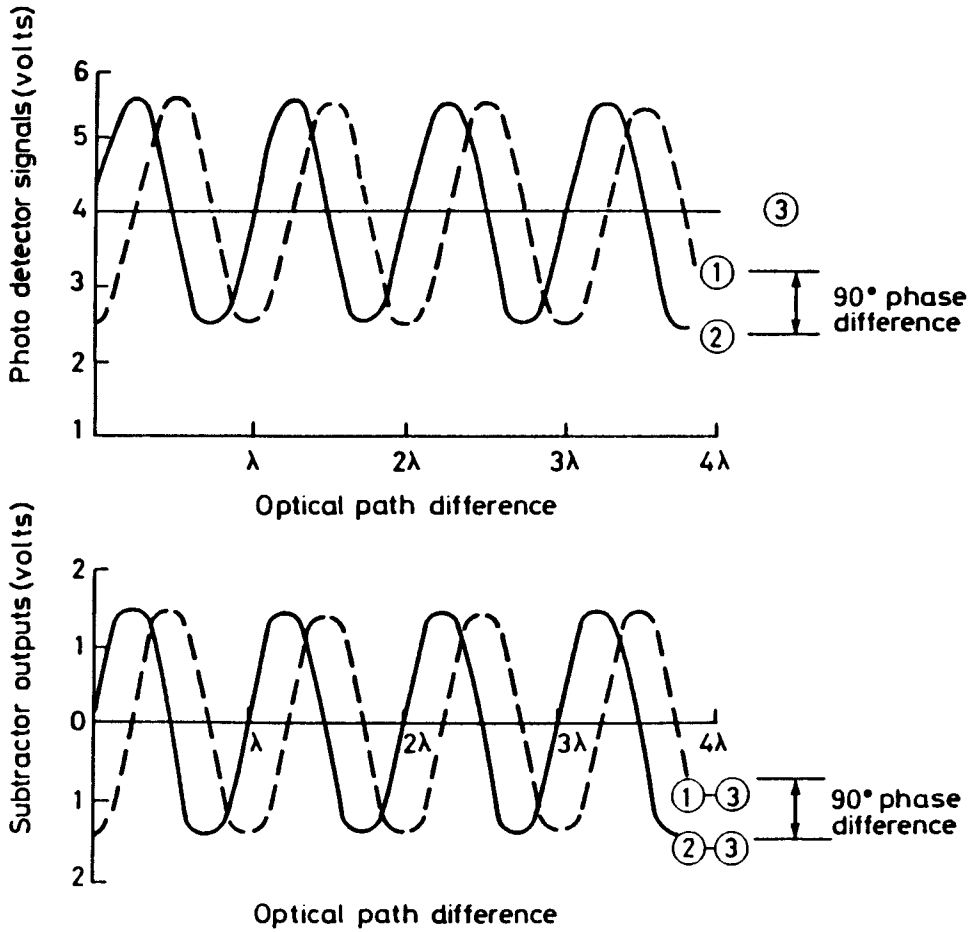


AIR REFRACTOMETER
(CH 2 FIG 18)

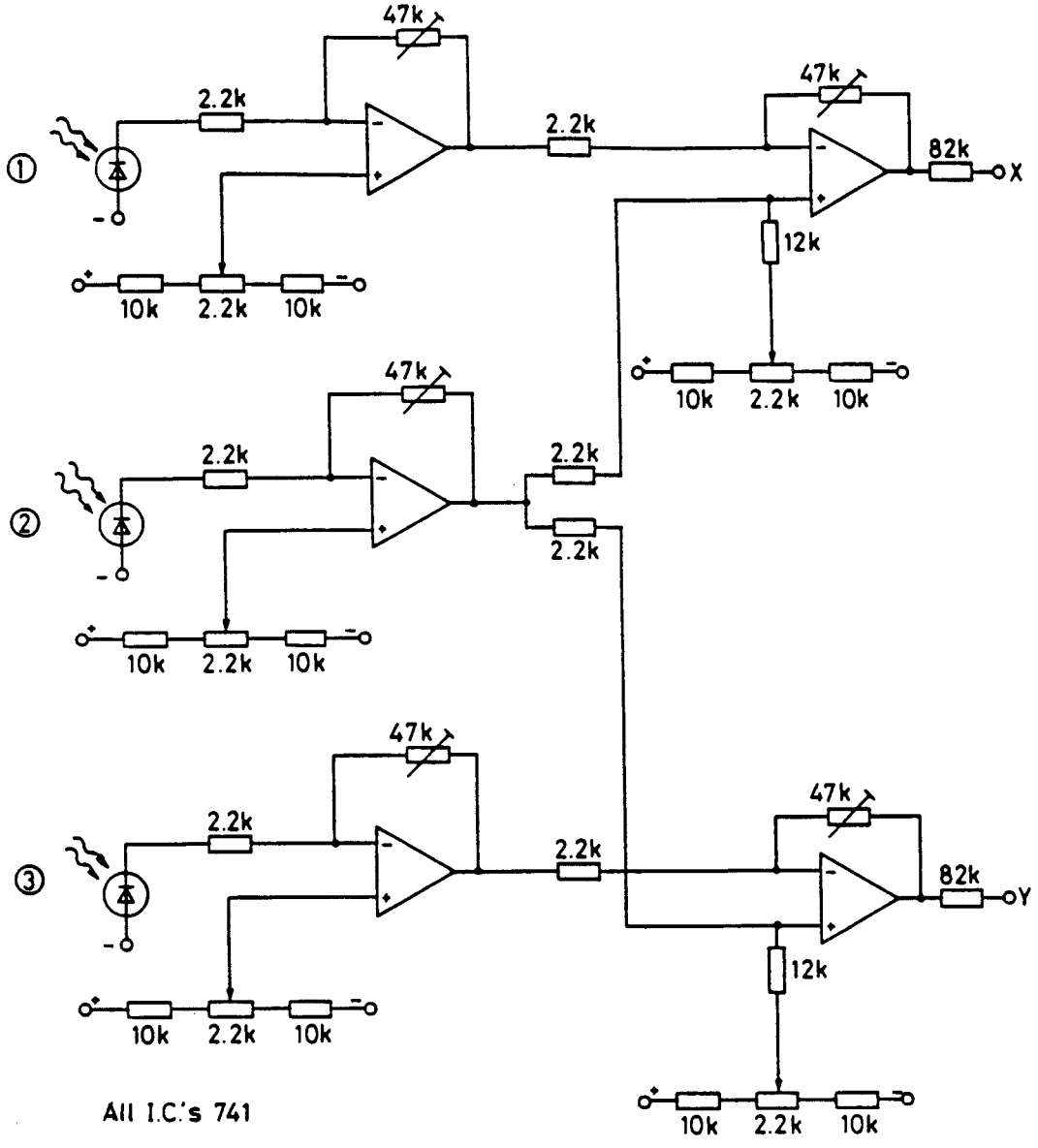


Low frequency interferometer electronics
(CH2 FIG 19)

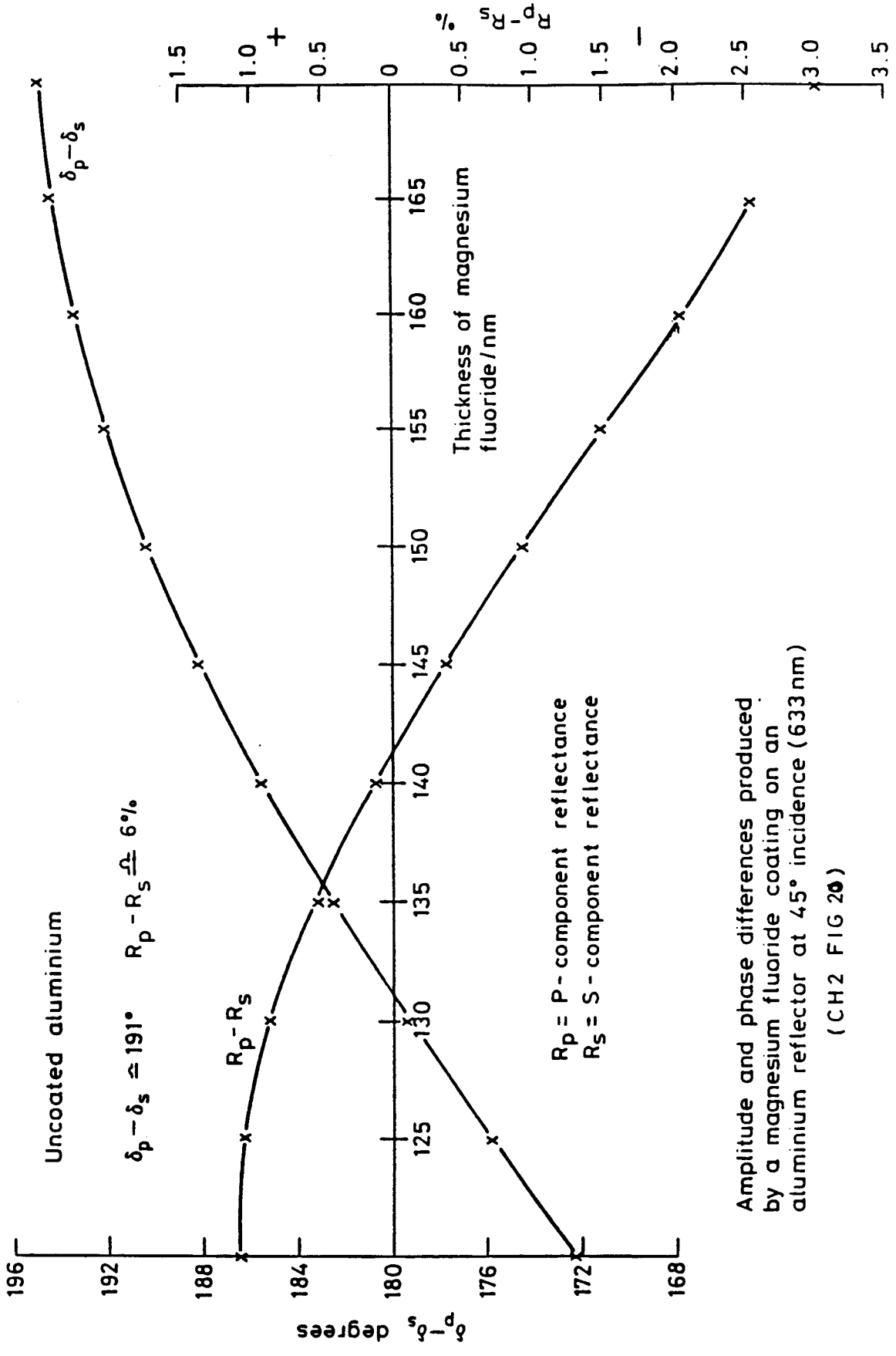


Amplitude and phase differences produced by a magnesium fluoride coating on an aluminium reflector at 45° incidence (633 nm)

(CH2 FIG 2b)

# C H A P T E R III

## ALIGNMENT AND OPERATION

### 3.1 Mechanical Alignment of length measuring interferometer

The six degrees of freedom affecting the position of an object in a single axis measuring system are shown in Figure 1. (It is worth noting that in a a 3 axis system there are 18 degrees of freedom together with the orthogonalities of the axes making 21 error sources.)

The two fundamental error sources generated by a single axis machine are Abbe and cosine errors and in addition there is the less significant 'deadpath' error. The effects of these can be reduced to an acceptable level by careful alignment and tracking of the measurement system.

Abbe error

Abbe errors are generated by angular motions of the measurement stage when the displacement measurement is taken at a location which is offset from the actual displacement to be measured. They can be almost completely eliminated by aligning the measurement point of the system to be coincident with the measurement direction of the interferometer which, as previously described, is a line through the apex of the corner cube retroreflector and parallel to the laser beam direction. The tolerance to this alignment is shown in Appendix VI. Alignment of the measurement point and direction of the system was achieved using a variable aperture centred on the laser beam with the capability of reducing the beam to 0.1 mm in diameter for alignment purposes.

The pitch and yaw of the scale positioning system was measured with a Rank Taylor Hobson photoelectric autocollimator by mounting a mirror on the substrate stage. The results of measurements from 20 runs over the 150 mm range of the stage indicated a pitch and yaw of 2.1 seconds of arc, both approximately in the centre of the movement with a repeatability of ± 0.25 seconds arc.

These angular movements would result in a maximum Abbe error in the system with a 0.1 mm Abbe offset of 0.001 μm (1 part in $10^8$). Reducing

this error to an acceptable level is of course only achievable by the use of a high quality tracking stage.

Cosine error

If the axis of motion of the measurement stage is not aligned with the axis of the laser beam an error is generated between the measured distance and the actual distance travelled. This is normally referred to as the cosine error as it is directly proportional to the cosine of the angle between these two axes, the cosine error always causes the interferometer to read shorter than the actual distance travelled. In order to achieve the accuracy of alignment required, it was necessary to construct the position sensitive quadrant photodetector system shown in Figure 2. The electronic circuit for this system is shown in Figure 3.

The quadrant cell detector was used, as shown in the diagram below, to measure the position of the retro-reflected laser beam. Using the detector in this configuration doubled the sensitivity to displacements resulting from tracking misalignment. As shown in the diagram, the laser beam direction was controlled by vertical and horizontal micrometer motions attached to both the front and rear of the laser tube; these not only provided angular adjustment but also enabled the position of the laser beam to be controlled and maintained in the optimum position through the centre of the interferometer block.

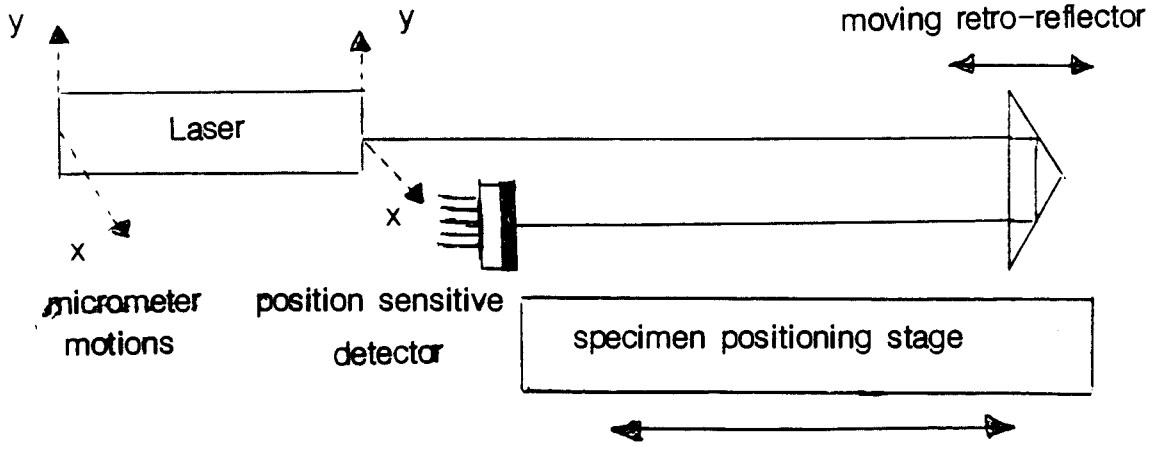


The position sensitive cell was calibrated using an X-Y micrometer motion and the tracking alignment achieved using the system was 20 μm in 150 mm. This is equivalent to 27.5 seconds of arc and due to the non-linearity of the cosine function results in a cosine error of 0.001 μm in 100 mm (1 part in $10^8$).

Two main characteristics of plate beam splitters are the displacements

they cause owing to the thickness of the plate and the deviations produced by the wedge angle introduced into the plate to prevent problems resulting from the unwanted energy reflected from the anti reflection coated rear surface of the beam splitter.

In order to be capable of both removal and replacing the interferometer block and interchanging the beam splitter whilst maintaining the alignment of the system, a compensator plate was used. The beam splitter and compensator plate were fabricated as a single optically flat element flatness specification (1 tenth fringe per 10 mm) which was cut into two pieces and used in the configuration shown in Figure 4. Using this technique the laser beam direction could be aligned with or without the interferometer block in the beam and the overall flexibility of the system was greatly improved. It is worth noting that the configuration used also corrects for chromatic effects should a multi-wavelength system ever be required.

## DEADPATH ERROR

Deadpath errors results from a difference in the optical paths of the two arms of the interferometer at the zero position. They are generated by atmospheric changes during the measurement cycle causing anomalous path differences in the uncompensated light path.

The 'deadpath' error in the system was minimised by appropriately positioning the interferometer block; this eliminated the need to apply a correction to the zero position. It will be appreciated however that where a 'deadpath' is inevitable in a system it is not required to be known to a high precision as the error is typically very small. In a single axis system the technique of taking a 'zero' reading before and after a scale measurement gives an indication not only of the repeatability and setting accuracy of the system, but also of whether any 'deadpath' or thermal expansion errors have been generated during the measurement cycle.

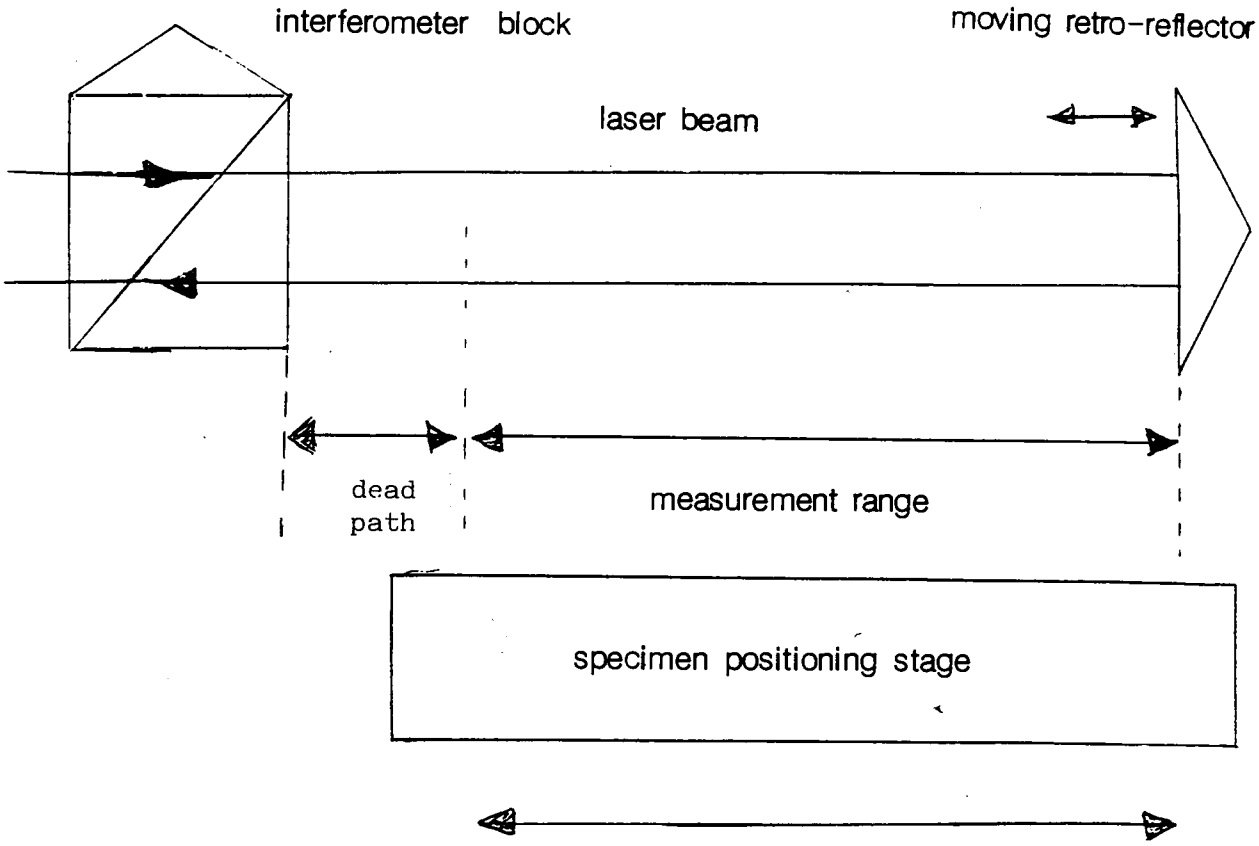


## 3.2 Operation of the Scale Positioning Stage

The optical scale being measured was mounted on the positioning stage shown schematically in Figure 5 and pictorially in Chapter II, Figure 7. The differential screw micrometers allowed both fine angular and positional control to be achieved. All the ball ends of these micrometers were held in contact with hardened steel pads using tension springs. A PI piezo-electric ceramic stack with a range of 10 µm was incorporated between this stage and the tracking stage to enable fine control of the position of the scale to be achieved remotely from the system using a 1 Kilovolt power supply.

Initially mechanical clips were used to hold the scale in position. However, when the scale was removed and remounted variations of the order of 0.2 µm in the 80 mm length were noted. After some investigations these were found to be attributable to mounting stress and the use of optical mounting wax was found to eliminate these variations and provide sufficient restraint to prevent the scale from moving when the stage was tracking during measurement. Further investigations were to show that the combined use of a mechanical clip at one end and wax at the other also provided a satisfactory mounting.

The results obtained using a 10 mm wide strip from an NPL 2-dimensional calibration plate with chrome features written on a low expansion glass substrate ($3 \times 10^{-6}$) are shown below. The measured lengths were calculated from the fringe count and fraction measured by the length interferometer and the calibrated vacuum wavelength for the Spectra-Physics 117 laser (632.99113 nm). Corrections for the refractive index of the atmosphere were obtained by measuring the temperatures in the air paths of the length interferometer and air refractometer using Platinum Resistance Thermometers and applying a suitable correction to the measured refractive index value for this temperature differential. Zero readings were taken before and after each scale measurement and meaned to eliminate systematic errors, and the scale temperature was measured with a PRT and a suitable correction applied. Each distance value is the mean of ten measurements.

| Measured distance (mm) between points 1 and 5 at 20 °C | Scale Mounting Technique (Substrate removed and remounted for each set of measurements) |
|---|---|
| 80.000 76 | |
| 61 | Mechanical Clip |
| 59 | both ends |
| 68 | |
| 83 | |
| 80.000 56 | |
| 57 | Wax both ends |
| 55 | |
| 54 | |
| 56 | |
| 80.000 57 | Mechanical clip one end, |
| 56 | flexible restraint the |
| 54 | other end |
| 80.000 56 | Mechanical clip one end, |
| 57 | wax restraint the |
| 55 | other end |

At first it was thought that these variations were because the scale was being mounted flat on a glass plate and not using one of the more traditional methods of mounting scales such as at the Airy points.

The Airy support points are two points on a standard bar, of length $\ell$, each distant from its centre point by $\frac{1}{2\sqrt{3}}\ell$.

When it is supported at these two points, varying flexure of bar, arising from changes in the intensity of gravity or small errors in the exact point of support has least effect on the horizontally projected length of the bar.

However it can be shown that it would take APPRECIABLY large bending or lack of flatness of the scale to cause the changes in length measured (see Appendix 5). The length changes due to mounting stress arising from the fact that the scale was being either stretched or compressed. Calculations for the scale measured indicated that an error of 0.01 μm could be incurred by a force of approximately 20 grms.
(Material silica dimensions 100 mm long, 10 mm wide and 3 mm thick)

This was confirmed by the results obtained by mechanically clipping the scale at one end and red waxing the other. The red wax being sufficiently pliable to prevent forces being developed along the scale whilst still performing the function of holding the scale flat. However it should be recognised that where the distances between several points are being measured, lack of flatness would result in focus variations in the optical setting system on the edges of the scale markings which could result in length measurement errors due to offsets in the optical setting where the setting technique is sensitive to focus (see Chapter II, Section 7).

Wax would be unsuitable for this application other than a research situation and a flexible mount was successfully developed that used a PTFE pad on the end of a compression spring.

The technique of having one of the mounts with lateral flexibility could form the basis of a design for all mechanical substrate restraints. The technique would also well be applicable to vacuum restraints if one of the final constraints was a bellows for example.

## 3.3 Results of Atmospheric Homogeneity Study

In order to access the magnitude of the problems caused to precision length interferometry by variations in the parameters of the atmosphere the humidity, pressure and temperature were measured at a number of positions within the Laboratory.

The two pressure measuring sensors used were Negretti and Zambra Aviation Ltd (Croydon) precision aneroid barometers. These instruments had been previously calibrated to an accuracy of ± 0.1 millibar (equivalent to ± 3 parts in $10^8$ of refractive index). The two type MIK3000 dual humidity and temperature sensor used were manufactured by Novasina AG (Zurich). The temperature readouts were calibrated to ± 0.1°C (equivalent to ± 1 part in $10^7$ of refractive index) and ± 1% relative humidity (equivalent to ± 1 part in $10^8$ of refractive index). By using pairs of instruments accurate differential measurements could be achieved.

The humidity sensors were also checked using calibration salts (Young, J F).

A schematic diagram of the measurement points within the laboratory is shown below:

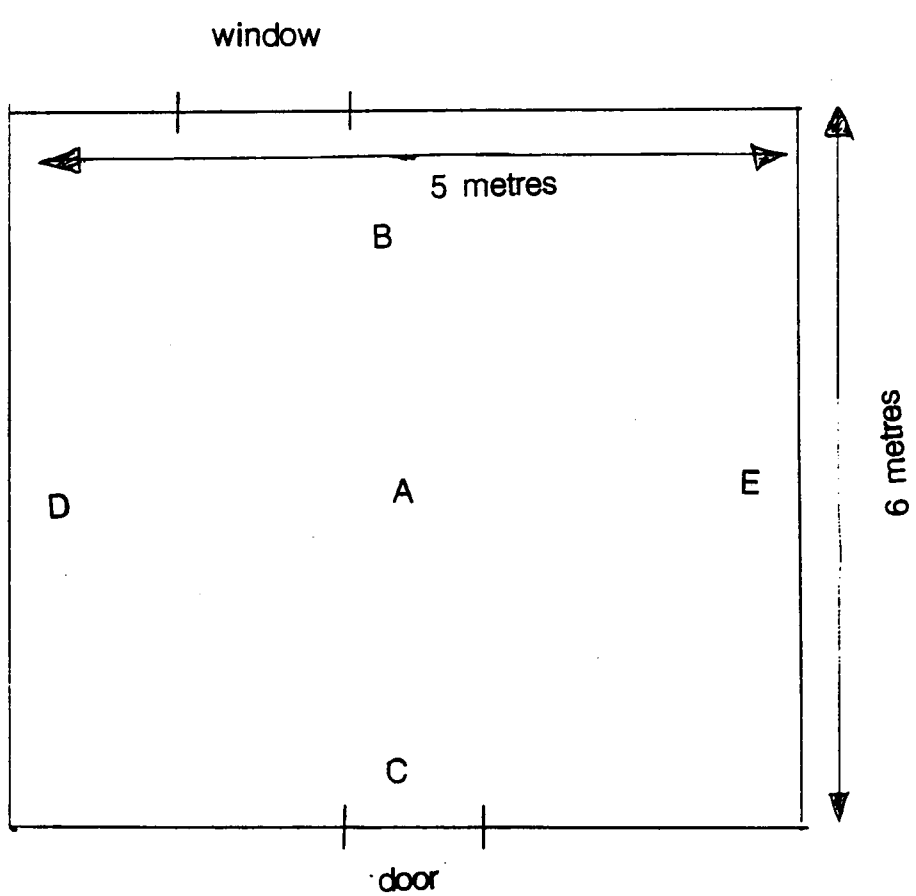

The ceiling height was 5 metres and all the measurements were taken at bench height. Temperature and relative humidity measurements were taken with one of the gauges in the centre of the laboratory and the other moved from this position to each of the other 4 points, returning to the central position between each measurement in order to establish a differential measurement reference point. A typical example of the results obtained from this study are shown below:

| GAUGE I | DIFFERENTIAL READING (II-I) | GAUGE II | POSITION |
|---|---|---|---|
| 20.6 °C<br>41.5 % RH | + 0.1 °C<br>- 1.7 % | 20.7 °C<br>39.8% RH | A |
| 20.5<br>41.7 | - 0.1<br>- 2.5 | 21.4<br>39.2 | B |
| 20.6<br>42.2 | + 0.1<br>- 1.0 | 20.8<br>41.2 | A |
| 20.7<br>41.6 | + 0.2<br>- 1.8 | 20.9<br>39.8 | C |
| 20.8<br>41.3 | + 0.1<br>- 1.1 | 20.9<br>40.2 | A |
| 20.8<br>41.1 | - 0.4<br>- 0.6 | 20.4<br>40.5 | D |
| 20.8<br>41.1 | + 0.1<br>- 0.9 | 20.9<br>40.2 | A |
| 20.7<br>41.8 | - 0.3<br>- 1.8 | 20.4<br>40.0 | E |
| 20.7<br>41.3 | + 0.1<br>- 1.0 | 20.8<br>40.3 | A |

The total range of temperature variation from these results of 0.6 °C would be equivalent to a refractive index variation of 6 parts in $10^7$. The total range of humidity variation measured of 2% relative humidity would be equivalent to a refractive index variation of 2 parts in $10^8$. The results of the pressure measurements obtained by gauge B436 at the centre of the laboratory and gauge B864 measuring at the four other measurement points are shown as follows:

| READING (GAUGE B436) | DIFFERENTIAL READING | READING (GAUGE B864) | POSITION OF B864 |
|---|---|---|---|
| 994.75 millibar | + 0.30 | 994.45 millibar | A |
| 4.70 | + 0.28 | 4.42 | B |
| 4.75 | + 0.27 | 4.48 | A |
| 4.80 | + 0.35 | 4.45 | C |
| 4.75 | + 0.28 | 4.50 | A |
| 4.70 | + 0.25 | 4.45 | D |
| 4.75 | + 0.33 | 4.42 | A |
| 4.80 | + 0.32 | 4.48 | E |
| 4.75 | + 0.30 | 4.45 | A |

The total pressure variation measured of 0.1 millibar would be equivalent to a change in refractive index of 3 parts in $10^8$.

The results of this study indicated that temperature variations throughout the atmosphere are a major limitation in achieving precision interferometric measurements in the free atmosphere; however to achieve and maintain an absolute pressure measurement accuracy of ± 0.1 millibar is extremely difficult and the contributions from both pressure and humidity cannot be ignored if a calculated refractive index value is to be employed.

## 3.4 Problems encountered with the Refractometer Cell Design

As shown in Chapter II, Figure 16, the air refractometer can be used with either a dual compartment or single compartment cell and experimental results were to show that the choice of cell would have distinct advantages and disadvantages dependent upon the measurement situation.

With the dual compartment cell the refractive index measurement is achieved by first evacuating the inner and outer compartments and then admitting air into one of these compartments, the bi-directional fringe counting system measuring the number of counts produced by this vacuum to air change; the fringe fraction interpolation being obtained in the

same way as for the length interferometer by measuring the angular orientation of the voltage vector produced on an oscilloscope by the counting signals (Figure 6) and electronically from the fractioning unit. Initial designs of these cells used a single inlet/outlet part for each compartment; however, in order to circulate a specimen through the cell for a short period to stabilise the specimen conditions within the cell, replacing for example any water vapour pumped from the cell walls during the vacuum phase, the cell was designed to have an inlet and outlet part for each compartment. The design of this dual compartment cell which can be seen in Figure 7; has the advantage that during the measurement cycle one of the refractometer readings is taken with both cells (EVACUATED) providing an absolute 'zero path' difference condition in the interferometer totally independent of temperature.

A second advantage of a dual compartment cell is that, unlike a single compartment cell, it does not confine the instrument to the measurement of the refractive index of the atmosphere; for, by introducing different gases into the compartments, comparative refractive indices can be measured. The latter advantage allows synthesised air with accurately known constituents to be measured and compared with values calculated using Edlen's equation. For these reasons a dual compartment cell was initially chosen for the measurement of the refractive index of the atmosphere. However, this was to prove far from ideal in this measurement application. In order to discover in this thesis the limitations to precision length measurement in the free atmosphere and to develop techniques for maintaining high measurement accuracies in typical laboratory conditions, no attempt was made to control the environment in the laboratory. The laboratory temperature, for example, could rise by several degrees Celsius during the day changing at rates approaching one degree an hour. When the refractive index values measured with a dual compartment cell were compared with those calculated by measuring pressure, temperature and humidity accurately and using Edlen's equations, the results indicated that the Platinum Resistance Thermometers measuring the temperature of the air within the cell were giving completely false readings. The errors in these readings were being generated by the thermal dynamics of the measurement situation underlining the difficulty of measuring the temperatures of gases with their low thermal capacitances and slow thermal transfer characteristics.

In spite of their small physical dimensions the thermal capacitances of

the Platinum Resistance Thermometers used were producing a lag in their response to temperature changes and large errors in the measured temperature were generated by the fluctuating temperature of the air specimen. In order to measure the air refractive index to a few parts in $10^8$, accuracies of a few hundredths of a degree Celsius were essential. Having encountered this problem, and knowing from the atmospheric study in Section 3, that temperature measurement would be the major limitation to the accuracy achievable, an investigation of temperature sensors was carried out and this is described in Section 6. The results obtained by this investigation were to rule out the use of a dual compartment cell other than in a thermally controlled situation such as a temperature bath.

Unsuccessful attempts were made to allow time for the PRTs to respond to the air temperature by switching of the circulating pump and allowing the air specimen to stand in the cell compartment. The poor agreement between measured and calculated values of refractive index persisted and the temperature measurement indicated that the air was taking up the temperature of the cell body because of its dominant thermal capacitance. In addition to this the small volume of the cell would prevent convection taking place to reduce any thermal gradients generated in the air specimen.

Both the thermal control of the cell with a liquid bath and thermal control of the air specimen were considered; however, the object of the research was to develop a simple and economic technique for measuring the refractive index of the atmosphere for use with precision length interferometers, and at this point it was decided to re-appraise the situation.

The results with a dual compartment cell had shown that one of the fundamental problems to be solved was the accurate measurement of the temperature of the air in the cell and it is a fact that one of the main advantages of a single compartment cell is that it does not suffer from this problem.

With a single compartment cell (shown in Figure 8) the air specimen is continuously in contact with the atmosphere and does not require circulation. Because the air has been within the vicinity of the cell for a reasonable time, it has achieved a stable temperature condition and the temperature sensors are accurately measuring the temperature. In

practice with the use of shielding to prevent draughts from the laboratory, and with several PRTs suitably spaced close to the interferometer path to average out any temperature gradients. An accuracy of a hundredth of a degree Celsius was achieved equivalent to a part in $10^8$ of refractive index. The fact that the use of a single cell restricted the instrument to the measurement of the atmosphere was not a limitation in this application and the only real disadvantage remaining was the fact that with a single cell the 'zero path' difference reading had to be performed with air in both paths of the interferometer. On first examination this appeared to reintroduce the problem of temperature measurement within the single compartment of the cell; however, in the 'zero path' difference situation with air in both paths, the interferometer is effectively measuring the temperature of the air at a speed limited by the electrical response of the system. This fact was used to preclude the need to measure temperature in either optical path at the 'zero path' point by slowly circulating a representative sample of air from the open path through the central compartment. The circulation of the specimen now permitted by the fast temperature measurement minimised the effects of temperature changes caused by the high thermal capacitance of the cell body. The air specimen was obtained by the four branched inlet manifold shown with the cell in Figure 8. Four pvc tubes of equal length were connected to this manifold and by sampling the air at several suitable points around the cell and circulating the sample obtained by the manifold through the inner compartment of the cell, an extremely stable air to air zero of 1/200th of a fringe could be achieved. (Equivalent to 1 part in $10^8$ of Refractive Index with a 158 mm long cell).

It was important not to circulate this specimen at an excessive rate as heating of the cell body was then found to take place. The cell compartment consists of a stainless steel tube 158 mm long and 8 mm inner diameter (volume 8 ccs). A flow rate of 0.2 litres/minute was found to be suitable, replenishing the specimen in the cell every 3 seconds without unduly disturbing the stable conditions around the cell itself by extracting too much air.

The temperature measurements shown below indicate that the frictional forces involved with a flow of 2 litres per minute would raise the temperature of the cell body 0.11 $^{o}$C and a flow of 5 litres per minute 0.22 $^{o}$C.

| AIR TEMPERATURE IN OPEN CELL PATH | FLOW RATE (litres/min) | TEMPERATURE OF CELL BODY (2 PRT's) |
|---|---|---|
| 19.85<br>19.84 MEAN 19.84 °C<br>19.82<br>19.84 | 0.2 | 19.82 MEAN 19.84 °C<br>19.87 |
| 20.24<br>20.18 MEAN 20.19 °C<br>20.19<br>20.15 | 2.0 | 20.28 MEAN 20.30 °C<br>20.32 |
| 20.38<br>20.34 MEAN 20.35 °C<br>20.34<br>20.35 | 5.0 | 20.51 MEAN 20.57 °C<br>20.62 |

This temperature rise was accompanied by a corresponding change in the air to air 'zero path' measurement.

| AIR TO AIR ZERO (FRINGE FRACTION) | FLOW RATE (litres/min) |
|---|---|
| 0.5 | 0.2 |
| 0.43 | 1.0 |
| 0.42 | 2.0 |
| 0.415 | 3.0 |
| 0.41 | 4.0 |
| 0.4 | 5.0 |

0.1 FRINGE = 2 PARTS IN $10^7$ (for a 158 mm long cell) OF REFRACTIVE INDEX

It should be noted that the above measurements were deliberately taken on a day when the temperature in the laboratory was relatively stable, minimising the problems due to thermal response characteristics.

## 3.5 Single Compartment Refractometer Cell Design

The design of the single compartment cell finally employed is shown in Figure 8. This cell incorporated a number of features designed to overcome problems encountered during the construction of the dual compartment cell. The design is shown diagramatically in Figure 9. The compartment of the cell was fabricated together with its inlet and outlet from stainless steel; this allowed a strong demountable cell to be fabricated by polishing the ends of the stainless tube, allowing vacuum seals to be obtained via o-rings onto the windows. The length of the cell, effectively its calibration, is defined by three silica rods each acting as a length standard with a very low coefficient of linear

expansion. (For a 158 mm length cell a change in length of 5 μm is equivalent to a change 1 part in $10^8$ of refractive index).

The temperature of the air in the open path of this cell was measured by four PRTs spaced at suitable distances apart close to the laser beam path. Shields were used to prevent direct draughts from the room and results indicated that even when the laboratory temperature was changing at a rate of 1 $^{o}$C an hour, the gradients measured across the volume of the outer interferometer path never exceeded 0.1 $^{o}$C and that typically the PRTs would accurately measure the average temperature of the air to a hundredth of a degree centigrade.
(Equivalent to a part in $10^8$ of refractive index)

## 3.6 Thermal Measurement Techniques

When one considers that air is a poor thermal conductor it is not surprising that the results of the study of the thermal homogeneity of the atmosphere indicated that large thermal gradients existed in the laboratory atmosphere, making temperature variations of the air one of the main limitations to precision length measurement in the free atmosphere. Unfortunately as the results of the temperature measurements of the air sample in the refractometer cell indicated, this problem is further complicated by both the very low thermal capacity of the air and the slow thermal response of the suitably accurate temperature measuring sensors available. Thermal sensors are typically 50 times slower in response and exhibit up to 50 times more self heating effect when measuring gases with only natural convection rather than circulating fluids. For example, one manufacturer's data states that a 1.6 mm diameter, 25 mm length standard 100 OHM PRT detector has a self heating characteristic of 0.015 $^{o}$C/mW in water flowing at 1 metre per second. In air with only natural convection this can be between 20 and 40 times greater.

A detector passing a current of 1mA dissipates 0.1 mW of heat at 0$^{o}$C. This will give a self heating effect of 0.6 millidegrees in flowing water and 12-24 millidegrees in naturally circulating air. Thus a reasonable figure for the measuring current for a PRT in a naturally circulating air application would be 0.3 mA. Smaller detectors requiring even less current for the same error level. In spite of the increasing accuracies of flat film devices, thermistors and semiconductor devices, Platinum Resistance Thermometers (LABFACILITY, Middlesex and Eurotherm,

Worthing) still provide the most accurate and stable sensors for measuring temperature. Platinum as a sensing element in a resistance thermometer resists contamination, and is electrically and mechanically stable. The relationship between temperature and resistance is nearly linear and drift and errors associated with normal ageing and use are negligible.

Standard 100 Ω four-lead devices encapsulated in ceramic and manufactured by Sensing Devices Ltd (Merseyside) were chosen for temperature measurement, two of the leads supply the constant current required by the device and two leads for measuring the voltage difference this current generates across the platinum resistance coil eliminating the effect of any lead resistance in the copper leads.

Fifteen of these devices were calibrated against standard thermometers by inserting them down metal tubes immersed in a liquid bath at temperatures of 15, 20 and 25 °C. The results of these calibrations are shown below:

| Temp | Thermometer Corrections °C (all +) | | | | | | | | | | | | | | |
|---|---|---|---|---|---|---|---|---|---|---|---|---|---|---|---|
| oC | 1 | 2 | 3 | 4 | 5 | 6 | 7 | 8 | 9 | 10 | 11 | 12 | 13 | 14 | 15 |
| 15 | .97 | 1.12 | 1.10 | 1.15 | 1.16 | 1.10 | 1.04 | 1.33 | 1.06 | 1.14 | 1.11 | 1.07 | 1.06 | 1.13 | 1.38 |
| 20 | .98 | 1.13 | 1.11 | 1.15 | 1.16 | 1.10 | 1.04 | 1.33 | 1.07 | 1.15 | 1.11 | 1.08 | 1.07 | 1.13 | 1.37 |
| 25 | .99 | 1.13 | 1.12 | 1.15 | 1.17 | 1.11 | 1.04 | 1.34 | 1.07 | 1.16 | 1.11 | 1.08 | 1.07 | 1.14 | 1.38 |

The PRTs were switched via a suitably high quality multiway switch into a common display unit.

In order to provide a portable system for monitoring and checking the accuracy of the PRTs in the laboratory at Southampton University, two 0.01 °C Mercury in glass thremometers with a temperature range of 18 to 24 °C were calibrated for both horizontal and vertical use and installed in the lagged enclosures shown in Figure 10. These purpose built

enclosures had 50 mm thick insulating foam on the insides of all the walls and a triple glazed viewing panel. The temperatures measured by these thermometers were always found to agree to better than ± 0.02 degree centigrade with the temperatures measured by PRTs inserted through a small hole in the enclosure and attached to the thermometer bulb. The calibration tables for the two mercury in glass thermometers for both vertical and horizontal use are shown below:

| THERMOMETER READING °C | REQUIRED CORRECTION TO THERMOMETER READING °C | | CORRECT TEMPERATURE (VERTICAL) |
|---|---|---|---|
| | VERTICAL | HORIZONTAL | |
| 17.980 | - 0.022 | - 0.049 | 17.958 °C |
| 18.506 | - 0.026 | - 0.057 | |
| 19.008 | - 0.030 | - 0.065 | |
| 19.508 | - 0.028 | - 0.067 | |
| 20.006 | - 0.022 | - 0.064 | |
| 20.496 | - 0.018 | - 0.064 | |
| 21.034 | - 0.022 | - 0.072 | |
| 21.496 | - 0.026 | - 0.079 | |
| 21.998 | - 0.022 | - 0.079 | |
| 22.508 | - 0.022 | - 0.083 | |
| 22.990 | - 0.028 | - 0.092 | |
| 23.516 | - 0.024 | - 0.092 | |
| 24.004 | - 0.018 | - 0.090 | |

TOTAL UNCERTAINTY ± 0.005 °C
AMBIENT BAROMETRIC PRESSURE 996 MILLIBAR
THERMAL REFERENCE 2048 NPL 84

| | | | |
|---|---|---|---|
| 17.982 | - 0.024 | - 0.053 | 17.958 °C |
| 18.506 | - 0.024 | - 0.057 | |
| 19.000 | - 0.022 | - 0.058 | |
| 19.502 | - 0.022 | - 0.062 | |
| 20.004 | - 0.020 | - 0.063 | |
| 20.500 | - 0.024 | - 0.071 | |
| 21.036 | - 0.024 | - 0.074 | |
| 21.494 | - 0.024 | - 0.078 | |
| 22.00 | - 0.022 | - 0.079 | |
| 22.512 | - 0.026 | - 0.087 | |
| 22.988 | - 0.026 | - 0.090 | |
| 23.516 | - 0.022 | - 0.090 | |
| 24.006 | - 0.022 | - 0.094 | |

TOTAL UNCERTAINTY ± 0.005 °C
AMBIENT BAROMETRIC PRESSURE 996 MILLIBAR
THERMOMETER REFERENCE 2051 NPL 84

This technique provided a continuous check on the temperature measurement system as, for example, failure of either the PRTs and their associated electronics or the mercury sticking in the thermometer column would result in a fundamental disagreement between the two measured

temperatures. The PRT electronics could have been tested using a standard resistance however, the comparison of two completely independent temperature measuring systems was considered to be a more comprehensive test. The absolute temperature provided by the PRTs was required to calculate a value for the refractive index of the atmosphere to check against the measured value obtained from the refractometer. However it was recognised at the outset that once it was confirmed that the refractometer was measuring the correct value it would no longer be necessary to have an absolute temperature measurement and that an accurate differential temperature measurement between the air in the measurement path of the length interferometer and the specimen in the refractometer would allow a suitable correction to be applied to the measured refractive index value.

The measurement of differential temperature has the distinct advantages that self heating effects ideally cancel out and the effects of thermal response delays are minimised. A ten junction copper constantan thermopile was constructed to perform the required differential temperature measurement. These devices are mechanically robust and do not require a reference junction when used in a differential mode. They also work directly into a sensitive digital voltmeter (1 μV) and do not require calibration as tables are readily available for thermocouple outputs as shown below:

COPPER CONSTANTAN THERMOCOUPLE

| DIFFERENCE TEMPERATURE $^{o}C$ | OUTPUT PER JUNCTION (mV) | OUTPUT 10 JUNCTION (mV) | OUTPUT THERMOPILE (μV) |
|---|---|---|---|
| - 5 | - 0.193 | - 1.93 | - 1930 |
| - 4 | - 0.154 | - 1.54 | - 1540 |
| - 3 | - 0.116 | - 1.16 | - 1160 |
| - 2 | - 0.077 | - 0.77 | - 770 |
| - 1 | - 0.039 | - 0.39 | - 390 |
| 0 | 0 | 0 | 0 |
| 1 | 0.039 | 0.39 | 390 |
| 2 | 0.078 | 0.78 | 780 |
| 3 | 0.117 | 1.17 | 1170 |
| 4 | 0.156 | 1.56 | 1560 |
| 5 | 0.195 | 1.95 | 1950 |

(For a 10 junction thermopile 0.01 $^{o}C$ = 3.9 μV)

The only real disadvantage of using a thermopile is its slow thermal response. However, provided the two temperatures being compared are changing at the same rate, the response errors cancel out between identical sensors. The results of a comparison between a PRT and thermopile are shown below:

PERFORMANCE RESULTS FOR TWO IDENTICAL THERMOPILES (I and II)

| | TEMPERATURE DIFFERENCE | | THERMOPILE CONFIGURATION |
|---|---|---|---|
| | μv | °C | |
| (a) | I - 4 | - 0.010 | Both junctions taped together and |
| | II + 6 | + 0.015 | inserted in the same position in |
| | | ------- | a foam block |
| | II - I = | 0.025 | |
| (b) | I - 15 | - 0.387 | One junction of each pile taped together |
| | II - 161 | - 0.413 | and inserted in two different foam |
| | | ------- | blocks |
| | II - I = | 0.026 | |
| (c) | I - 203 | - 0.521 | As for (b) |
| | II - 210 | - 0.538 | |
| | | ------- | |
| | II - I = | 0.027 | |
| (d) | I - 2012 | - 5.159 | One pair of junctions heated by hand and |
| | II - 2015 | - 5.167 | reinserted into block together with a PRT |
| | | ------- | (PRT temperature difference 5.18 °C) |
| | II - I = | 0.008 | |
| (e) | I + 2322 | + 5.954 | As for (d) but other junction heated |
| | II + 2316 | + 5.938 | |
| | | ------- | |
| | II - I = | - 0.016 | (PRT temperature difference + 5.96 °C) |

The results indicated that the thermopiles would achieve accuracies of a few hundredths of a degree centigrade in differential temperature measurement providing a valuable alternative measuring technique in this application.

In order to assess the magnitude of the problems caused by the dynamic response of the temperature sensors in air with only natural convection, an electrical model was developed. (Appendix VII)

The model predicted the cooling curve of a temperature sensor to be an

exponential function of the simple form:

$$\phi_t = \theta + (\phi_o - \theta)e^{-t/\tau}$$

where $\theta$ = air temperature

$\phi$ = sensor temperature at time t ($\phi_o$ at t = 0)

t = time

$\tau$ = response time of the sensor

It was found experimentally that the cooling curve of a temperature sensor was indeed an exponential function of this simple form justifying the assumption of the simple model and its electrical equivalent. The model may be used with confidence to predict the temperature response behaviour in situations of changing air temperature knowing the thermal history of the device [Dantzig, 1985].

Experimental results were obtained using a hair-dryer as a heat source to raise the temperature of the sensors about 20 $^{o}$C above ambient and then timing their cooling rates using a stop watch. The results obtained from both PTRs and thermopiles are shown graphically in figures 11 and 12.
These readings are the means of measurements from two identical devices and two runs for each. The computer fitted exponential functions shown graphically in Figures 13 and 14 gave $\tau$ values of 22 and 170 seconds for the PRTs and thermopiles respectively.

It can be shown that when the air temperature is changing at a constant rate the sensor is in error by a constant E where

$$E = \phi_t - \theta_t = \frac{d\theta}{dt}\tau .$$

As can be seen from the results from the PRTs, when the temperature is changing at 1 $^{o}$C per hour and $\tau$ = 22 seconds, the steady state response error E assuming a constant temperature rise is given by

$$E = \frac{1\ ^{o}C \times 22secs}{3600\ secs} = \underline{0.006\ ^{o}C}$$

The results also show why it was not possible to achieve accurate temperature measurements with a dual compartment cell in an uncontrolled environment where a rate of change of temperature of the air specimen of 0.5$^{o}$C per minute was typical.

It may have been possible to differentiate the output of the sensor and

feed this differential signal into an amplifier with a time constant equal to the response function of the sensor, enabling a correction to be applied to the sensor. However, as described, the different sampling technique for the air specimen when using an open path cell circumvented this requirement.

In order to assess the thermal response characteristics of material cooling rates in the atmosphere to assist in the design of both refractometer cells and scales, three identical sized bars of silica, stainless steel and duralumin were also measured. The results for these materials are shown in Figures 15 - 22 and the response functions listed below indicate that the cooling rates are almost directly proportional to their thermal capacitances as is shown by the agreement between the ratios of their $\tau$ functions and thermal capacitances.

| MATERIAL | THERMAL CAPACITANCE ($J\ cm^{-3}\ ^{o}C^{-1}$) | NORMALISED | $\tau$SECONDS | NORMALISED |
|---|---|---|---|---|
| Silica (fused) | 1.85 | 1.00 | 376 | 1.00 |
| Aluminium | 2.52 | 1.36 | 496 | 1.32 |
| Stainless steel | 3.98 | 2.15 | 819 | 2.18 |

| MATERIAL | THERMAL CONDUCTIVITY ($Wm^{-1}\ K^{-1}$) |
|---|---|
| Silica (fused) | 1.33 |
| Aluminium | 236 |
| Stainless Steel | 24.5 |

This relationship with thermal capacitance and insensitivity to thermal conductivity would only apply to thin bars where the heat transfer characteristics within the material are faster than the thermal response function in a particular application.

These measurements indicate that aluminium with its high thermal conductivity and low thermal capacitance would be a better choice thermally for constructing the body of a refractometer cell than stainless steel, however as the results of the study of physisorption in this thesis underline (paper appended) it is vitally important to polish the surfaces of the refractometer cell to achieve the smoothest possible

finish and minimise water adsorption problems.

Depending upon the area of surface exposed to the atmosphere approximate calculations could be made for the thermal response characteristics of a component, and as the results obtained with the silica and aluminium bars lying flat on a foam block indicate (Figures 21 and 22), care must be taken where there is a possibility of a restricted circulation or even stagnation of the surrounding air.

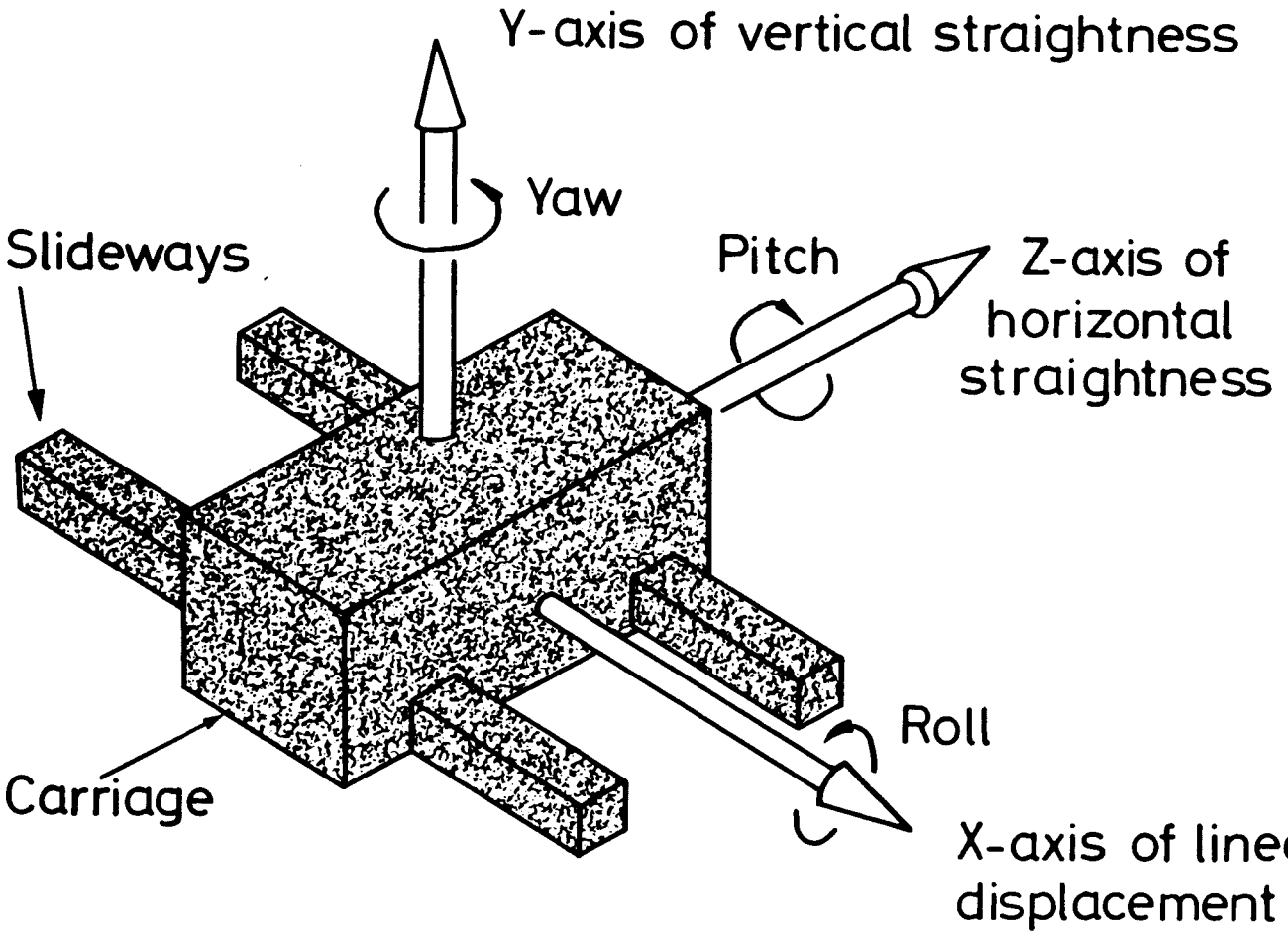


The six degrees of freedom of a single axis positioning system

(CH3 FIG 1)

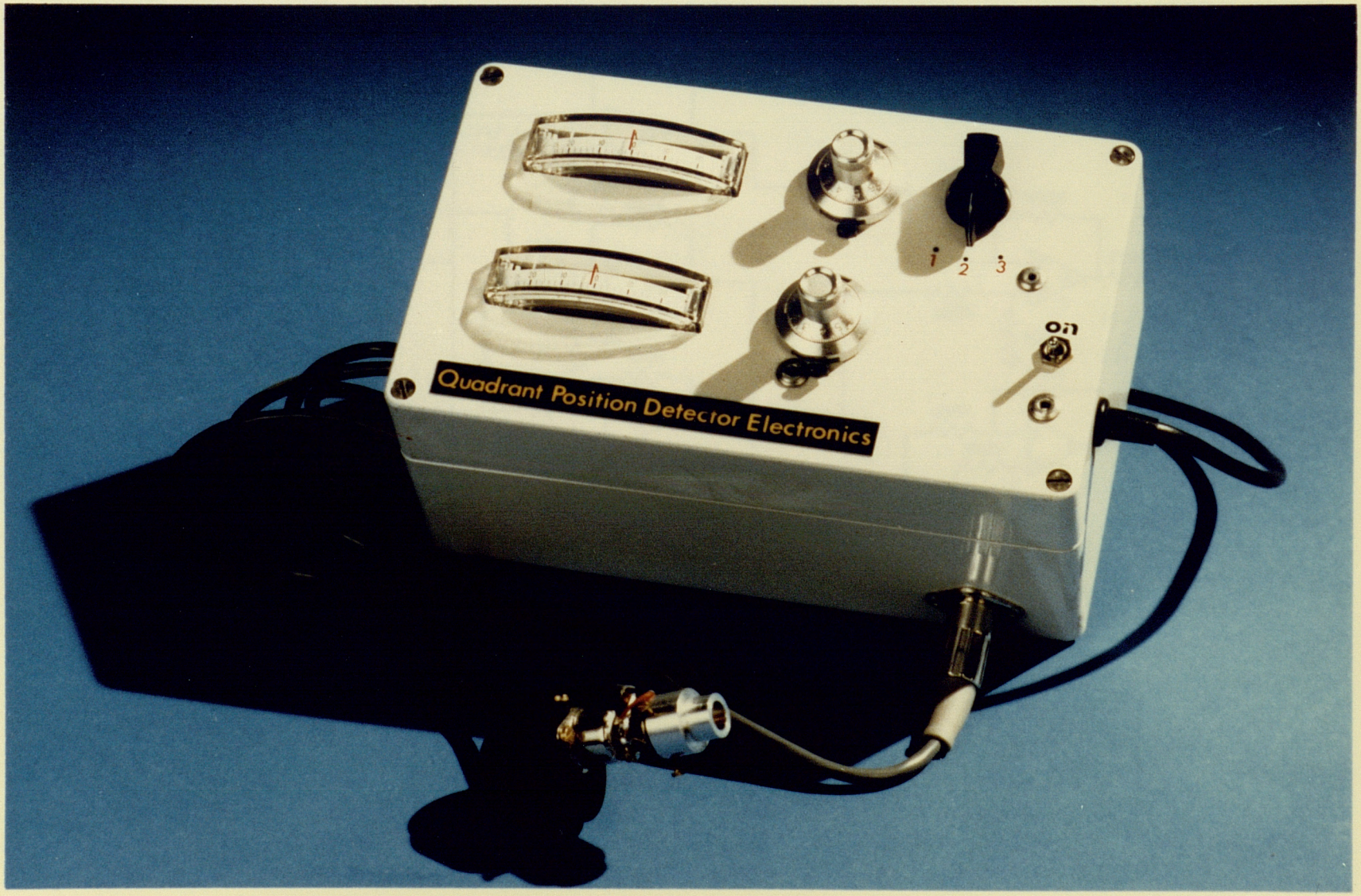


TRACKING ALIGNMENT CELL
(CH3 FIG 2)

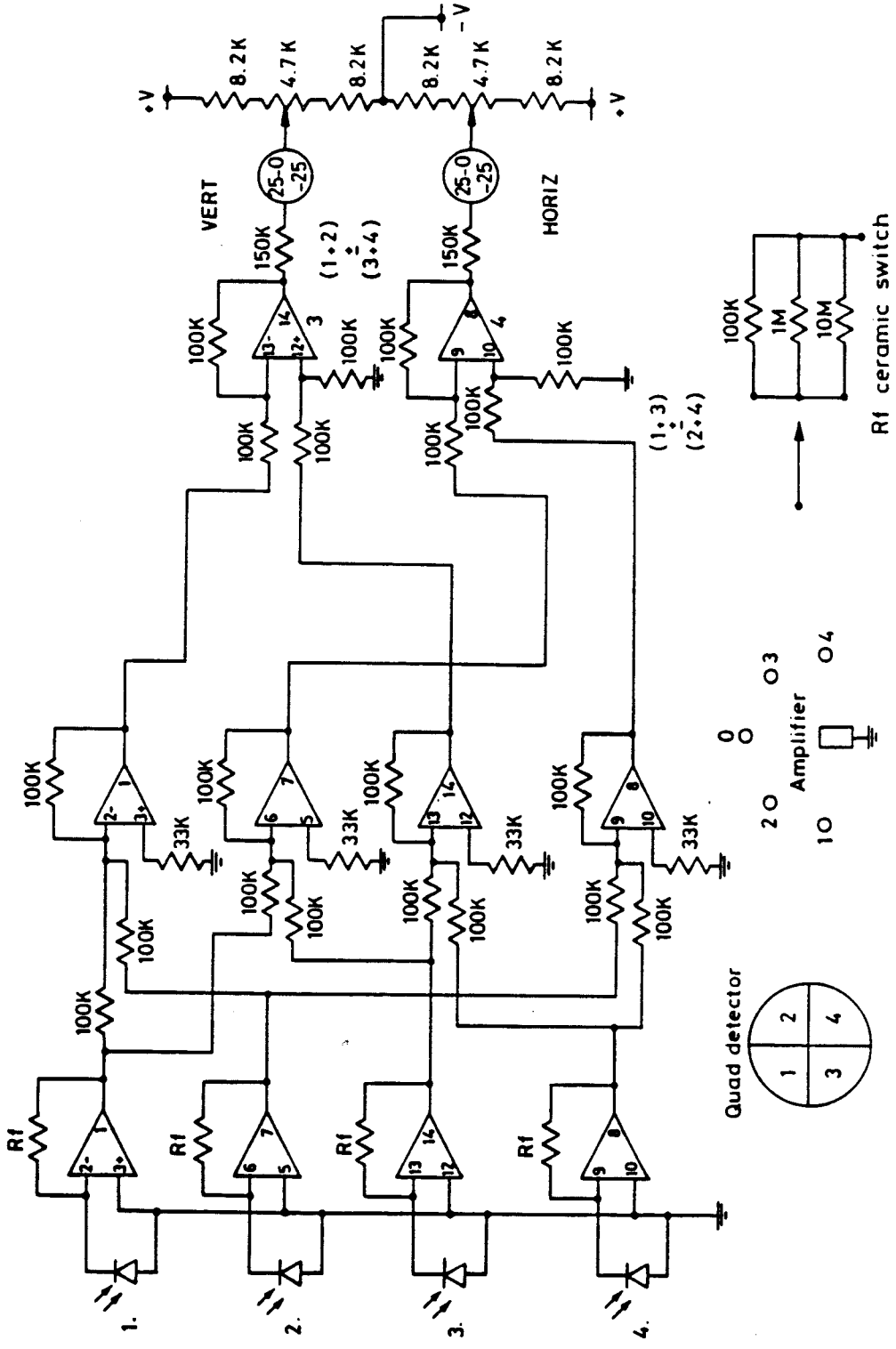


Quadrant photodetector drive circuit

(CH 3 FIG 3)

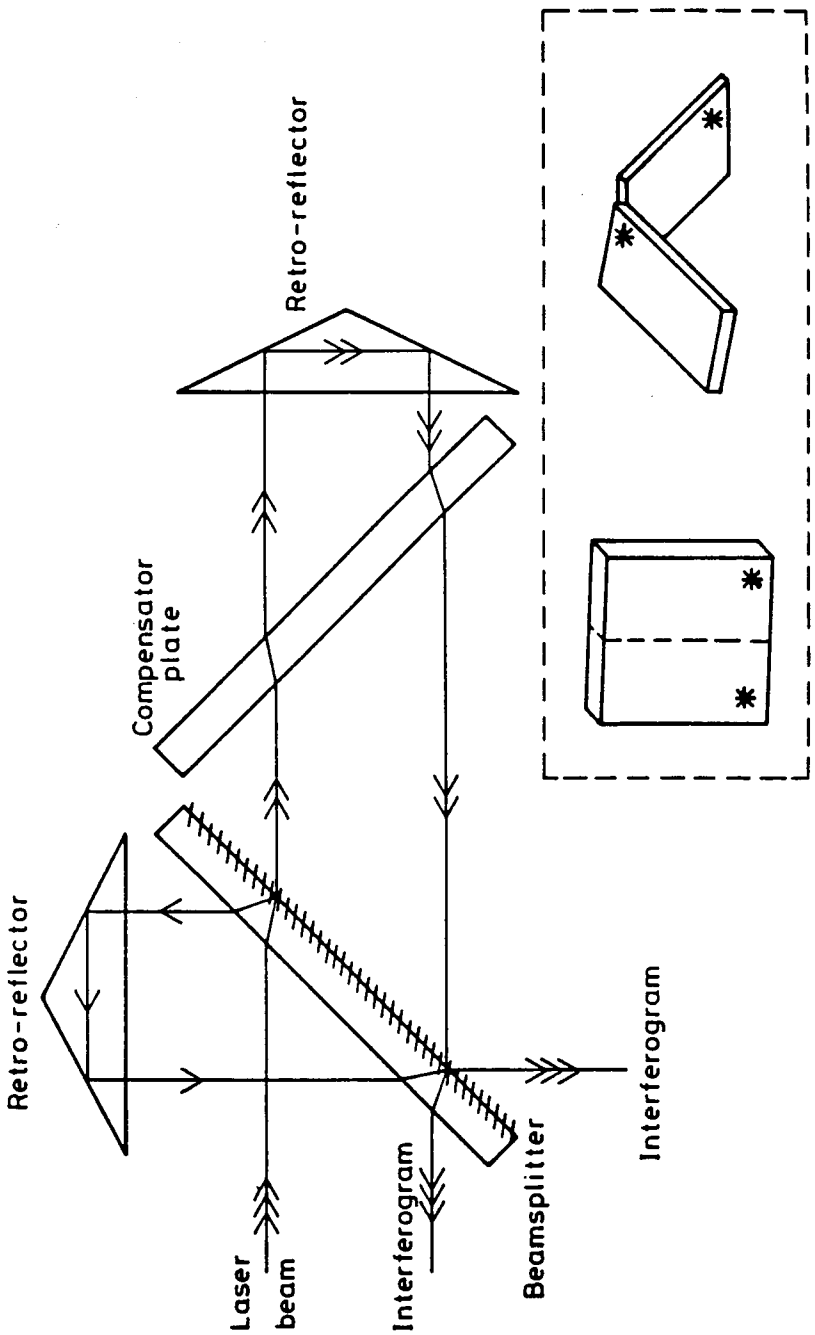


Michelson interferometer with compensator plate
(CH 3 FIG 4)

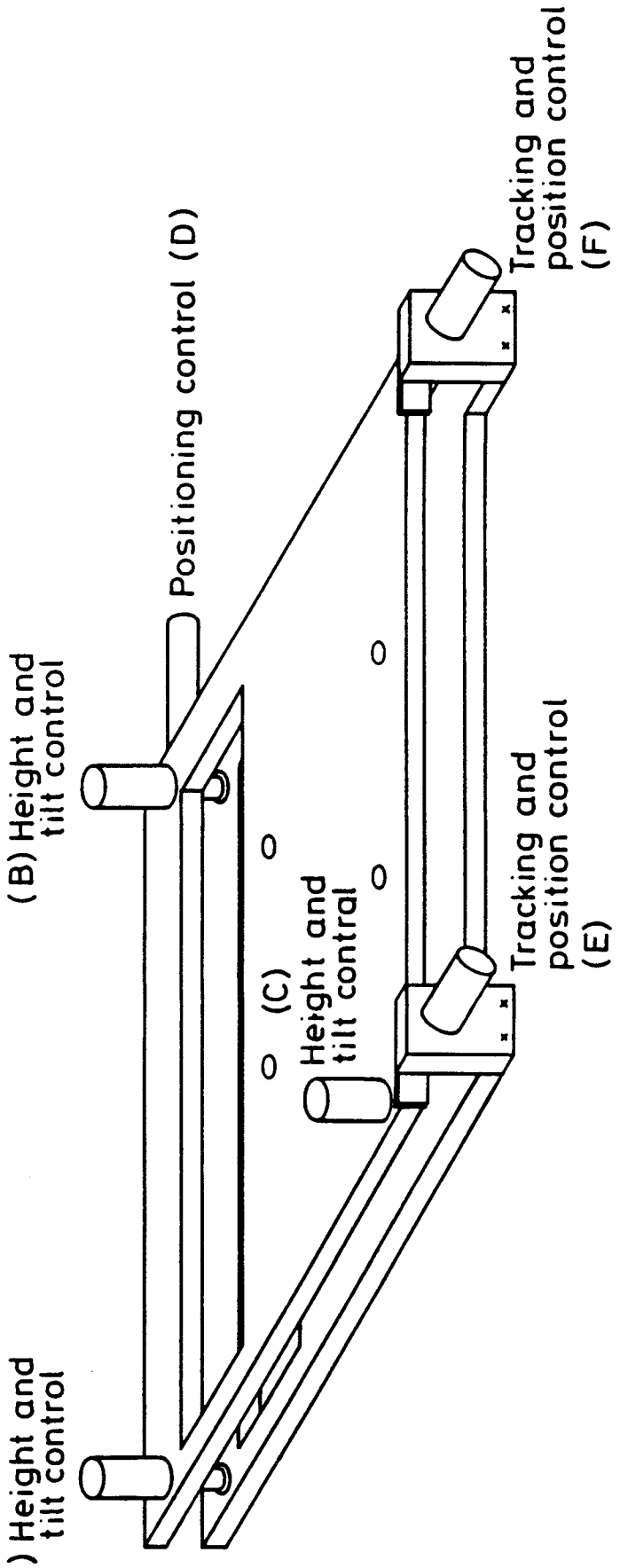


Substrate positioning stage

(CH 3 FIG 5)

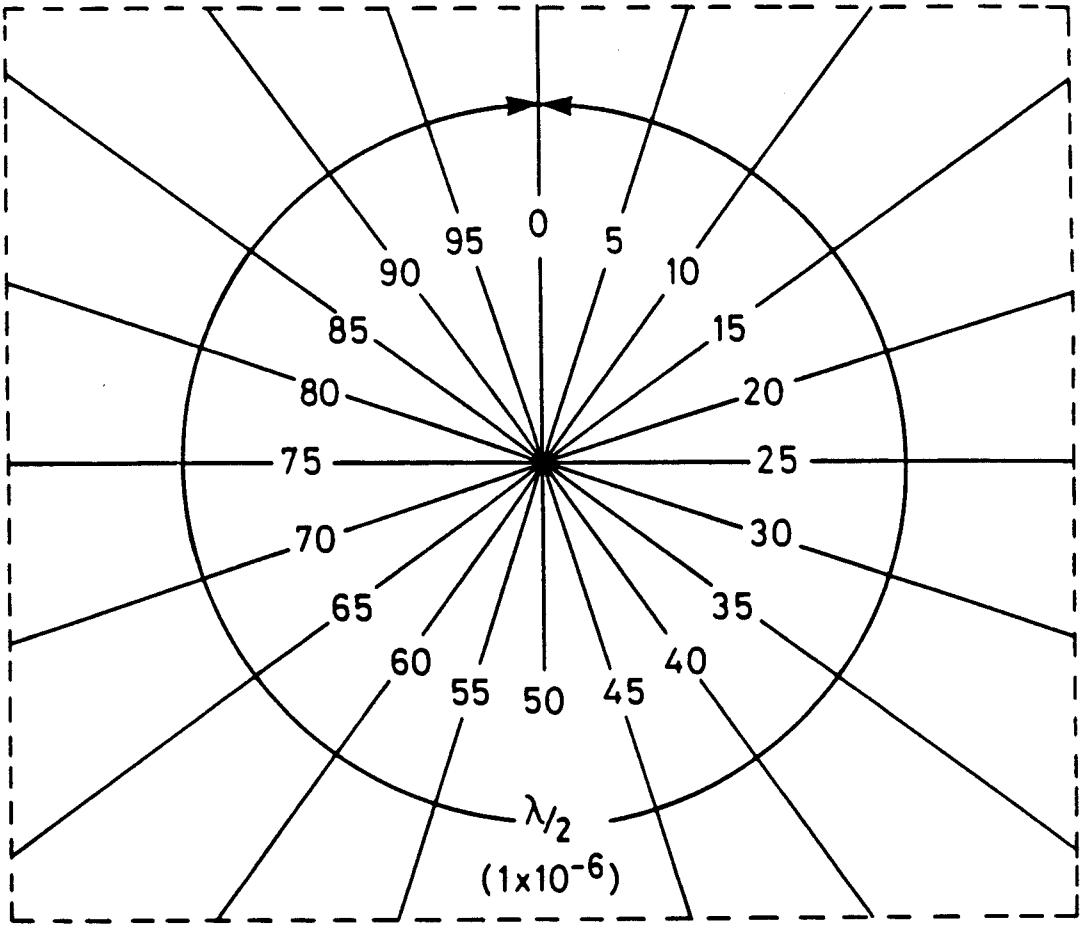


Fringe fractioning
air refractometer
(CH3 FIG 6)

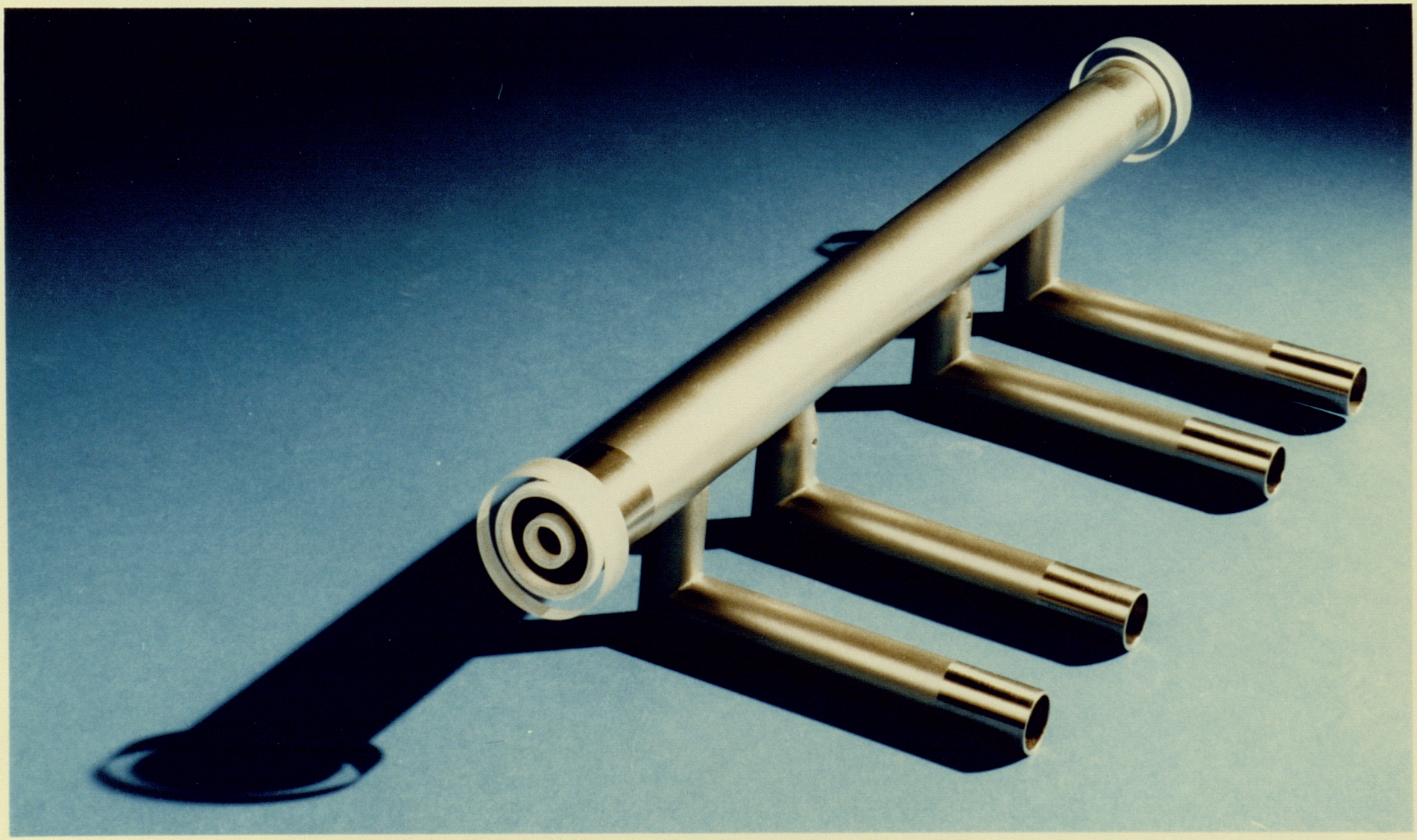

DOUBLE COMPARTMENT CELL
(CH3 FIG 7)

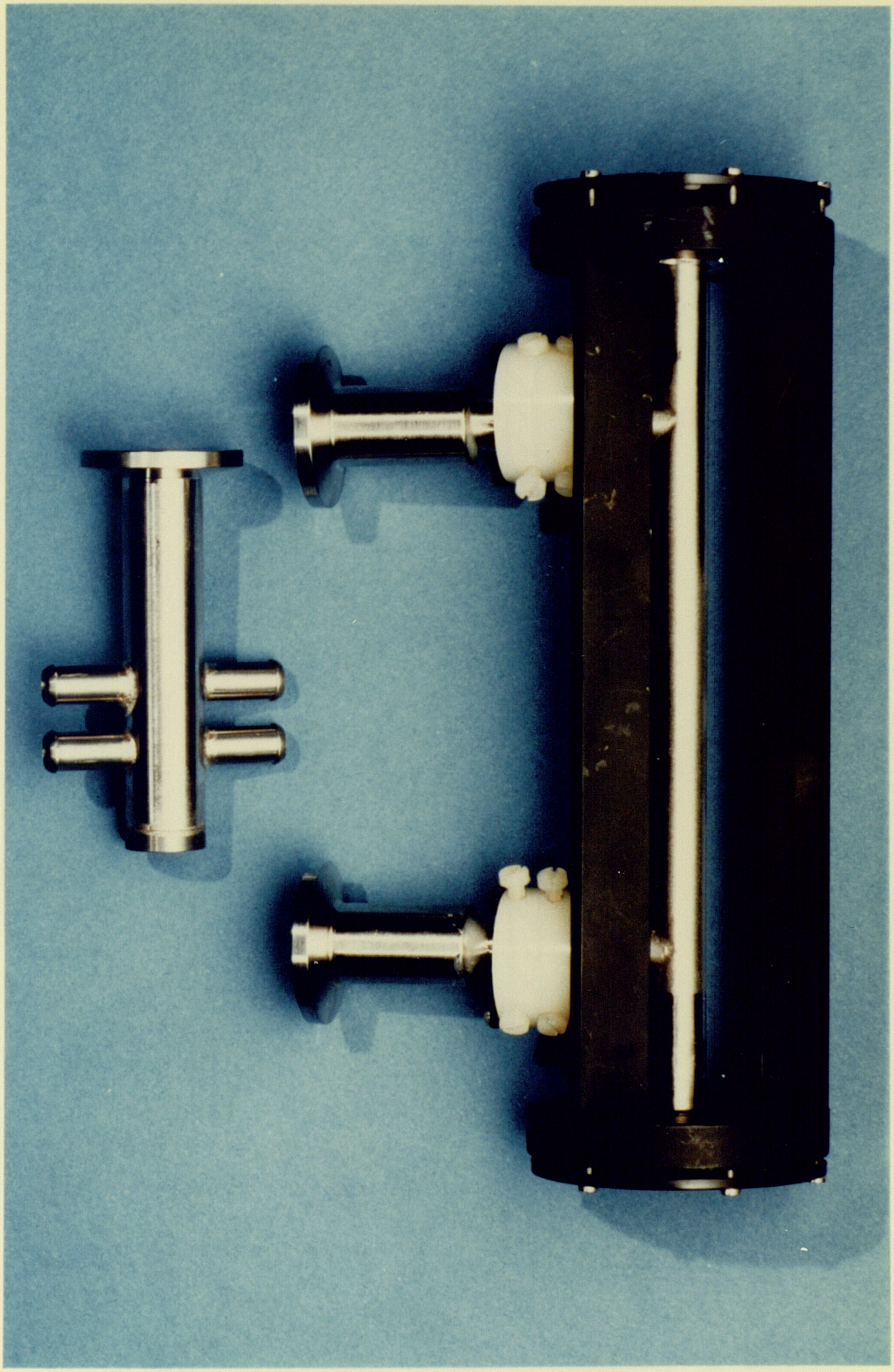

SINGLE COMPARTMENT CELL
(CH3 FIG 8)

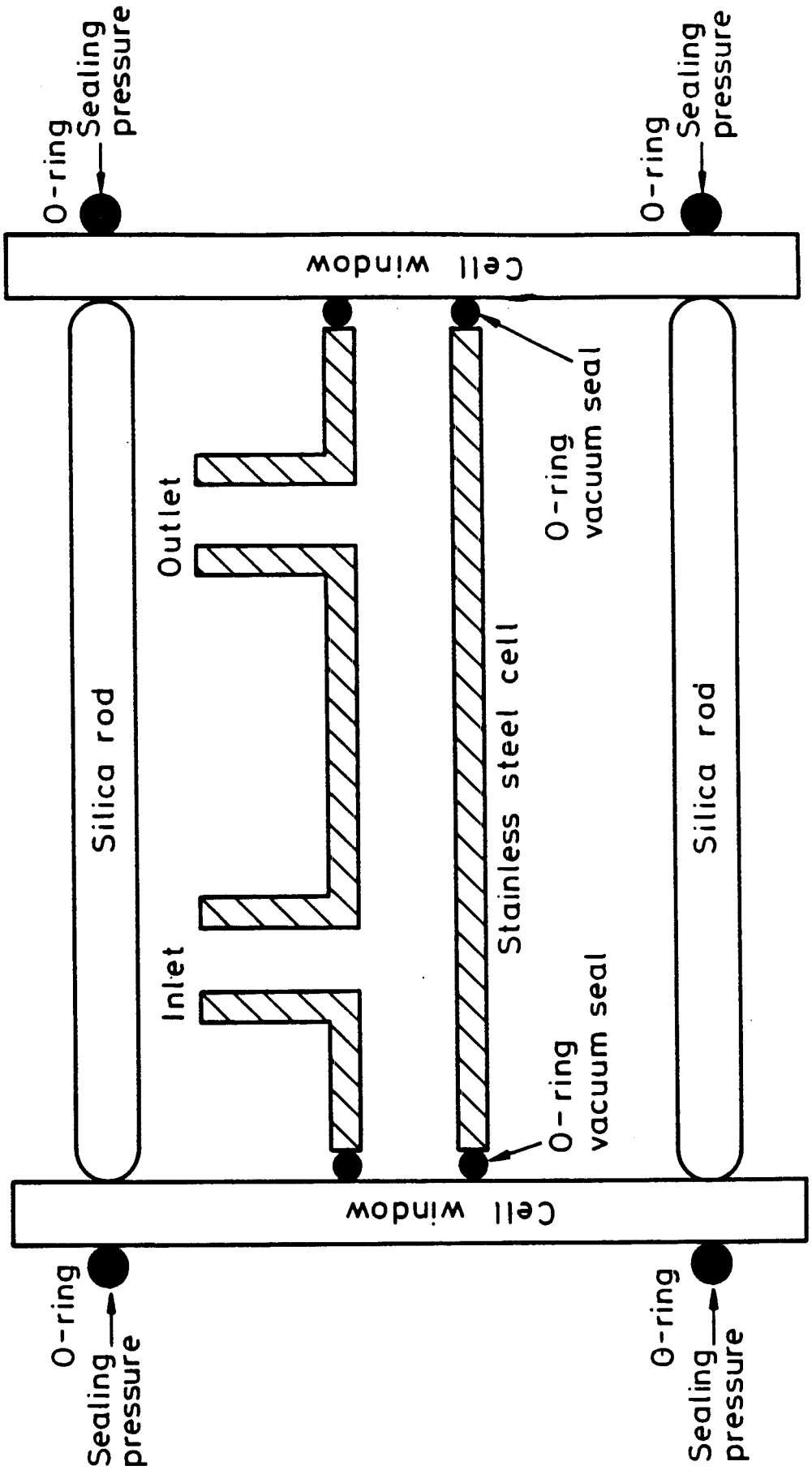


Air refractometer cell
(CH3 FIG 9)

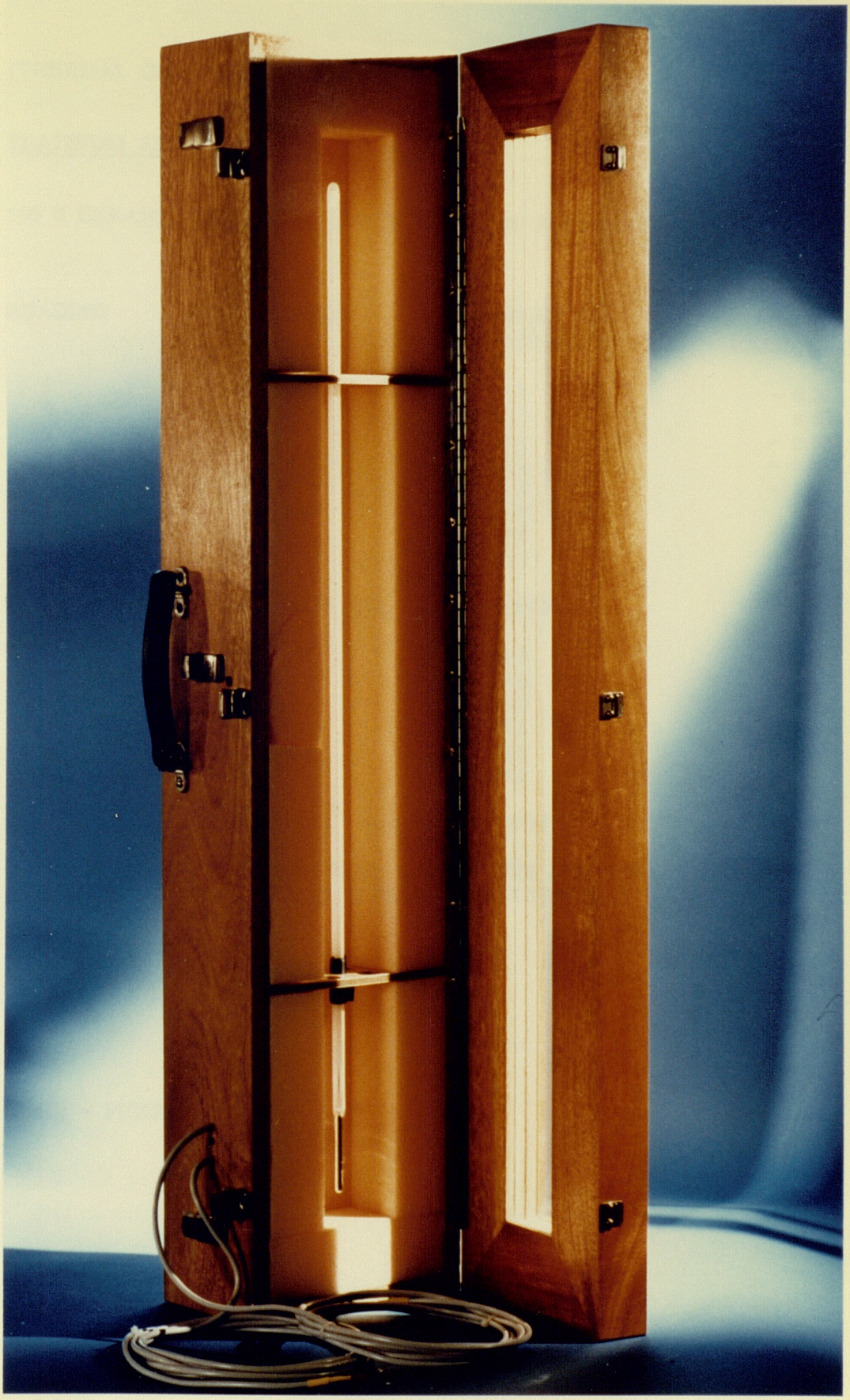

THERMOMETER ENCLOSURE
(CH3 FIG 10)

(THERMAL CHARACTERISTIC $y = Ke^{-t/\tau} + C$)

PLATINUM RESISTANCE THERMOMETER

100 Ω CERAMIC ENCAPSULATED (0.2 mm outer diameter 10 mm Long)

| READING | TIME SECONDS | TEMPERATURE DIFFERENCE °C | OBSERVED - CALCULATED °C |
|---|---|---|---|
| 1 | 0 | 15.3 | - 0.28 |
| 2 | 9 | 11.3 | 0.60 |
| 3 | 21 | 6.3 | - 0.18 |
| 4 | 36 | 3.3 | - 0.15 |
| 5 | 44 | 2.3 | - 0.16 |
| 6 | 59 | 1.3 | 0 |
| 7 | 71 | 0.8 | 0.03 |
| 8 | 105 | 0.3 | 0.15 |

K = 15.6 $\tau$ = 24 secs C = - 0.05

| | | | |
|---|---|---|---|
| 3 | 21 | 6.3 | 0 |
| 4 | 36 | 3.3 | 0.02 |
| 5 | 44 | 2.3 | - 0.04 |
| 6 | 59 | 1.3 | 0.03 |
| 7 | 71 | 0.8 | - 0.01 |
| 8 | 105 | 0.3 | 0 |

K = 15.8 $\tau$ = 22 secs C = 0.17

'STEADY STATE' TEMPERATURE ERROR DUE TO THERMAL RESPONSE IN AN ATMOSPHERE CHANGING AT A CONSTANT RATE OF 1 °C PER HOUR.

$$= \frac{1}{3600} \times 22 = 0.006 \text{ °C}$$

---

(CH 3 - FIGURE 11)

(THERMAL CHARACTERISTIC $y = Ke^{-t/\tau} + C$)

COPPER/CONSTANTAN THERMOPILE

10 JUNCTION USED IN DIFFERENTIAL TEMPERATURE MODE NO REFERENCE JUNCTION REQUIRED

ENCAPSULATED IN A STAINLESS STEEL TUBE 6 mm OUTER DIAM 0.5 mm wall thickness and 25 mm long.

| READING | TIME SECONDS | TEMPERATURE DIFFERENCE °C | OBSERVED - CALCULATED °C |
|---|---|---|---|
| 1 | 0 | 16.3 | - 0.06 |
| 2 | 16 | 15.0 | 0.12 |
| 3 | 30 | 13.8 | 0.03 |
| 4 | 46 | 12.5 | - 0.03 |
| 5 | 64 | 11.3 | - 0.05 |
| 6 | 85 | 10.0 | - 0.03 |
| 7 | 108 | 8.8 | - 0.05 |
| 8 | 136 | 7.5 | - 0.01 |
| 9 | 168 | 6.3 | - 0.02 |
| 10 | 210 | 5.0 | 0.05 |
| 11 | 265 | 3.8 | 0.09 |
| 12 | 335 | 2.5 | 0 |
| 13 | 465 | 1.3 | - 0.04 |
| 14 | 622 | 0.6 | - 0.01 |

$K = 16.1$ $\tau = 172.0$ secs $C = 0.21$

'STEADY STATE' TEMPERATURE ERROR DUE TO THERMAL RESPONSE IN AN ATMOSPHERE CHANGING AT A CONSTANT RATE OF 1 °C/HOUR.

$$= \frac{1}{3600} \times 172.0 = 0.048 \text{ °C}$$

---

(CHAPTER 3 FIGURE 12)

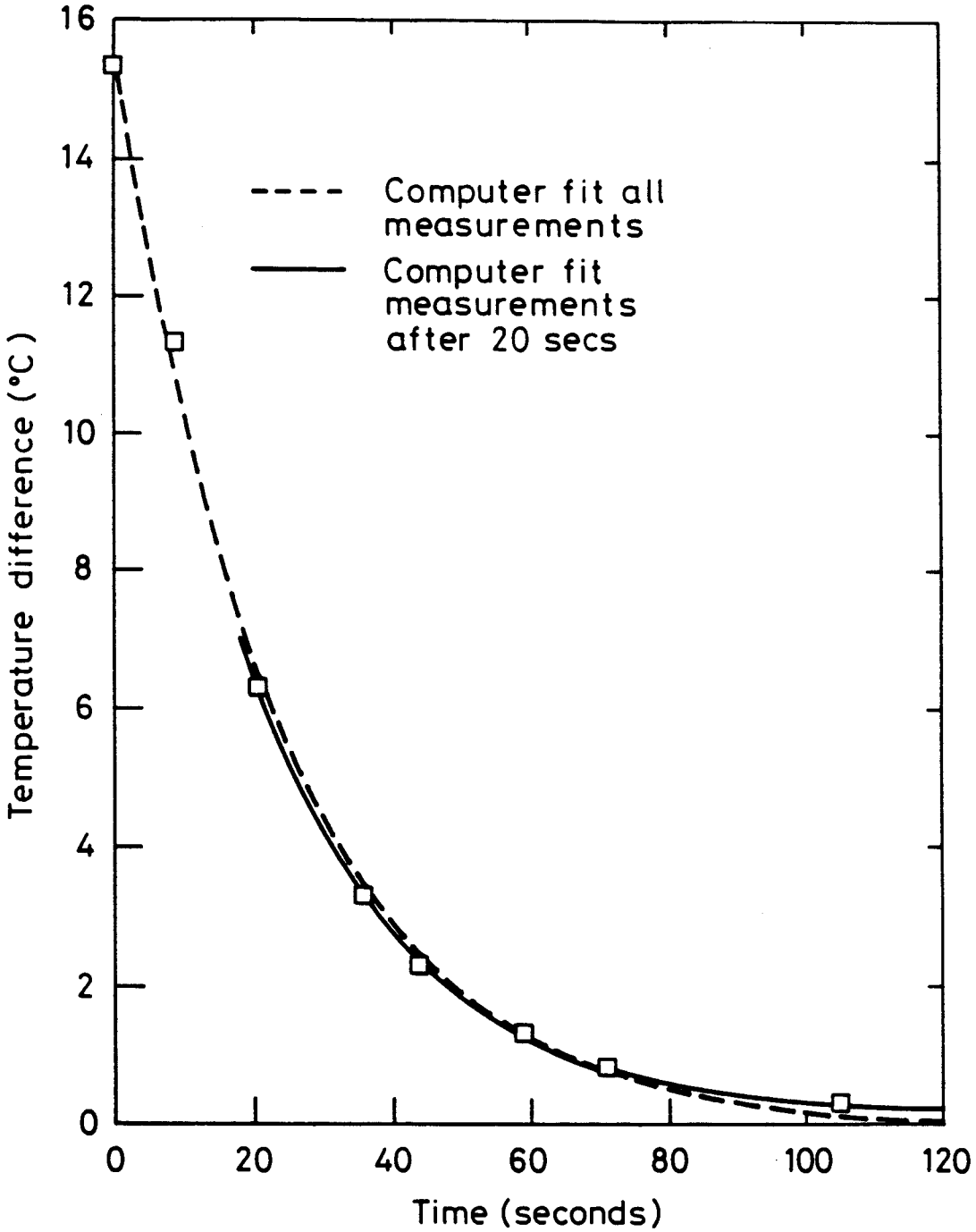


Thermal response characteristic of a platinum resistance thermometer ( in air )

(CH3 FIG 13)

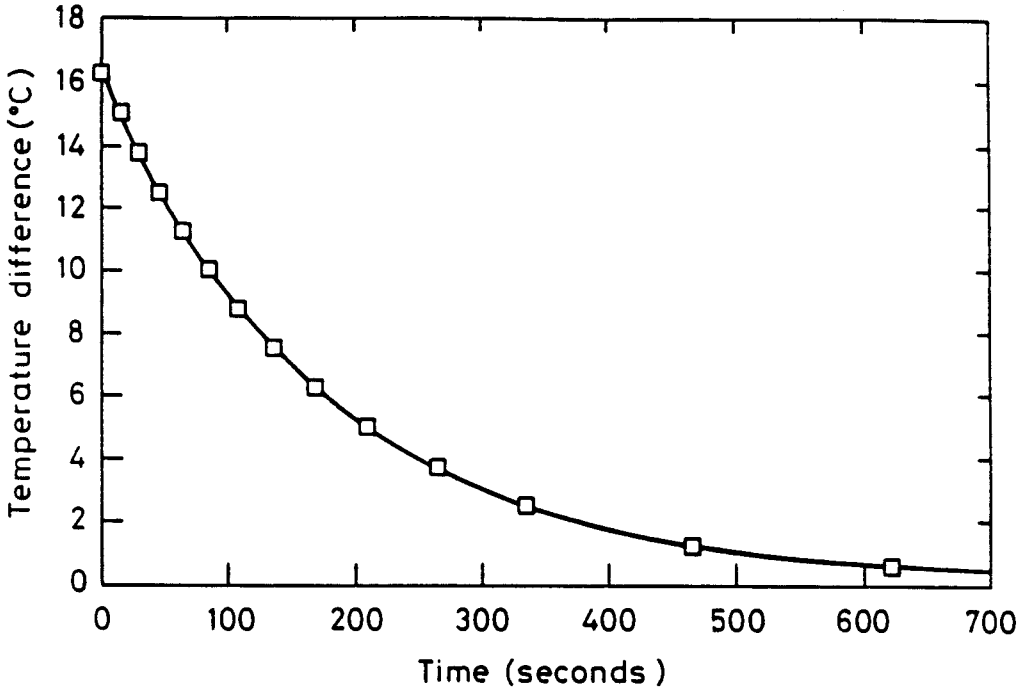


Thermal response characteristic of a copper/constantan thermop ile ( in air )

(CH 3 FIG 14)

(THERMAL CHARACTERISTIC $y = Ke^{-t/\tau} + C$)

SILICA

POLISHED BAR 160 × 25 × 5 mm (VOLUME 20 ccs)

THERMAL CAPACITY 1.85 J $cm^{-3}$ $^{\circ}C^{-1}$
SURFACE AREA EXPOSED TO ATMOSPHERE 90 sq cms.
THERMAL CONDUCTIVITY 1.33 $Wm^{-1}$ $K^{-1}$

| READING | TIME SECONDS | TEMPERATURE DIFFERENCE °C | OBSERVED - CALCULATED °C |
|---|---|---|---|
| 1 | 0 | 15.4 | 0 |
| 2 | 22 | 14.4 | 0 |
| 3 | 46 | 13.4 | 0 |
| 4 | 71 | 12.4 | 0 |
| 5 | 99 | 11.4 | 0 |
| 6 | 129 | 10.4 | 0 |
| 7 | 162 | 9.4 | 0 |
| 8 | 198 | 8.4 | 0 |
| 9 | 240 | 7.4 | 0 |
| 10 | 289 | 6.4 | 0.1 |
| 11 | 342 | 5.4 | 0.1 |
| 12 | 409 | 4.2 | 0.1 |
| 13 | 492 | 2.8 | - 0.2 |
| 14 | 602 | 1.8 | - 0.1 |
| 15 | 757 | 0.8 | 0.1 |

K = 16.9 $\tau$ = 375.5 secs C = - 1.5

'STEADY STATE' TEMPERATURE ERROR DUE TO THERMAL RESPONSE IN AN ATMOSPHERE CHANGING AT A CONSTANT RATE OF 1 °C/HOUR.

$$= \frac{1}{3600} \times 375.5 \text{ secs} = 0.104\ ^{\circ}C$$

---

CH 3 FIGURE 15

(THERMAL CHARACTERISTIC) $y = Ke^{-t/\tau} + C$

STAINLESS STEEL

LAPPED BAR 160 x 25 x 5 mm (VOLUME 20 ccs)
THERMAL CAPACITY 3.98 J $cm^{-3}$ $^{\circ}C^{-1}$
SURFACE AREA EXPOSED TO ATMOSPHERE 90 sq cms.
THERMAL CONDUCTIVITY 24.5 $Wm^{-1}K^{-1}$

| READING | TIME SECONDS | TEMPERATURE DIFFERENCE °C | OBSERVED - CALCULATED °C |
|---|---|---|---|
| 1 | 0 | 16.7 | - 0.11 |
| 2 | 55 | 15.7 | 0.02 |
| 3 | 113 | 14.7 | 0.06 |
| 4 | 170 | 13.7 | 0.04 |
| 5 | 234 | 12.7 | 0.06 |
| 6 | 301 | 11.7 | 0.05 |
| 7 | 373 | 10.7 | 0.03 |
| 8 | 453 | 9.7 | 0.02 |
| 9 | 540 | 8.7 | - 0.01 |
| 10 | 634 | 7.7 | - 0.07 |
| 11 | 748 | 6.7 | - 0.06 |
| 12 | 883 | 5.7 | - 0.04 |
| 13 | 1042 | 4.7 | - 0.03 |
| 14 | 1258 | 3.7 | - 0.06 |
| 15 | 1542 | 2.6 | 0.01 |
| 16 | 2003 | 1.5 | 0.01 |

K = 16.8 $\tau$ = 819.4 secs C = - 0.03

'STEADY STATE' TEMPERATURE ERROR DUE TO THERMAL RESPONSE IN AN ATMOSPHERE CHANGING AT A CONSTANT RATE OF 1 °C/HOUR.

$$= \frac{1}{3600} \times 819.4 \text{ secs} = 0.228\ ^{\circ}C$$

---

CH3 FIGURE 16

(THERMAL CHARACTERISTIC) $y = Ke^{-t/\tau} + C$

DURALUMIN

LAPPED BAR 160 × 25 × 5 mm (VOLUME 20 ccs)
THERMAL CAPACITY 2.52 J $cm^{-3}$ $^{\circ}C^{-1}$
SURFACE AREA EXPOSED TO ATMOSPHERE 90 sq cms.
THERMAL CONDUCTIVITY 236 $Wm^{-1}$ $K^{-1}$

| READING | TIME SECONDS | TEMPERATURE DIFFERENCE °C | OBSERVED - CALCULATED °C |
|---|---|---|---|
| 1 | 0 | 16.8 | 0.06 |
| 2 | 32 | 15.8 | 0.05 |
| 3 | 65 | 14.8 | 0.01 |
| 4 | 101 | 13.8 | - 0.01 |
| 5 | 140 | 12.8 | - 0.03 |
| 6 | 182 | 11.8 | - 0.06 |
| 7 | 229 | 10.8 | - 0.06 |
| 8 | 280 | 9.8 | - 0.08 |
| 9 | 340 | 8.8 | - 0.05 |
| 10 | 409 | 7.8 | - 0.01 |
| 11 | 490 | 6.8 | 0.04 |
| 12 | 587 | 5.8 | 0.10 |
| 13 | 704 | 4.8 | 0.12 |
| 14 | 860 | 3.7 | 0.06 |
| 15 | 1074 | 2.6 | - 0.06 |
| 16 | 1456 | 1.6 | - 0.08 |

$K = 15.9$ $\tau = 496.3$ secs $C = 0.83$

'STEADY STATE' TEMPERATURE ERROR DUE TO THERMAL RESPONSE IN AN ATMOSPHERE CHANGING AT A CONSTANT RATE OF 1 °C/HOUR.

$$= \frac{1}{3600} \times 496.3 \text{ secs} = 0.138\ ^{\circ}C$$

---

CH3 FIGURE 17

(THERMAL CHARACTERISTIC) $y = Ke^{-t/\tau} + C$

SILICA

POLISHED BAR 160 × 25 × 5 mm (VOLUME 20 ccs)
SURFACE AREA EXPOSED TO ATMOSPHERE 56 sq cms.
BAR LYING FLAT ON FOAM INSULATING BLOCK.

| READING | TIME SECONDS | TEMPERATURE DIFFERENCE °C | OBSERVED - CALCULATED °C |
|---|---|---|---|
| 1 | 0 | 14.3 | 0.05 |
| 2 | 34 | 13.3 | 0.12 |
| 3 | 70 | 12.0 | - 0.14 |
| 4 | 112 | 11.0 | - 0.02 |
| 5 | 153 | 10.0 | - 0.02 |
| 6 | 198 | 9.0 | - 0.03 |
| 7 | 249 | 8.0 | - 0.01 |
| 8 | 302 | 7.0 | - 0.07 |
| 9 | 365 | 6.0 | - 0.09 |
| 10 | 436 | 5.2 | 0.07 |
| 11 | 521 | 4.3 | 0.13 |
| 12 | 622 | 3.3 | 0.07 |
| 13 | 748 | 2.3 | - 0.03 |
| 14 | 922 | 1.5 | 0.08 |
| 15 | 1166 | 0.5 | - 0.12 |

$K = 14.8$ $\tau = 453.4$ secs $C = -0.51$

'STEADY STATE' TEMPERATURE ERROR DUE TO THERMAL RESPONSE IN AN ATMOSPHERE CHANGING AT A CONSTANT RATE OF 1 °C/HOUR.

$$= \frac{1}{3600} \times 453.4 \text{ secs} = 0.126 \text{ °C}$$

---

CH3 FIGURE 18

(THERMAL CHARACTERISTIC) $y = Ke^{-t/\tau} + C$

DURALUMIN

LAPPED BAR 160 x 25 x 5 mm (VOLUME 20 ccs
SURFACE AREA EXPOSED TO ATMOSPHERE 56 sq cms.
BAR LYING FLAT ON FOAM INSULATING BLOCK.

| READING | TIME SECONDS | TEMPERATURE DIFFERENCE °C | OBSERVED - CALCULATED °C |
|---|---|---|---|
| 1 | 0 | 13.8 | 0.10 |
| 2 | 60 | 12.7 | - 0.03 |
| 3 | 124 | 11.7 | - 0.06 |
| 4 | 193 | 10.7 | - 0.08 |
| 5 | 267 | 9.8 | - 0.02 |
| 6 | 350 | 8.8 | - 0.03 |
| 7 | 441 | 7.8 | - 0.04 |
| 8 | 539 | 7.0 | 0.12 |
| 9 | 649 | 6.0 | 0.08 |
| 10 | 778 | 5.0 | 0.07 |
| 11 | 930 | 4.0 | 0.07 |
| 12 | 1108 | 2.8 | - 0.16 |
| 13 | 1342 | 1.8 | - 0.13 |
| 14 | 1665 | 1.0 | 0.11 |

$K = 15.3$ $\tau = 910.8$ secs $C = -1.56$

'STEADY STATE' TEMPERATURE ERROR DUE TO THERMAL RESPONSE IN AN ATMOSPHERE CHANGING AT A CONSTANT RATE OF 1 °C/HOUR.

$$= \frac{1}{3600} \times 910.8 \text{ secs} = 0.253 \text{ °C}$$

CH3 FIGURE 19

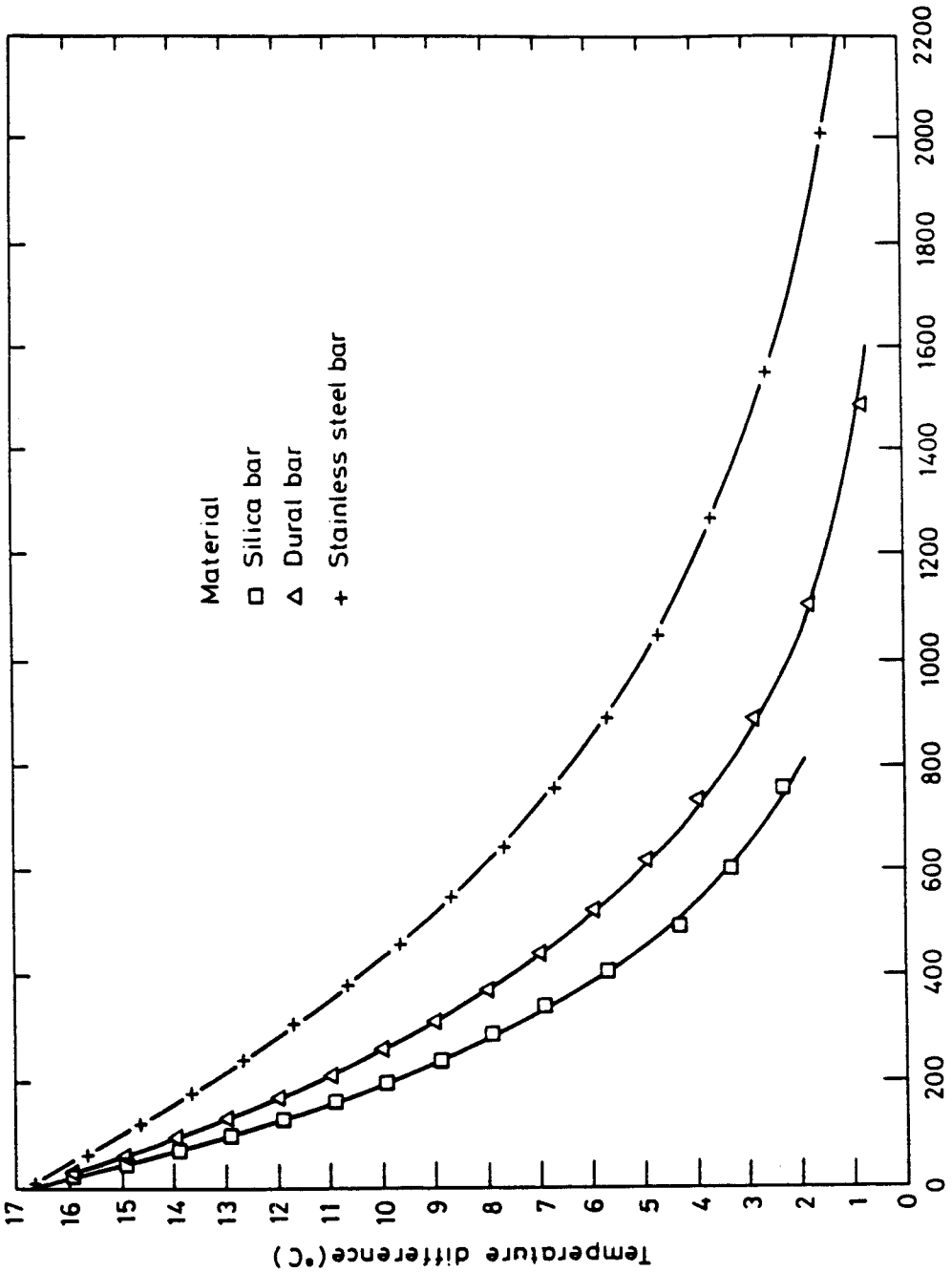


Thermal response characteristic of bar(160x25x5mm)

(CH 3 FIG 20)

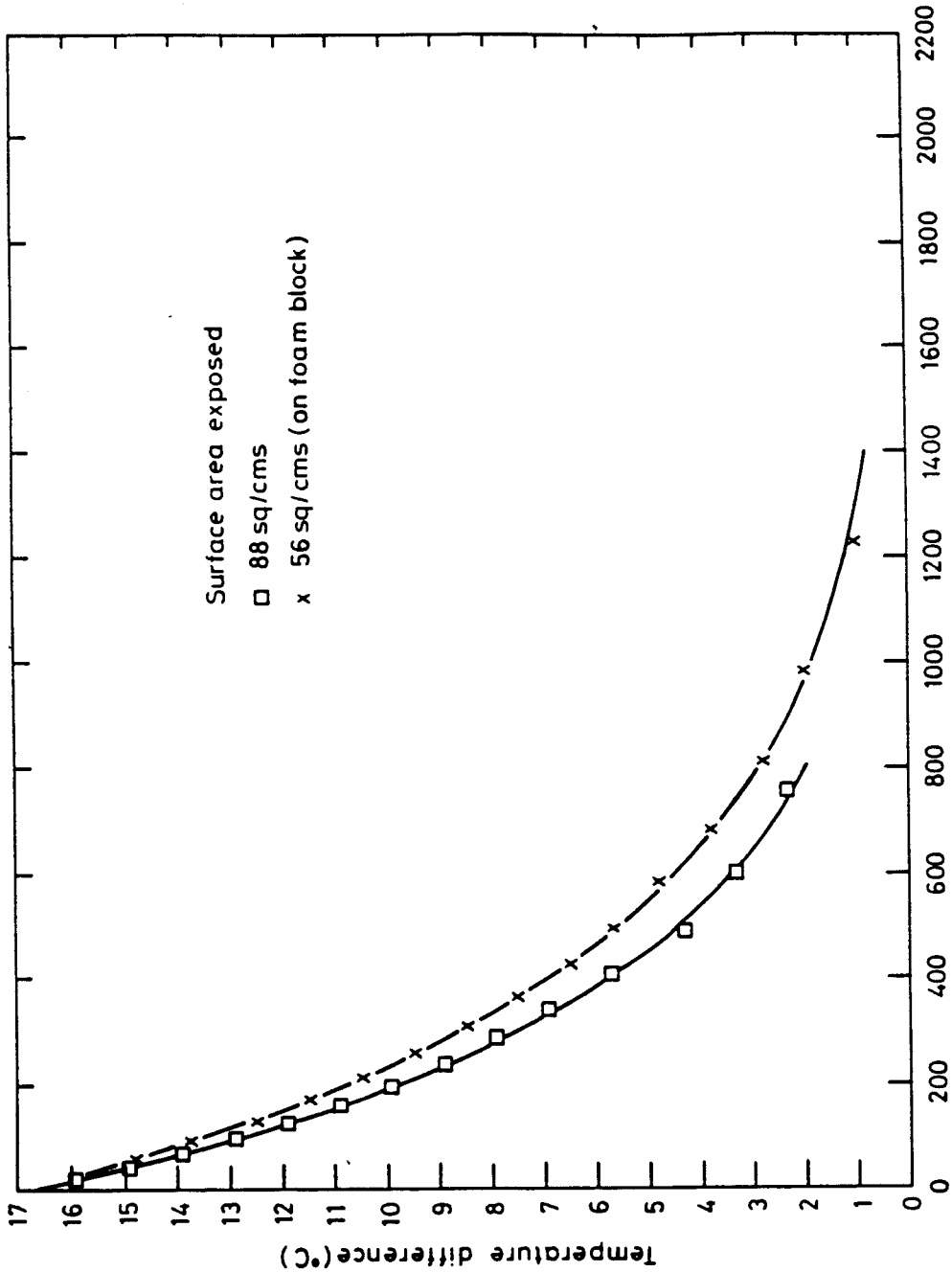


Thermal response characteristic of silica bar
(CH 3 FIG 21)

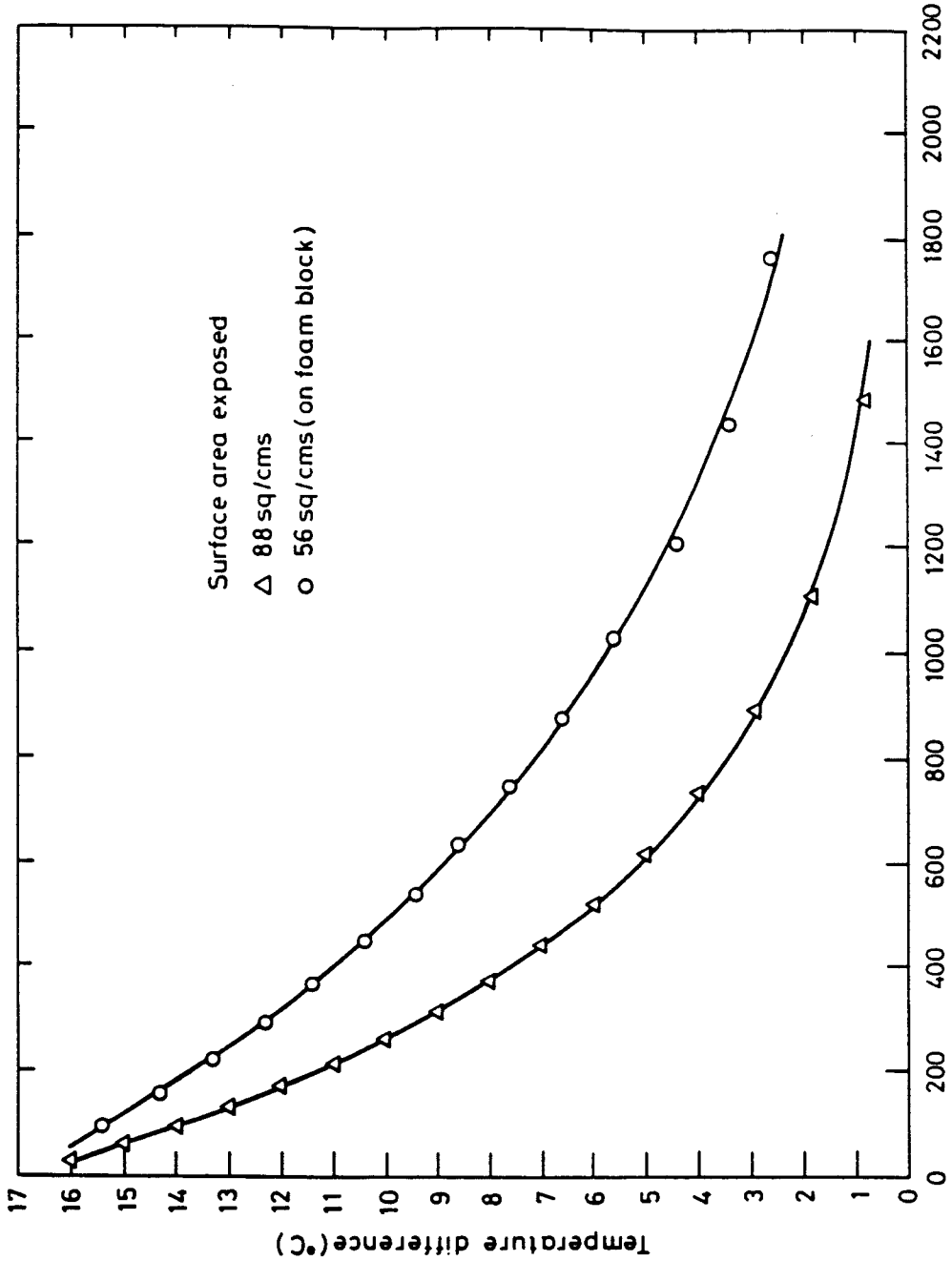


Thermal response characteristic of dural bar

(CH 3 FIG 22)

# CHAPTER IV

## PERFORMANCE AND CALIBRATION

### 4.1 Results of comparisons between measured and calculated values of atmospheric refractive index

The accurate length measurement of the refractometer cell was achieved with two inductance transducers and an accurate end bar. The mechanical configuration for this is shown in Figure 1. The distance between the centres of the cell windows was measured and the sum of the thicknesses of two windows was then subtracted from this value to find the internal cell length. The cell length could be measured using this technique to an accuracy of a few micrometers. A change in length of 10μm in a 316 mm cell being equivalent to a change in refractive index of 1 part in $10^8$. The length of the 158 mm long cells used was calibrated using a Tropel laser rule. The mechanical probe on this instrument has a measurement range of 180 mm with an absolute accuracy of 1 part in $10^6$, the accuracy being limited by the use of an unstabilised laser source in the interferometer system used for measuring the position of the probe. This instrument was also checked using calibrated end bars and measurement repeatabilities of 1 to 2 micrometers were readily achieved. Before assembling the 158 mm demountable cell shown in Chapter III, Figure 9, the three silica spacer rods were measured together with the thicknesses of the windows. An example of the results of these measurements is given below:

| | |
|---|---|
| Rod 1 | 158.247 mm |
| Rod 2 | 158.248 mm |
| Rod 3 | 158.248 mm |
| | |
| Window 1 | 5.093 mm |
| Window 2 | 5.092 mm |

The calculated outside length of the cell was 168.433 mm. The measured outside length was found to be 168.415 mm showing that 6 mm diameter silica rods had been compressed 18 μm by the O-ring sealing pressure. The cell length was measured under vacuum and the length was found to decrease by

a further 2 μm. A change in cell length in a 158 mm cell of 5 μm is equivalent to 1 part in $10^8$ and a correction of + 4 parts in $10^8$ was applied to the measured value of the refractive index to take account of the cell being slightly shorter than the ideal value of 158.2479 mm; which corresponds to one quarter of the vacuum wavelength x $10^6$ and makes 1 fringe of path difference equal to 2 parts in $10^6$ of refractive index.

The results of the comparisons between refractive index of the atmosphere measured directly with the 158 mm stainless steel cell in the refractometer and those calculated using Edlen's equation are shown below:

| DATE | MEASURED - CALCULATED x $10^{-7}$ | TIME (Hours) |
|---|---|---|
| 17.6.86 | 1.4 | 11.00 |
| | 1.6 | 12.00 |
| | 1.7 | 13.00 |
| | 1.8 | 15.00 |
| | 2.0 | 17.00 |
| 26.6.86 | 1.4 | 12.00 |
| 3.7.86 | 1.3 | 10.00 |
| | 1.4 | 11.00 |
| | 1.5 | 12.00 |
| | 2.0 | 16.00 |
| 28.8.86 | 1.3 | 10.00 |
| | 1.5 | 11.00 |
| | 1.4 | 12.00 |
| 11.9.86 | 1.4 | 11.00 |
| 18.9.86 | 1.3 | 10.00 |
| | 1.5 | 11.00 |
| | 1.6 | 12.00 |

The $CO_2$ content of the atmosphere in the laboratory at Southampton was both calculated (Appendix IX) and measured and a $CO_2$ correction of -1 part in $10^8$ per hour for 1 person in the 150 cu metre laboratory applied to the measured results starting at 0900 hours. The results corrected for $CO_2$ are shown below:

| | MEASURED - CALCULATED $CO_2$ corrected x $10^{-7}$ | TIME (hours) |
|---|---|---|
| 17.6.86 | 1.2 | 11.00 |
| | 1.3 | 12.00 |
| | 1.3 | 13.00 |
| | 1.2 | 15.00 |
| | 1.2 | 17.00 |
| 26.6.86 | 1.3 | 12.00 |
| 3.7.86 | 1.3 | 10.00 |
| | 1.2 | 11.00 |
| | 1.2 | 12.00 |
| | 1.2 | 16.00 |
| 28.8.86 | 1.3 | (No $CO_2$ allowed to |
| | 1.2 | develop in Laboratory |
| | 1.4 | by leaving between measurements) |
| 11.9.86 | 1.4 | 11.00 |
| 18.9.86 | 1.3 | 10.00 |
| | 1.5 | 11.00 |
| | 1.6 | 12.00 |
| mean of $CO_2$ corrected measured-calculated | 1.3 x $10^{-7}$ | |

The $CO_2$ corrected results, together with those not requiring correction, gave an average difference between the measured and calculated values of 1.3 x $10^{-7}$. The calibrations of the pressure, temperature and humidity sensors used were re-checked against primary National Standards at the NPL and the total uncertainty in the absolute accuracy expected from these was calculated to be ± 3 parts in $10^8$. It was decided to check for any hydrocarbons in the air using a gas chromatography facility at the NPL. An evacuated aluminium cylinder was used to obtain a specimen of Southampton air and as the results below indicate, there were no unusual levels of hydrocarbon present.

APPROXIMATE LEVELS (ppm) OF CONTAMINANTS IN A SAMPLE OF AIR FROM SOUTHAMPTON (+2)

| | |
|---|---|
| Methane | 2 |
| Carbon Monoxide | 5 |
| Carbon dioxide | 200 |
| Propane | $< 0.005$ |
| 2-methyl butane | 0.04 |

It has been known for years that adsorption of water onto surfaces can significantly modify the humidity of a moist gas and that this could cause an error in the measurement of its refractive index. The surface of the stainless steel tube used in the cell was extremely rough which would enhance this problem, so a single compartment smooth surfaced silica tube cell was employed and immediately the difference between the measured and calculated values fell to 6.5 parts in $10^8$. Adsorption effects in the refractometer cell were consequently investigated.

## 4.2 Physisorption effects in the refractometer cell

The refractometer was used to study this problem (paper appended) fabricating a cell from both silica and stainless steel tubes as shown in Figures 2 and 3, with one of the interferometer areas enclosed in silica, the other in stainless steel. The technique of using the common inlet manifold shown in the diagram makes the system completely insensitive to the composition, temperature and pressure of the gas; any differences measured between the two optical paths being induced by the materials being compared.

The adsorption of water onto an optically polished silica surface was examined using internal reflection ellipsometry and less than a molecular layer of water was measured when changing the exposure of the surface from laboratory air with a relative humidity of 50% to vacuum. As this level of adsorption would not cause significant humidity changes even in a cell constructed with narrow bore tubing, this material was chosen to effectively act as a reference standard for the 'dual-material' cell.

The results indicated that with fully humidified air differences of the order of 15% in relative humidity (15 parts in $10^8$ of refractive index)

could be induced in a stationary specimen by a stainless steel tube 7 mm in diameter. This effect accounted for the 6.5 parts in $10^8$ difference obtained by changing from stainless steel to silica; however, it still left a difference of 6.5 parts in $10^8$ between the measured and calculated values and as the water term in the Edlen's equation is based on original work by Barrell and Sears (NPL) where the air was exposed to a number of rough metal surfaces, an investigation of the accuracy of the water term in the Edlen's equation was carried out.

## 4.3 Examination of the Accuracy of the Water Term

Although it has been found essential in this thesis to employ a single compartment smooth surface silica cell in an environment where the temperature is not controlled, a dual compartment silica cell may be used in this type of environment to perform accurate comparison between gases as the problem of any temperature differences occurring between the specimens in the two compartments can be minimised by starting with the specimens from the same source and flowing them slowly through the cell. This technique was used to check the humidity term in Edlen's equation using the dual compartment cell optical configuration shown in Chapter II Figure 16, to compare dry and humidified air. The air was humidified by bubbling it through two flasks of water in series and the air was dried by passing it over silica gel (shown in Figure 3). A 'zero-setting' was obtained by passing either dry or humidified air through both compartments and the path difference induced by either humidifying the dry air or drying the humidified air was then measured. The humidity of the air was measured after the cell using dew point hygrometers. The value calculated using the water term in the Edlen's equation was found to be 13 parts in $10^8$ higher than the measured value for fully humidified air. This would account for the remaining difference of 6.5 parts in $10^8$ between the measured single compartment silica cell and calculated values of laboratory air at 50% RH and 20 $^{o}$C. The use of a corrected water term in the Edlen's equation resulted in the calculated values agreeing to the measured values to better than $\pm$ 3 parts in $10^8$.

It should be noted that the limitations to the accuracy of both the equation and of measuring the parameters required for calculating the refractive index produce an uncertainty of $\pm$ 3 parts in $10^8$; the value measured by the refractometer is accurate to $\pm$ 1 part in $10^8$.

## 4.4 Path changes induced in refractometer cell windows

In order to realise the highest possible accuracy in the measured value of refractive index the possibility of errors resulting from optical path changes induced in the cell windows by the pressure changes taking place during measurement cycle were investigated. The Lorent-Lorentz equation was differentiated and the rate of change of refractive index with thickness calculated. The mechanical changes were then calculated using PAFEC - a finite element analysis technique. The results of both practical measurements with vacuum cells with etalon windows (Figure 4), short refractometer cells and these calculations confirmed that if reasonably thin silica cell windows were employed no significant errors would be produced (paper appended).

## 4.5 Results of Measurements on an Optical Scale

The L-shaped feature (Figure 5) used on the scale in this thesis was written in a 100 nm thick chromium film on a fused quartz plate by an electron beam pattern generator used in the microelectronics industry for the lithographic fabrication of mask plates. This particular feature enables the optical microscope setting system used on the equipment in this thesis to set an extremely high positional accuracy on the edges of the features in both the X and Y direction. The distances between features 1 and 5 on this mask plate (shown in Figure 6) was measured on two Helium Neon laser interferometer systems at the NPL in a temperature controlled environment. Both the NPL systems employ a Hewlett Packard interferometer system with a dual frequency Zeeman split frequency stabilised source; the stabilisation technique being completely different from that used on the laser source at Southampton. In addition, optical path changes in the Hewlett Packard systems are measured using a measurement of frequency difference and this method is also electronically very different from the fringe counting technique at Southampton. Another difference between the systems was that the correction for air refractivity was generated using Edlen's equation. The fundamental differences between the interferometric measurement in the instruments providing an additional check on techniques when the results were compared.

The results at NPL measured the distance between the points 1 and 5 as 79.9999 mm ± 0.05 μm (3 sigma) on a single axis interferometer system and 79.9998 mm ± 0.1 μm (3 sigma) on a two dimensional measuring system.

The measurement on the two-axis systems being more sensitive to the effects of vibration. These measurements have been corrected for thermal expansion to a plate temperature of 20 $^{o}$C, but the calculated values of the atmospheric refractive index used for generating the wavelength had not been corrected either for the error in the water term of the Edlen's equation or for the carbon dioxide content of the atmosphere.

The system at Southampton measured the distance between the features 1 and 5 as 79.99989 mm ± 0.02 μm (3 sigma) using the measurement procedure employed in chapter III section 2. The NPL values were corrected for the error in the Edlen's formula and compared with the Southampton measurements and the result of this comparison is shown below:-

| | |
|---|---|
| Southampton system | 79999.89 μm ± 0.02 (3 sigma) |
| NPL single axis system | 79999.895 μm ± 0.05 (3 sigma) |
| NPL Two Axis system | 79999.80 μm ± 0.10 |
| Electron Beam Pattern Writer (Two axis system) | 79999.992 μm ± 0.10 |

The results indicate that agreement of better than 1 part in $10^{7}$, 0.008 μm on an 80 mm scale, had been obtained between the single axis systems. The direct measurement of the refractive index of the atmosphere at Southampton enabling this precision to be achieved in a typical laboratory environment. However, it should be stressed that the limit of setting accuracy on a feature of ± 0.01 μm was a significant part of the measurement repeatability of ± 0.02 μm. If a higher resolution from this type of measurement system is required a different technique of positional location would need to be applied, probably involving the identification of a position by the integration of a feature with a large area, such as a grating or zone plate. Similarly, although the research in this thesis was carried out at Southampton in an ordinary laboratory environment in order to isolate the physical problems involved in perfoming measurements on these types of systems, it is obviously not recommended as a standard practice. Where the highest measurement or control accuracy is required it is advisable to minimise the effects of temperature, vibration etc, on the system by controlling the environmental parameters. In particular, the results in this thesis have underlined the importance of controlling the rate of change of temperature in the measurement environment.

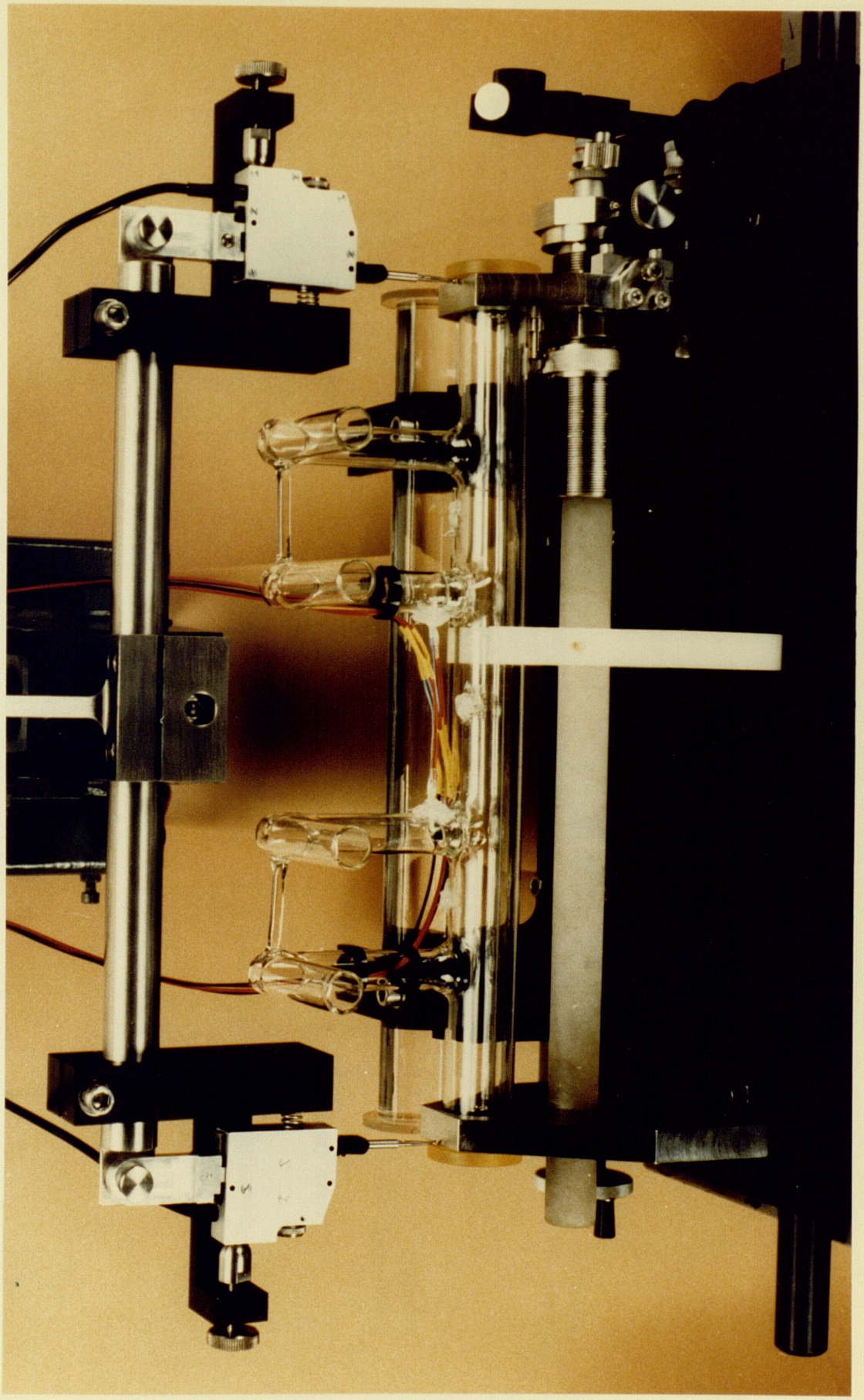

CELL LENGTH CALIBRATION EQUIPMENT
(CH4 FIG 1)

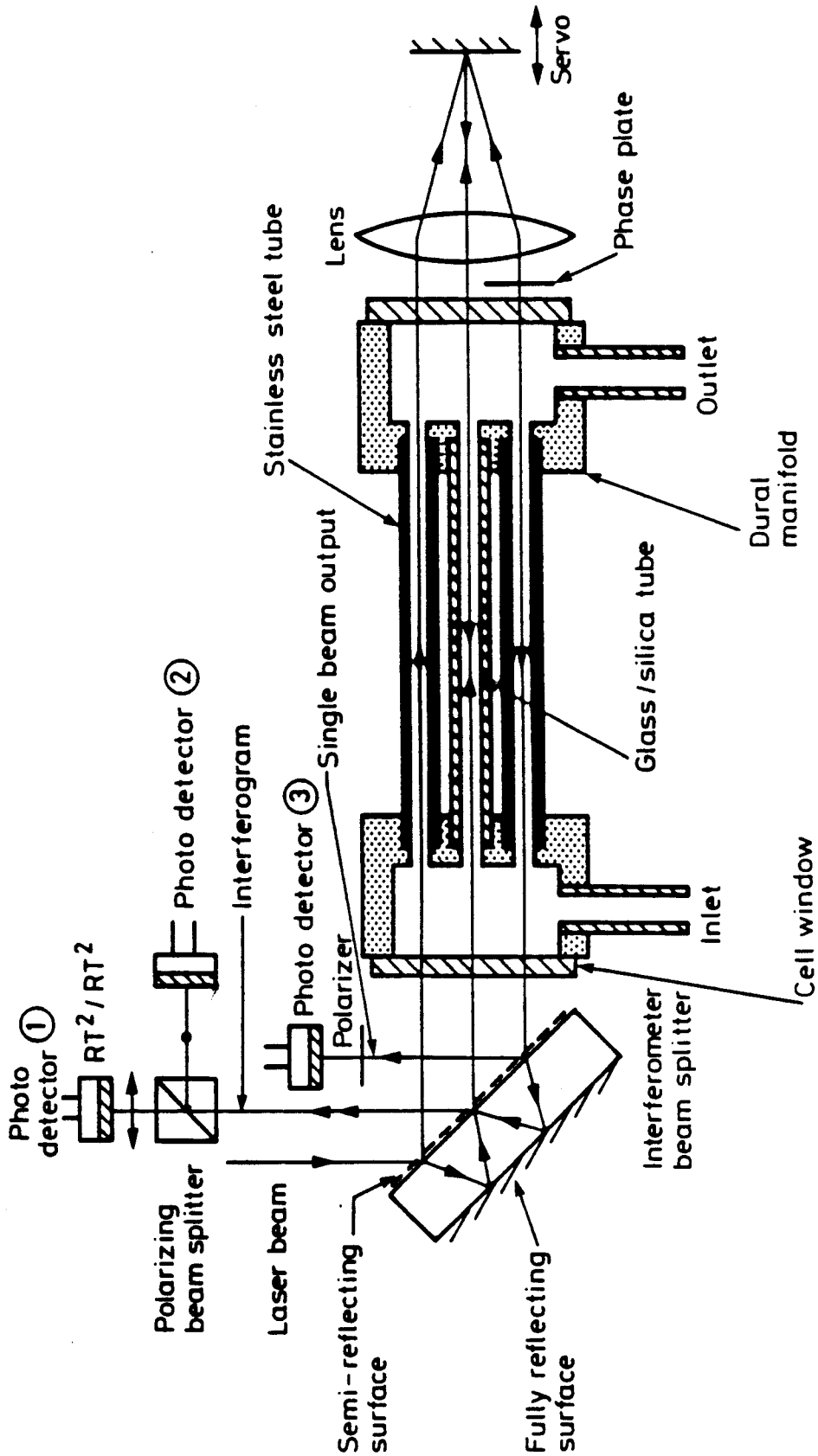


(CH4 Fig 2) NPL Refractometer configuration for examining water vapour absorption effects

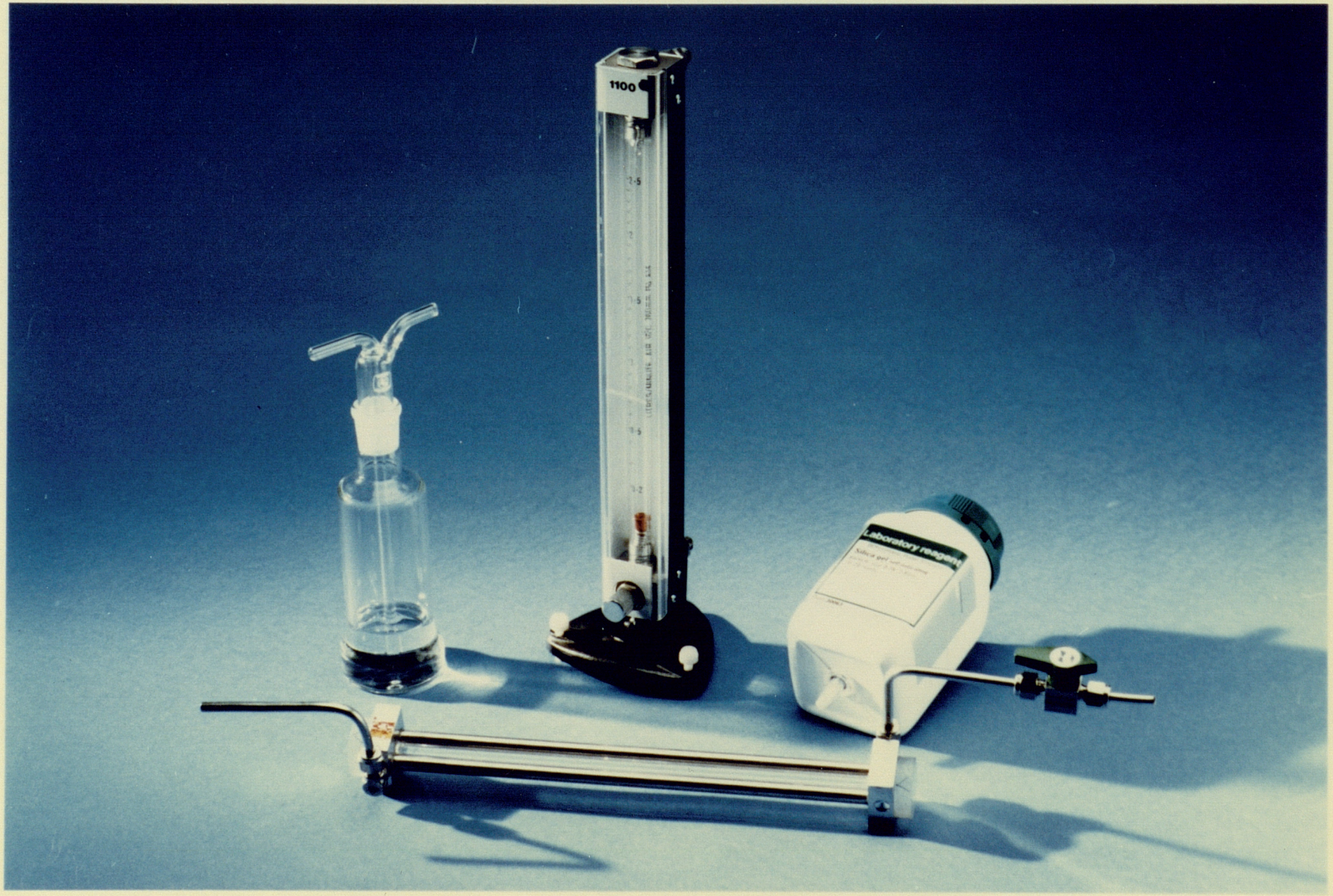


REFRACTOMETER CELL WITH A COMMON MANIFOLD
(CH4 FIG 3)

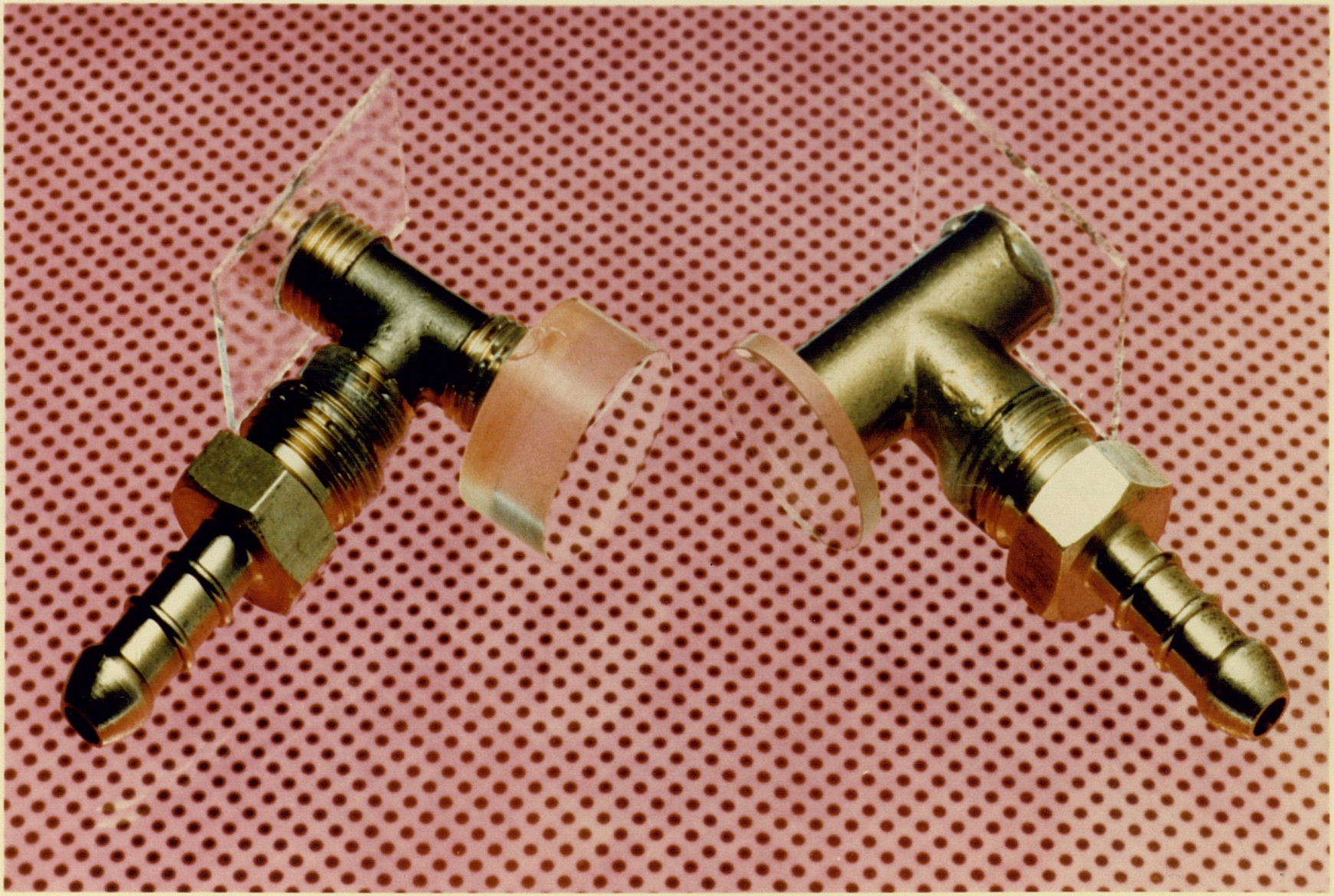

VACUUM CELL WITH AN ETALON WINDOW

(CH 4 FIG 4)

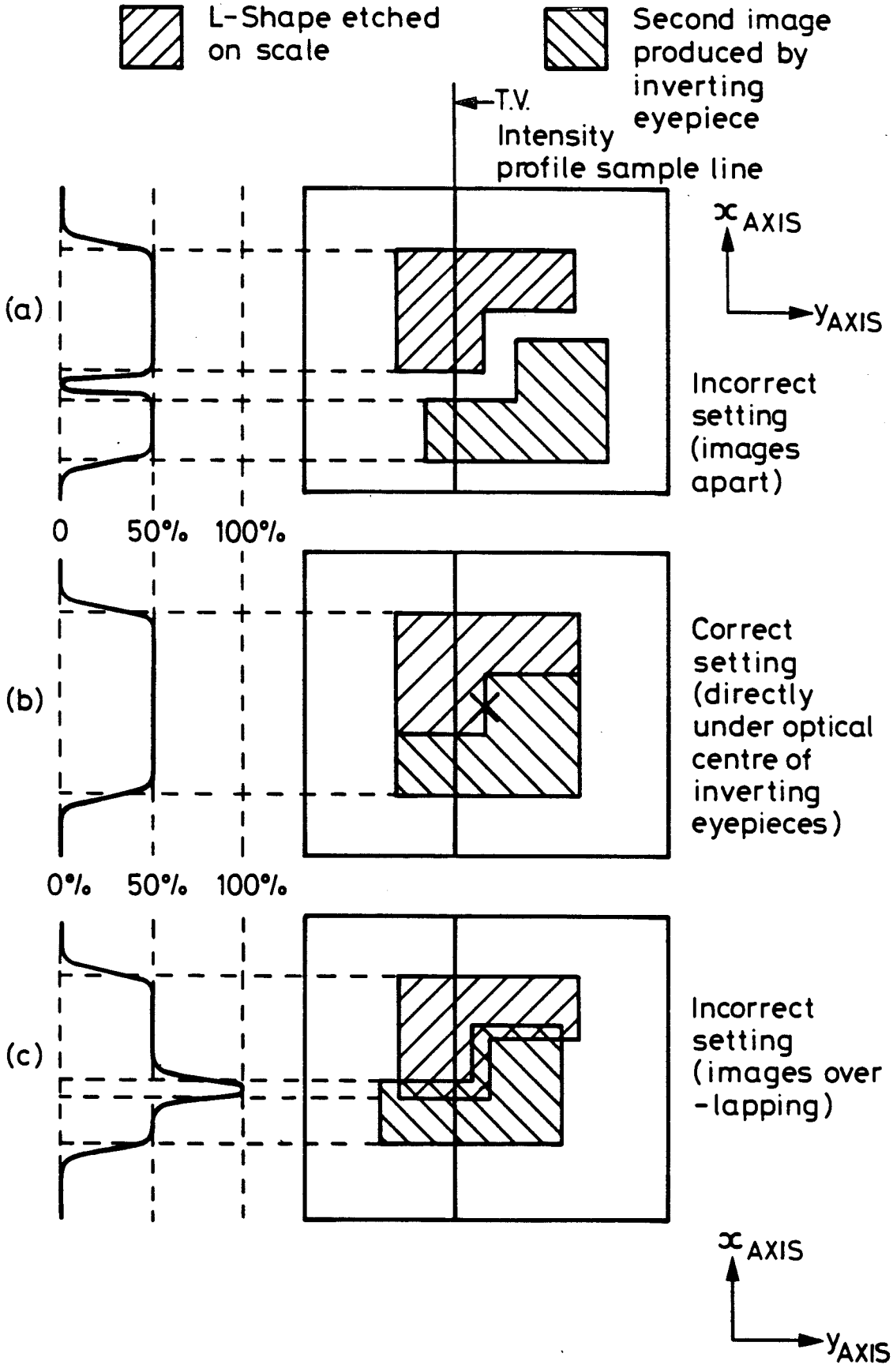


Location feature viewed through inverting eyepiece
(CH4 FIG 5 )

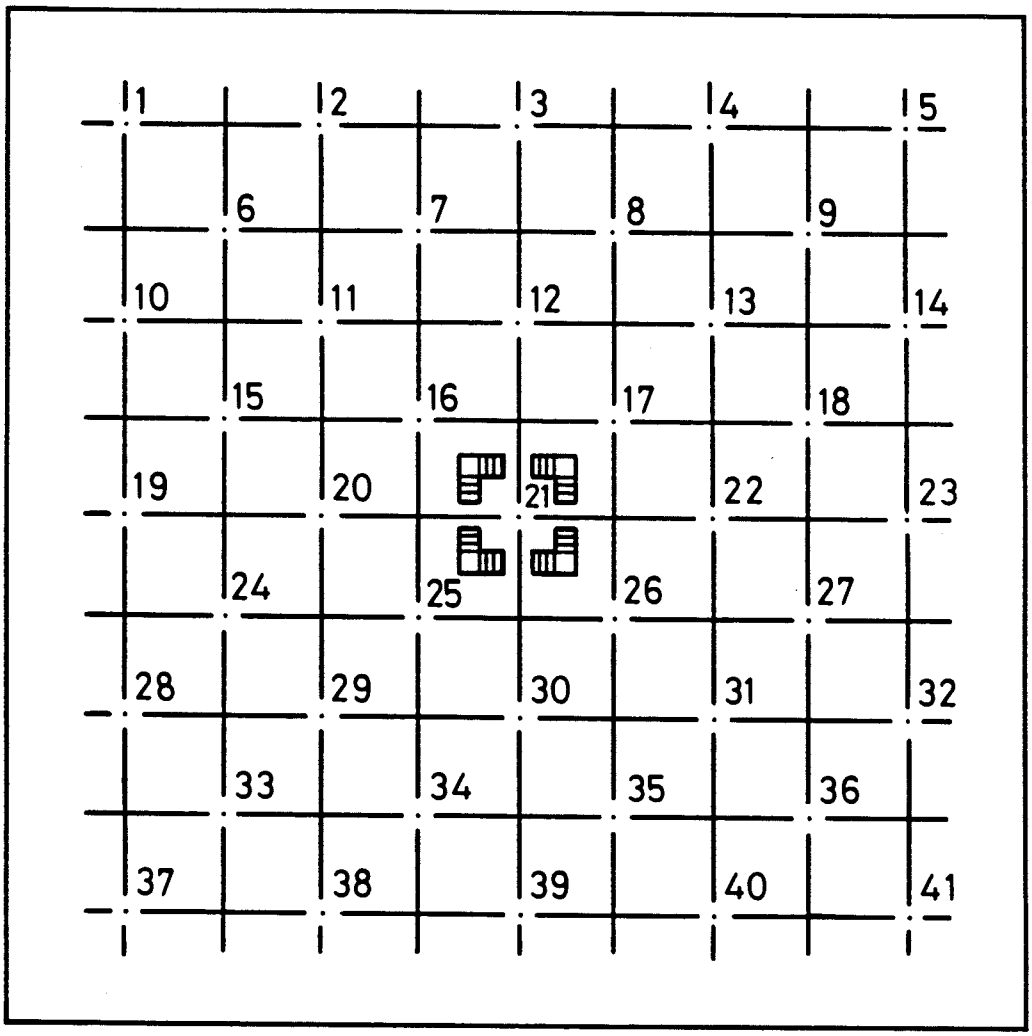


Location feature layout on photomask plate
(CH4 - FIG 6)

# C H A P T E R V

## 5.1 ACHIEVEMENTS

The achievements of the research in this thesis in the areas of length interferometry and measurement of refractive index are listed below:

### LENGTH INTERFEROMETRY

(a) New Michelson beamsplitter design

It is standard practice in Michelson interferometer beamsplitters to minimise the effects of the radiation reflected from the non-beamsplitting interface by both employing a proprietary anti-reflection coating on the surface and slightly wedging the beamsplitter plate. Although the latter practice is the most efficient way of solving the problem it effectively turns the beamsplitter into a weak prism and together with the beam displacement caused by the $45^{o}$ angle of incidence onto the plate, imposes the condition that the beamsplitter must be in position when the system is aligned.

In practice this makes the alignment procedure extremely difficult, and in addition prevents the interchange of beamsplitters other than those fabricated with a specified thickness and wedge angle. As the objective of the instrument in this thesis was to realise the ultimate performance from these interferometers, a novel beamsplitter was designed involving the use of two components, allowing the optimum alignment of the system to be achieved and enabling the beamsplitter to be then introduced into the system leaving this alignment completely unaffected. The technique involved fabricating a beamsplitter plate twice the required size and cutting this into two parts, these are then used in an optical configuration in which one plates acts as a compensator cancelling out the beam displacement and deviation from the beamsplitter plate (Chapter 3, Figure 4). This design is completely insensitive to the thickness and wedge angle of the components and chromatically corrects the system, an additional advantage in applications where a multi-wavelength source is employed.

(b) Mechanical mounting technique

An important problem identified as a major limitation to the resolution in the precision length measurement of optical scales was that the mounting restraints used to prevent a typical scale from moving during measurement could cause significant mechanical deformation of the scale producing errors in the measured length.

Initially the differences obtained from measurements were thought to be due to variations in the flatness of the scale; however, calculations indicated that this was unlikely to be the cause, and after experimenting with different types of mounting the problem was identified as being due to mechanical forces generated between the restraints at the ends of the scale either stretching or compressing the scale.

The problem was solved using a mounting technique in which one of the restraints used at the ends of the scale was designed to be incapable of sustaining a significant sideways force.

Initially successful experiments were carried out using a conventional optical mounting wax; however, this was not considered to be an ideal method as it could contaminate the optical-scale, and a mount consisting of a PTFE pad on the end of a compression spring was used. An ordinary clamp was fixed at one end of the scale to prevent it from moving whilst the PTFE pad held the other end of the scale down flat whilst preventing any significant forces existing along the length of the scale.

The principles of this technique could be incorporated into other forms of mounting employed in precision measurement systems including vacuum chucking by using bellows.

(c) Optical setting technique

One of the major limitations to the resolution of an interferometer system when applied to the measurement of optical scales is the capability of the system to set on the lines on the scale. The optical setting head used on the equipment in this thesis was specifically developed to investigate the ultimate resolution achievable by these instruments when using optical setting techniques. An image inverting eyepiece was incorporated into an optical microscope to provide an accurate positional setting technique on the edges of the lines on the scale. This system was then further improved by the use of a television

camera, allowing both the positional settings to be made remotely from the interferometer and additional electronics to be used in conjunction with the signal from the television camera to further enhance the sensitivity of the technique.

Positional setting accuracies of 0.01 μm were achieved using this method on the edges of lines produced in a 100 nm thick chromium film on a silica substrate using conventional photo-lithography.

## ATMOSPHERIC REFRACTIVITY

### (a) Refractometer cell

In the atmospheric study of the laboratory at Southampton the measurements of humidity, pressure and temperature showed that the most critical parameter to measure was the temperature of the air. The sensors available for measuring with the required accuracy were slow to respond to the fluctuating temperatures in the laboratory, and this imposed a severe limitation on their measurement accuracy.

The thermal problems were investigated and, an examination of the response functions of the thermal sensors and the relative thermal capacitances of the air specimens and the refractometer cells, led to the inevitable conclusion that the measurement accuracy of an interference refractometer fitted with a dual compartment cell would be severely limited in an environment without temperature control. The realisation of the optimum performance from these instruments in this application making the use of a single compartment cell design essential. The subsequent use of a single compartment cell 'open path' design and the technique described in this thesis of obtaining the air specimen from several points within the vicinity of the cell, enabled the interference refractometer to achieve a measurement repeatability of ± 1 part in $10^8$ in the laboratory environment at Southampton.

### (b) Water adsorption in the refractometer cell

The repeatability of the results of measurements of air refractivity using single compartment cell fabricated with both silica and stainless steel tubes indicated that a larger difference between the measured and calculated values was being measured by the stainless steel cell than

the silica cell. As the surface finish of the stainless steel was significantly rougher than the silica, an investigation of water adsorption effects was carried out using a cell constructed with a common manifold and a different material enclosing each optical path [Birch *et al*, 1988 paper appended]. The results of this study indicated that with fully humidified air the physisorption of water onto the surface of the stainless steel would modify the humidity of the air and increases the difference between the measured and calculated values by up to 1.5 parts in $10^7$. The results enabled the errors induced by the stainless steel to be quantified and corrections could have been made for them, however because the adsorption effect varied slightly the absolute measurement accuracy achieved this way was found to be ± 3 parts in $10^8$ rather than the ± 1 part in $10^8$ from silica cells and at this stage a single compartment silica cell was fitted to the refractometer.

(c) Error in the water term of Edlen's equation

The results of refractive index measurements by the refractometer fitted with a single compartment silica cell still showed a difference of 6.5 parts in $10^8$ between the measured and calculated values. Because the water term in the Edlen's formula was based on experiments carried out by Barrell and Sears where rough metal surfaces would have been in contact with the gas and water adsorption could have taken place, an investigation of the accuracy of the water term was carried out using a dual compartment smooth surfaced silica cell in a comparator mode in conjunction with a cylinder of dry air and a humidifying system. These experiments were to identify an error in the water term in the formula of 13 parts in $10^8$ for fully humidified air at 20 $^{o}$C. [Birch and Downs 1988, paper appended].

This error source accounted exactly for the remaining difference of 6.5 parts in $10^8$ between the measured and calculated values of the laboratory atmosphere (Temperature 20 $^{o}$C and relative humidity 50%). By using a modified water term in the Edlen's equation (Appendix I), agreement to better than ± 3 parts in $10^8$ was achieved. However, it is worth noting that the major sources of uncertainty lie both in the formula and in the measurement accuracies of the atmospheric parameters required for the theoretically calculated value, and that the refractometer was measuring to an absolute accuracy of ± 1 part in $10^8$.

(d) Complete length measuring system

Optical scales 80 mm long with chromium features on a silica substrate were measured on the completed system at Southampton and the results obtained compared with values measured on interferometer systems at the National Physical Laboratory. The instruments at the NPL measure in a controlled environment and are used for disseminating international primary standards of length.

The results of the means of several measurements on an 80 mm optical scale were in agreement to better than ± 0.008 μm, achieving a major objective of the research in this thesis of measuring length with an accuracy of 1 part in $10^7$ in the free atmosphere.

## 5.2 SUMMARY AND CONCLUSIONS

In order to identify the limitations to the accuracy and resolution achiev able by interferometry in the precision measurement of length in the free atmosphere, a number of aspects of the physics in these systems has been researched.The frequencies of the Helium Neon laser radiation sources used in these instruments typically change by only 1 or 2 parts in $10^8$ in the lifetime of the laser tube and, providing the correct optical and mechanical alignment procedures discussed in this thesis are followed, then in a vacuum an absolute measurement accuracy approaching a few parts in $10^8$ can be achieved from these systems.

When optical systems are used on length measurement applications in the free atmosphere, corrections for the atmosphere wavelength variations can now be made in any one of the two ways described to an accuracy of a few parts in $10^8$ as a result of the research. Firstly by measuring the parameters of pressure, temperature and humidity and calculating the refractive index of the air using the modified Edlen's equation, and secondly by measuring the refractive index directly using an interference refractometer. The first technique involving the corrected Edlen's formula has a theoretical accuracy of approaching ± 3 parts in $10^8$ but being dependent on the constituents of the atmosphere, whereas the refractometer technique is independent of the constituents and is capable of an absolute accuracy approaching ± 1 part in $10^8$. However, as has been described, care must be taken to ensure that the temperature of the gas specimen in the refractometer is the same as that in the path of the length interferometer or alternatively that a suitable correction applied by accurately measuring any temperature differences that exist. The measurement of differential temperature avoids the problems encountered in absolute temperature measurement of self-heating in the sensors and non-linearities in the sensor electronics and, in addition minimises the thermal response errors in environments where the temperature is varying.

The results of length measurements on an optical scale have shown that an absolute accuracy of better than 1 part in $10^7$ can be achieved by these systems in the free atmosphere, with a lower resolution limit of ± 0.02 μm. A major part of this limit is the optical setting capability; however the results have also underlined the importance when resolving to this level of the care that must be taken in the mechanical stability of the scale with respect to both the material and its

physical dimensions.

The results of the research in this thesis, including the discussions and descriptions of the various techniques developed, together with the information contained in the various appendices, provide a compendium of information for achieving the optimum performance in both accuracy and resolution from length measuring interferometer systems, particularly when used in applications in the free atmosphere.

## REFERENCES

BAER, T., KOWALSKI, F.V. and HALL, J.L.
Frequency calibration of a 0.633 μm He-Ne Longitudinal Zeeman Laser. *Applied Optics*, Vol 19, No 18,(Sept 1980) p 3173-3177.

BALDWIN, Richard R., TRUHE, Larry E. and WOODRUFF, David C.
Laser Optical Components for Machine Tool and Other Applications. Hewlett-Packard Journal(April 1983)

BALHORN, R., KUNZMANN, H. and LEBOWSKY, F.
Frequency Stabilization of Internal Mirror Helium-Neon Lasers. *Applied Optics* (1972), 11, p742.

BARRELL, H. and SEARS, J.E.
Trans. Roy. Soc. (London) A238, 1, (1939)

BENNETT, J.M.
A Critical Evaluation of Rhomb-Type Quarterwave Retarders. *Applied Optics* Vol 9, No. 9,(Sept 1970.)

BREBBIA, Dr Carlos
Boundary Element Analysis System (Beasy)
Computational Mechanics Institute Southampton.

BENNETT, S.J., WARD, R.E. and WILSON, D.C.
Comments on: Frequency Stabilisation of Internal Mirror He-Ne Lasers. *Applied Optics*, Vol 12, No 7 (July 1973)

BRUNAUER, S., EMMETT, P.H. and TELLER, E.
*J Amer Chem Soc*, 60, 309,(1938)

CIDDOR, P.E. and DUFFY, R.M.
Two-mode Frequency Stabilised He-Ne (633 nm) Lasers: Studies of Short and Long Term Stabilities. *J Phys E: Sci Instrum*, Vol 6, (1983).

DANTZIG, J.A.
Improved Transient Response of Thermocouple Sensors. *Rev Sci Instrum*, 56 (5)(May 1985.)

DICKSON, L.D.
Characteristics of a Propagating Gaussian Beam. *Applied Optics*, Vol 9, No 8,(August 1979,) p1854-1861.

DOWNS, M.J. and RAINE, K.W.
An Unmodulated Bi-Directional Fringe-Counting Interferometer System for Measuring Displacement. *Precision Engineering*, 1, 2 (1979), p85-88.

DOWNS, M.J. and BIRCH, K.P.
Bi-Directional Fringe Counting Interference Refractometer. *Precision Engineering* (July 1983), Vol 5, No 3, p105-110.

DOWNS, M.J. and McGIVERN, W.H.
Optically monitored, high efficiency thin film polarising beamsplitter cubes.
Commercially confidential NPL Report(1983.)

DOWNS, M.J.
High Precision Length Measurement using Helium-Neon Laser Interferometers. Proceedings Electro-Optics/Laser International UK(1984.)

DUARDO, A.J., WANG, S.C. and HUG, W.
Polarisation Properties of Internal Mirror He-Ne Lasers. *SPIE*, Vol 88, Polarised Light (1976), p34-49.

EDLEN, B.
The Dispersion of Standard Air. *J Opt Soc*, AM. 43, 339 (1953)

EDLEN, B.
*Metrologia*, (1966,) 2, p71.

ESTLER, Tyler W.
High-Accuracy Displacement Interferometry in Air. *Applied Optics*, Vol 24, No 6, (March 1985.)

EUROTHERM
Thermocouple EMF and Platinum 100 Resistance Thermometer Tables.
Eurotherm Ltd, Broadwater, Worthing, England.

HEYDEMANN, P.L.M.
Determination and Correction of Quadrature Fringe Measurement Errors in Interferometers. *Applied Optics*, 20, (1981), p3382-3384.

HOLMES, D.A.
Exact Theory of Retardation Plates. *Josa*, Vol 54, No 9, (Sept 1964,) p1115-1120.

JAVAN, A. and STOKES, A.
Isotope Shift and Saturation Behaviour of the 1.15 m Transition in Neon. Physics Review Letters. 15 (June 1983.)

JERRARD, H.G
The Calibration of Quarter-wave Plates *Josa, Vol 42, No 3, (March 1952).*

JERRARD, H.G. and McNEILL, D.B.
Theoretical and Experimental Physics. London: Chapman and Hall.

KING, R.J., and TALIM, S.P.
Some aspects of polariser performance. *J of Physics E; Vol 4* (1971)

KING, R.J., TURNER, N.P. and DOWNS, M.J.
Dimensional Measurement in Microelectronics. (2-3 Dec 1981). Internal Report Division of Mechanical and Optical Metrology. National Physical Labortory, Teddington, Middlesex.

KOCHSIEK, M.
$H_2O$ Adsorption Layers on Surfaces of Mass Standards. PTB-Mitt Eilungen Förschen und Prufen. (June 1977,) 87, p478-486.

Temperature Sensing with Thermocouples and Resistance Thermometers.
A Practical Handbook.
Lab Facility Ltd, 26 Tudor Road, Hampton, Middlesex, TW12 2NQ.

LYUBOMUDROV, O.V. and ETSIN, I. Sh.
Possibilities of Measuring Length by the Coincidence of Fractional Parts of Interference Orders. Sov. J Opt. Technol. SI (10), (Oct 1984,)
Machinery Handbook, 18th Edition, Industrial Press p422-423.

MATSUMOTO, H.
Recent Interferometric Measurements using Stabilised Lasers. *Precision Engineering* Vol 6, No 2 (1984) p87-94.

MARTIN, L.C.
The Theory of the Microscope. Published by Blackie & Son Ltd (1966)

MEHROTRA, Yogesh
New Materials for Precision Optics.
*Optical Engineering* (April 1986,) Vol 25, No 4, p513-518.

PECK, E.R.
Polarisation Properties of corner Reflectors and Cavities. *Josa*, Vol 52, No 3 (March 1962).

PTB Report ME-13 (Published by Physikalisch-Technische Bundesanstalt, Braunschweig, W Germany (1977,) p115.

ROARK, Raymond J. and YOUNG, Warren C.
Formulas for Stress and Strain 5th Edition. McGraw Hill Book Company.

ROWLEY, W.R.C.
Interferometric Measurement of Length and Distance. *Alta Frequenza*, Vol IXLI (1972), p887-896.

ROWLEY, W.R.C.
Analysis of Laser Frequency Stability by Heterodyne Measurement. National Physical Laboratory, Report MOM 78, (Feb 1986.)

SCHELLENKENS, P., WILKENING, G., REINBOTH, F., DOWNS, M.J., BIRCH, K.P. and SPRONCK, J.
Measurements of the Refractive Index of the Air using Interference Refractometers. *Metrologia*, 22 (1986), p279-387.

TAKASAKI, H., UMEDA, N. and TSUKIJI, M.
Stabilised Transverse Zeeman Laser as a New Light Source for Optical Measurement. *Applied Optics*, Vol 19, No 3, (Feb 1980,) p435-441.

TILFORD, Charles, R.
Analytical Procedure for Determining Lengths from Fractional Fringes. *Applied Optics*, Vol 16, No 7 (July 1977)

WALLARD, A.J.
The Frequency Stabilisation of Gas Lasers. *J of Physics E Scientific Instruments* (1973,) Vol 6, p793-807.

WECHTER, Stephen G. and KRAMER, Franklin Jnr.
Evaluation of Gas Phase Moisture Standards Prepared in Treated Aluminium Cylinders.
21st National Symposium of the Analysis Instrument Division, Instrument Society of America. King of Prussia, Pa (May 1975)

WUERZ, L.J. and QUENELLE, R.C.
Laser Interferometer System for Metrology and Machine Tool Applications. *Precision Engineering*, 5, 3 (1983) p111-114.

YOUNG, J.F.
Humidity Control in the Laboratory using Salt Solutions - A Review. *J Appl Chem* Vol 17 (Sept)

# APPENDIX I

## Edlen's formula

The refractive index of air is a well known function of atmospheric pressure (P), air temperature (T), partial pressure of water vapour or relative humidity (H), and carbon dioxide concentration by volume (y).

The empirical equation most widely used in metrology is due to Edlen and his most recently revised equation (1965). In this publication he expresses concern in the abstract about the validity of the standards for water vapour which are based on measurements by Barrell and Sears (1939) and the work in this thesis has in fact improved the accuracy of the water vapour term in the equation. In the revised equation for the refractive index ($n_s$) of dry standard air at 15 $^{o}$C and 101325 Pascals pressure is given by:

$$(n_s - 1) \times 10^8 = 8342.13 + 2406030\ (130 - \sigma^2)^{-1} + 15997\ (38.9 - \sigma^2)^{-1}$$

where $\sigma$ is the vacuum wavenumber in $\mu m^{-1}$.

The refractive of the carbon dioxide ($nCO_2$) is given by:

$$(nCO_2 - n_s) = (14485 + 117.8\ \sigma^2) \times 10^{-8}$$

Standard air defined as containing $CO_2$ to 0.0003 parts by volume, corresponding in the normal atmosphere to a partial pressure of 0.23 torr. As the refractivity of $CO_2$ is about 50% higher than that of air this $CO_2$ content increases the refractivity over that of $CO_2$-free air by approximately $0.5 \times 0.0003 \times (n_s - 1) = 4.5 \times 10^{-8}$.

The refractive index of water vapour is significantly lower than that of air and Edlen used Barrell and Sears (NPL 1939) measurements of the refractive index of water vapour in his final equation.

$$n_{tPf} = 1 + \frac{P(n - 1)_s}{96095.43} \cdot \frac{1 + P(0.613 - 0.00998t) \times 10^{-8}}{(1 + 0.0036610t)}$$

$$- f\ (4.2922 - 0.0343\sigma^2)10^{-10}$$

where $n_{tPf}$ is the refractive index of a standard composition of air at a temperature of $t^{o}C$, an atmospheric pressure of P pascals and a partial pressure of water vapour of f pascals.

As discussed in the appended paper resulting from the work in this thesis the errors measured in the refractive index values calculated using Edlen's equation may be attributable to physisorption effects in the original Barrell and Sears apparatus and the following modification to the water vapour term in the equation is recommended:

$$(n - 1)_{tPf} - (n - 1)_{tP} = - f(3.7209 - 0.0343\sigma^{2})10^{-10}$$

where $(n - 1)_{tP}$ is the refractivity of dry air at $t^{o}C$ and at atmospheric pressure P pascals: $(n - 1)_{tPf}$ is the refractivity of moist air under the same temperature and pressure conditions containing f pascals of water vapour; f is the partial pressure of water vapour in pascals and $\sigma$ is the vacuum wavenumber in $\mu m^{-1}$. The Edlen equation with this modification is expected to have an uncertainty of $\pm 3 \times 10^{-8}$ which is the limit at which the measurements were made.

The sensitivity of the refractive index of the atmosphere to the various parameters is shown below:

| Parameter | Nominal value | Change for which n = + 1 part in $10^{8}$ |
|---|---|---|
| Pressure | 101.3 kPa (760 mmHg) | + 3.73 Pa (+ 0.28 mmHg) |
| Temperature | 20.0 $^{o}C$ | -0.01 $^{o}C$ |
| Humidity | 40% | - 1% |
| Carbon dioxide concentration | 340 ppm | + 67 ppm |

# A P P E N D I X  II

## TILTING EFFECTS IN PHASE PLATES

| | ANGLE OF INCIDENCE IN AIR (degrees) | PHASE RETARDATION (degrees) | DIFFERENCE (degrees) |
|---|---|---|---|
| ROTATING MICA ABOUT THE FAST AXIS | 0 | 90 | 0 |
| | ± 5 | 88.2 | - 1.8 |
| | ± 10 | 83.1 | - 6.9 |
| | ± 15 | 74.6 | - 15.4 |
| | ± 20 | 62.9 | - 27.2 |
| ROTATING MICA ABOUT THE SLOW AXIS | 0 | 90 | 0 |
| | ± 5 | 91.8 | + 1.8 |
| | ± 10 | 96.8 | + 6.8 |
| | ± 15 | 105.4 | + 15.4 |
| | ± 20 | 117.2 | + 27.2 |
| ROTATING QUARTZ ABOUT THE FAST AXIS | 0 | 90 | 0 |
| | ± 5 | 89.86 | - 0.14 |
| | ± 10 | 89.43 | - 0.57 |
| | ± 15 | 88.73 | - 1.27 |
| | ± 20 | 87.78 | - 2.22 |
| ROTATING QUARTZ ABOUT THE SLOW AXIS | 0 | 90 | 0 |
| | ± 5 | 90.14 | + 0.14 |
| | ± 10 | 90.57 | + 0.57 |
| | ± 15 | 91.28 | + 1.28 |
| | ± 20 | 92.27 | + 2.27 |

Mica is a positive biaxial-crystal of which there are many different forms. The angle between the optical axes may be almost anything from $0^{\circ}$ to $42^{\circ}$ depending upon the chemical constitution as well as the crystal structure. The most common "muscovite" (page brown in colour) has an angle $2\alpha = 42^{\circ}$ between the optic axes. However, a clear colourless mica having a small angle $2\alpha = 0$ is to be preferred for $\lambda/4$ plates since the wave surfaces will then be approximately those of a positive uniaxial crystal. (A mica $\lambda/4$ plate is approximately 0.032 mm thick.)

Quartz is a positive uniaxial crystal ($N_e > N_o$) with no natural cleavage planes and has to be cut and the faces polished to optical flatness. A quartz $\lambda/4$ plate consists of two discs cut with their optical axes in the plane of the disc; these differ in thickness by $\lambda/4$ (0.016 mm) and

are cemented together with the fast axis of one disc aligned with the slow axis of the other.

For quartz $N_e = 1.553$ $N_o = 1.544$ ($\lambda$ 633 nm)

$\delta N = 0.009$

For calcite $N_e = 1.485$ $N_o = 1.656$ ($\lambda$ 633 nm)

$\delta N = 0.171$

For mica $\delta = 0.0045$

( $\lambda/4$ QUARTZ PHASE 633nm $\frac{\lambda}{4(n_e - n_o)} = 17.6\mu m$ )

When using waveplates with coherent light sources such as lasers, it is vitally important that the surfaces are anti-reflection coated to prevent multiple reflections within the place causing problems. (Bennett, J.M.and Holmes, D.A. JERRARD, H.G)

The ellipticity introduced by tilting both mica and quartz retardation plates is negligible up to 20 $^{o}$.

# APPENDIX III

## REFRACTION BY A THIN PRISM

The equation for the minimum deviation by a prism is:

$$\frac{n'}{n} = \frac{\mathrm{Sin}\frac{1}{2}(\alpha + \delta)}{\mathrm{Sin}\frac{1}{2}\alpha}$$

where $n'$ and $n$ are the refractive indices of the prism material and the surrounding media and $\alpha$ and $\delta_m$ are the angles of the prism and minimum deviation respectively. This equation is widely used for the most accurate refractive index by placing the sample in the form of a prism on the table of a spectrometer and measuring the angles $\alpha$ and $\delta m$. When the refracting angle $\alpha$ becomes small enough to ensure that its sine and the sine of the angle of deviation $\delta$ may be set equal to the angles themselves this equation; and for prisms having a refracting angle of only a few degrees we can write:

$$\frac{n'}{n} = \frac{\delta + \alpha}{\alpha}$$

Thus $\delta = (n' - 1)\alpha$ for a thin prism in air. It is worth noting that this widely used formula is not accurate at $45^{\circ}$ incidence as it has been derived for the minimum deviation equation. In practice with interferometer beamsplitters at $45^{\circ}$ incidence the angle of deviation is approximately 80% of the wedge angle introduced into the plate.

In order to prevent problems being introduced by energy reflected from the rear surface, beamsplitters are typically wedged up to 2 minutes of arc. This introduces 2 fringes per mm between the wavefronts and results in a beam deviation of some 48 seconds at $45^{\circ}$ incidence with a silica plate. Unless alignment of the system was carried out with the interferometer in place, this would result in a cosine error of 6 parts in $10^8$. The novel two-component beamsplitter design described in this thesis makes the plate independent of thickness and wedge angle and chromatically corrects the interferometer system.

# A P P E N D I X  IV

## DISPLACEMENT BY A PARALLEL PLATE

When a single ray traverses a glass plate with plane surfaces that are parallel to each other, it emerges parallel to its original direction but with a lateral displacement d which increases with the angle of incidence $\phi$. Using the notation shown in the Figure we may apply the law of refraction and some simple trigonometry to find the displacement d. Starting with the right triangle ABE, we can write

$$d = \ell \sin (\phi - \phi) \qquad (a)$$

which, by the trigonometric relation for *the sine of the difference between two angles*, can be written:

$$d = \ell(\sin \phi \cos \phi' - \sin \phi \cos \phi) \qquad (b)$$

From the right triangle ABC we can write:

$$\ell = \frac{t}{\cos \phi'}$$

which, substituted in Equation gives:

$$d = t \left[ \frac{\sin \phi \cos \phi'}{\cos \phi'} - \frac{\sin \phi' \cos \phi}{\cos \phi'} \right] \qquad (c)$$

From Snell's law

$$\sin \phi' = \frac{n}{n'} \sin \phi$$

which substituted in equation (c) gives

$$d = t \left[\sin \phi - \frac{\text{Cos } \phi}{\text{Cos } \phi'} \frac{n}{n'}, \text{ Sin } \phi \right]$$

$$d = t \text{ Sin } \phi \left[ 1 - \frac{n}{n'} \frac{\text{Cos } \phi}{\text{Cos } \phi'} \right].$$

It can be seen that from $0^{\circ}$ up to appreciably large angle, d is nearly proportional to $\phi$, for as the ratio of the cosines becomes appreciably

less than 1, causing the righthand factor to increase, the sine factor drops below the angle itself in almost the same proportion. For the 3 mm thick silica plate used in the length interferometer at $45^{o}$ incidence, the displacement of 0.95 mm was completely eliminated by the use of the compensator plate.

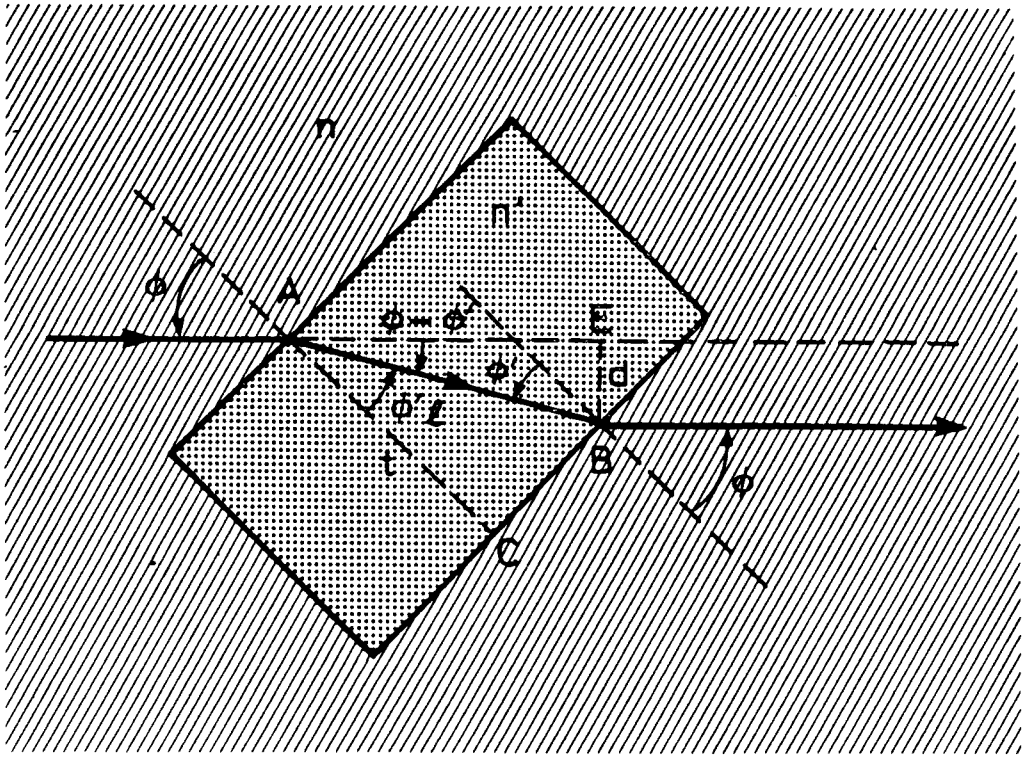


Refraction by a plane-parallel plate

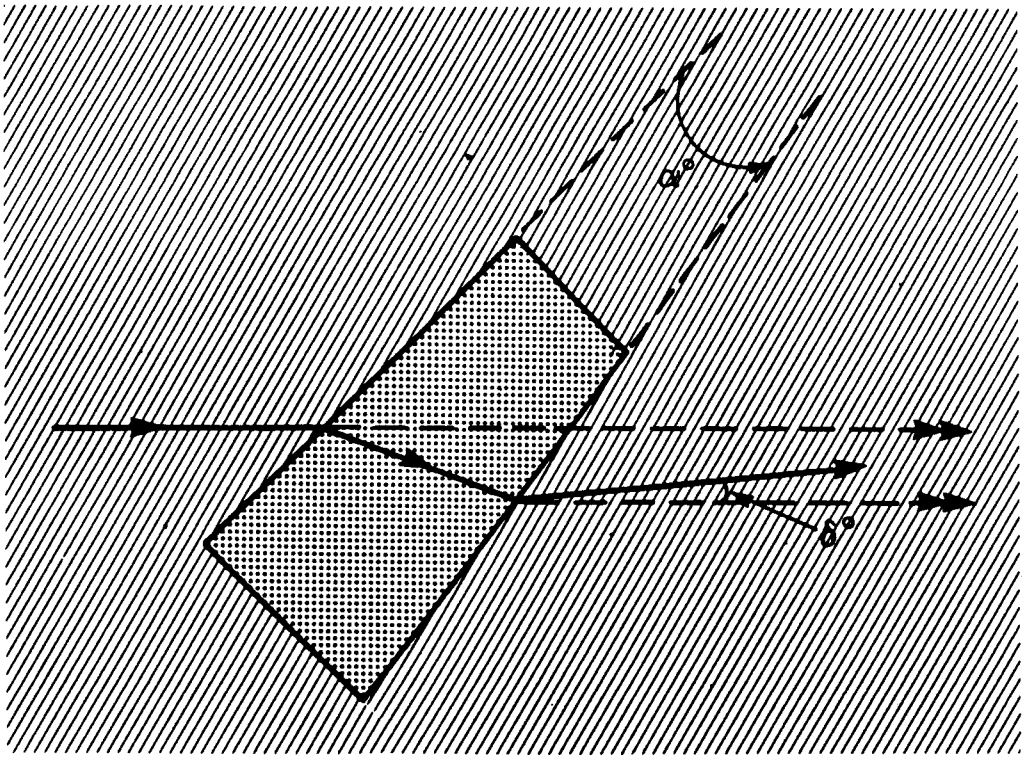


Deviation by a wedged plate
(Appendix III and IV)

APPENDIX V

Length errors due to bending or lack of flatness.

$$\varphi = \frac{a}{R} \qquad (1)$$

$$b^2 = d(2R - d) = 2dR - d^2$$

$$2Rd = b^2 + d^2$$

$$R = \frac{b^2 + d^2}{2d} \qquad (2)$$

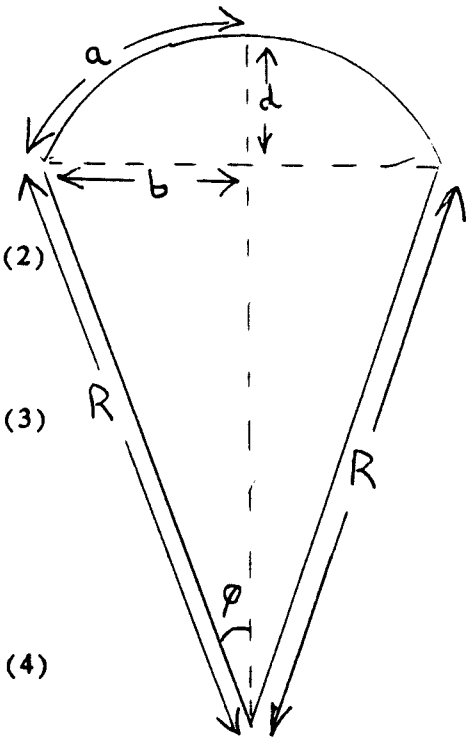


$$\frac{b}{R} = \sin\varphi \qquad (3)$$

Substituting $\varphi$ from (1) into (3)

$$\frac{b}{R} = \sin\frac{a}{R} \qquad (4)$$

Substituting R from (2) into (4)

$$\frac{2db}{b^2 + d^2} = \sin\frac{2da}{b^2 + d^2} \qquad (5)$$

---

First approximation : $d^2$ may be neglected by comparison with $b^2$

Second approximation : $\sin\varphi = \varphi - \frac{\varphi^3}{3!} + \frac{\varphi^5}{5!} \ldots\ldots$

$$\sin\varphi = \varphi - \frac{\varphi^3}{6}$$

Thus from (5)

$$\frac{2d}{b} = \frac{2ad}{b^2} - \frac{8d^3a^3}{6b^6}$$

$$6db^5 = 6adb^4 - 4a^3d^3$$

$$3b^5 = 3ab^4 - 2a^3d^2$$

$$3b^4(a - b) = 2a^3d^2$$

$$\therefore a - b = \frac{2a^3d^2}{3b^4} \qquad (6)$$

In (6) $\frac{a^3}{b^4} \approx 1/a$

Hence $a - b = \frac{2d^2}{3a}$ ← accurate formula

---

SIMPLE CASE

$$b^2 + d^2 = a^2$$

$$a^2 - b^2 = d^2$$

$$(a + b)(a - b) = d^2$$

$$a - b = \frac{d^2}{a + b}$$

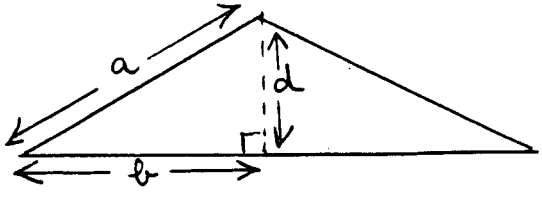


$$a - b \approx \frac{d^2}{2a}$$ ← approximate formula

It should be appreciated that these formulae are only applicable on the neutral axis and where thick scales are involved their thicknesses and shapes must be taken into consideration.
It can be shown that for a scale of thickness t the change in length a-b is approximately $\frac{2dt}{a}$.
The exact value depending upon the cross section of the scale and the mounting technique employed.

If a = 80mm and t = 3mm
for a-b = 0.01 m then d = 0.12 m (⅓ FRINGE)

## EXAMPLES OF CHANGES IN LENGTH DUE TO BENDING OR LACK OF FLATNESS (ON THE NEUTRAL AXIS)

$$(A - B) = \frac{2}{3}\frac{d^2}{A}$$

Deflection for 1 $\mu$m error in 100 mm

$$0.5 = \frac{2}{3}\frac{d^2}{50000} \qquad \underline{d = 194\ \mu m} \quad (613 \text{ fringes})$$

Deflection for 0.01 $\mu$m error in 1 mm

$$0.005 = \frac{2}{3}\frac{d^2}{500}$$

$\underline{d = 1.94\ \mu m}$ (6 fringes)

(0.01 $\mu$m in 100 mm 61 fringes)

## LENGTH ERRORS INDUCED BY TENSION OR COMPRESSION

$$\text{Stress} = \frac{\text{load}}{\text{area}} \qquad \text{Strain} = \frac{\text{change in length}}{\text{original length}}$$

$$\text{Load} = D \times \frac{dl}{l} \times A$$

where E is Young's modulus for the material
dl is the change in length
l is the original length
A is the cross sectional area
E for silica 73.1 $GNm^{-3}$ ($1 \times 10^7$ lbs/sq in)
E for steel 211.9 $Gnm^{-3}$ ($3 \times 10^7$ lbs/sq in)

For a silica scale 10 mm wide and 3 mm thick a force of 2.11 kg (4.65 lbs) is required to induce a 1 $\mu$m change in length over 100 mm.

[0.01 $\mu$m over 100 mm would require 21 grms (0.74 oz)]

## APPENDIX VI ERROR SOURCES IN LENGTH INTERFEROMETRY

| PARAMETER | 0.01 mm ERROR IN 100 MM LENGTH (1 PART IN $10^7$) | |
|---|---|---|
| **WAVELENGTH** | | |
| VACUUM WAVELENGTH | 1 PART IN $10^7$ | (EQUIVALENT TO A FREQUENCY CHANGE OF 50 MHz) |
| REFRACTIVE INDEX EQUATION | 1 PART IN $10^7$ | |
| AIR TEMPERATURE | 0.1 °C | |
| ATMOSPHERIC PRESSURE | 0.3 mm | |
| RELATIVE HUMIDITY | 12% | |
| CARBON DIOXIDE | 670 ppm | (NORMAL LEVEL 340 ppm) |
| **INTERFEROMETER ALIGNMENT** | | |
| COSINE ERROR | SINGLE AXIS 92 SECONDS/ARC (0.045 mm/100 mm) | |
| | TWO AXIS 65 SECONDS/ARC | |
| ABBE ERROR | 20 SECONDS/ARC (0.1 mm OFFSET) | |
| **LINEAR THERMAL EXPANSIONS** | | |
| DURAL | ($23 \times 10^{-6}$ °C$^{-1}$) | 0.004 °C |
| STEEL | ($11.5 \times 10^{-6}$ °C$^{-1}$) | 0.009 °C |
| GLASS | ($8.5 \times 10^{-6}$ °C$^{-1}$) | 0.012 °C |
| LOW EXPANSION GLASS | ($3 \times 10^{-6}$ °C$^{-1}$) | 0.033 °C |
| SILICON | ($2 \times 10^{-6}$ °C$^{-1}$) | 0.050 °C |
| INVAR | ($1.5 \times 10^{-6}$ °C$^{-1}$) | 0.067 °C |
| SILICA | ($5 \times 10^{-}$ °C$^{-1}$) | 0.2 °C |
| ZERODUR | ($2 \times 10^{-8}$ °C$^{-1}$) | 0.5 °C |

# ADDITIONAL ERROR SOURCES IN A TWO DIMENSIONAL MEASURING SYSTEM EMPLOYING PLANE MIRROR INTERFEROMETERS

Related to 0.1 $\mu$m in 100 mm (1 part in $10^6$)

ORTHOGONALITY OF PLANE MIRRORS

0.2 SECONDS/ARC

TOLERANCE ON FLATNESS OF PLANE MIRRORS

(a) Direct displacement error — 1/3 fringe (0.1 $\mu$m)

(b) Angular variation in the perpendicular to the mirror surface — 1/25 fringe in 100 mm (0.013 $\mu$m)
0.2 SECONDS/ARC

## ANGULAR SENSITIVITY TO FLATNESS

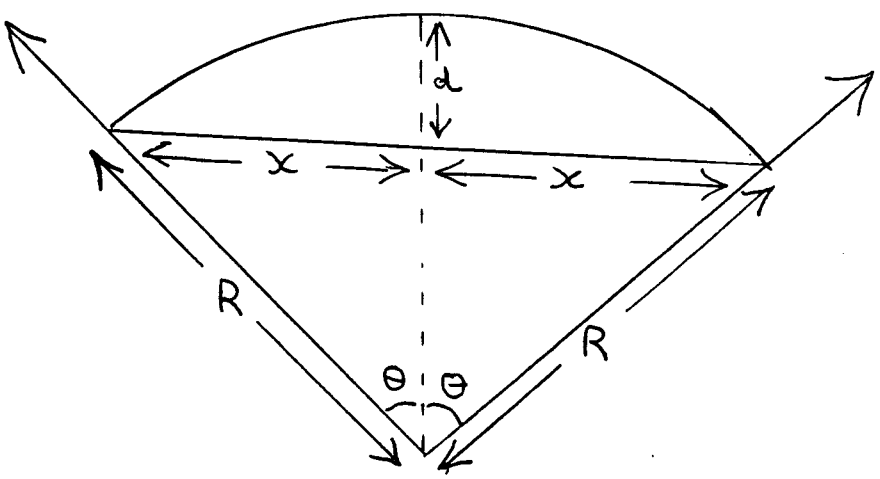


$$d(2R - d) = x^2 .$$

(i) $\rightarrow \quad x^2 \approx 2dR \qquad R >>> d.$

(ii) $\rightarrow \quad \sin\theta = \frac{x}{R} .$

Subst (i) in (ii) $\quad \sin\theta = \frac{x}{R} = \frac{2d}{x}.$

For 1 fringe per 1 inch (0.3 $\mu$m in 25.4 mm)

$$\sin\theta = \frac{2 \times 0.3}{12.7} \quad . \quad \theta = 10 \text{ SECONDS ARC.}$$

For 1 fringe per inch $2\theta$ = 20 SECONDS/ARC.

# APPENDIX VII
# DYNAMIC RESPONSE OF A THERMAL SENSOR

The behaviour may be analysed by the following model

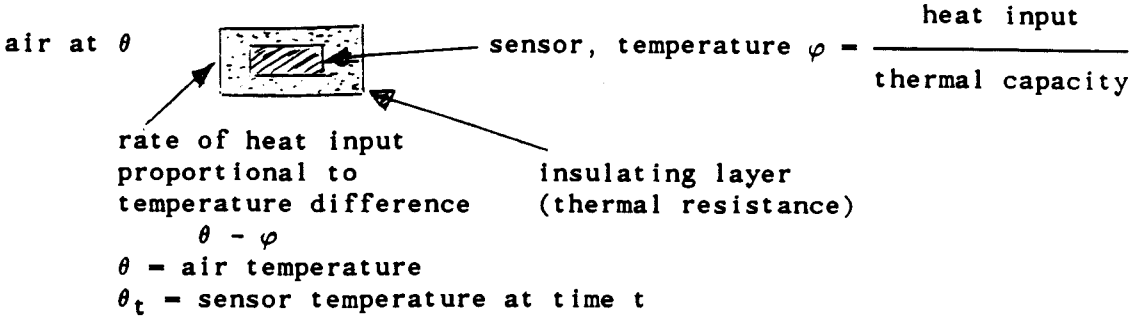


$\theta$ = air temperature
$\theta_t$ = sensor temperature at time t

The model is more easily treated as its electrical equivalent:

| | | |
|---|---|---|
| temperature | → | voltage |
| rate of heat input | → | current |
| thermal resistance | → | electrical resistance |
| thermal capacity | → | electrical capacitance |
| heat input | → | electrical charge |

Thus the equivalent electrical circuit model is:

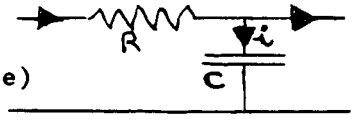


input voltage = $\theta$ (≡ air temperature)

$\varphi$ = output voltage (≡ sensor temperature)

The voltages and current are functions of time, t

$$i_t = \frac{\theta_t - \varphi_t}{R}, \qquad \frac{d\varphi}{dt} = \frac{i_t}{C}$$

Thus $$\frac{d\varphi}{dt} = \frac{\theta_t - \varphi_t}{RC} = \frac{\theta_t - \varphi_t}{\tau}$$ (where $\tau$ = RC, the time constant)

$$\tau \frac{d\varphi}{dt} + \varphi_t - \theta_t = 0$$

This is a standard form of differential equation which has the solution

$$\varphi_t - \theta = \alpha e^{-t/\tau}$$ , in which $\alpha$ is a constant (unknown)

We know however that at t = 0, $\varphi_t = \varphi_o$.

ie $\varphi_o - \theta = \alpha$

Thus $\varphi_t = \theta + (\varphi_o - \theta)^{-t/\tau}$

Eg for $\theta < \varphi_o$ (cooling)

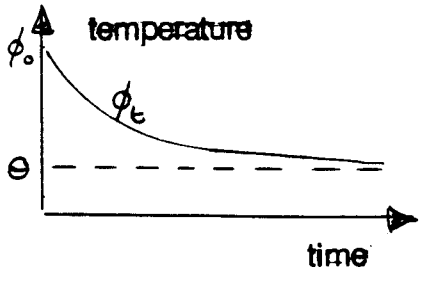

Air temperature changing at a constant rate $\frac{d\theta}{dt} = \beta$

$$\theta_t = \theta_o + \beta t$$

$$i_t = \frac{\theta_t - \varphi_t}{R} = \frac{\theta_o + \beta t - \varphi_t}{R}$$

Thus $$\frac{d\varphi}{dt} = \frac{1}{C}\frac{(\theta_o + \beta t - \varphi_t)}{R} = \frac{1}{\tau}(\theta_o + \beta t - \varphi_t)$$

$$\tau \frac{d\varphi}{dt} + \varphi_t - \theta_o = \beta t$$

This is a standard form of differential equation, which has the solution:

$$\varphi_t - \theta_o = \alpha e^{-t/\tau} + (t - \tau)\beta \quad , \quad \text{where } \alpha \text{ is an unknown constant}$$

But $\theta_t = \theta_o + \beta t$ , $-\theta_o = -\theta_t + \beta t$

Thus $\varphi_t - \theta_t = \alpha e^{-t/\tau} - \beta\tau$ , but when $t = 0$, $\varphi_o = \theta_o$ $\therefore 0 = \alpha - \beta t$

Hence $\varphi_t - \theta_t = \beta\tau(e^{-t/\tau} - 1)$

When t is large, compared to $\tau$

$$E = \varphi_t - \theta_t = -\beta\tau$$

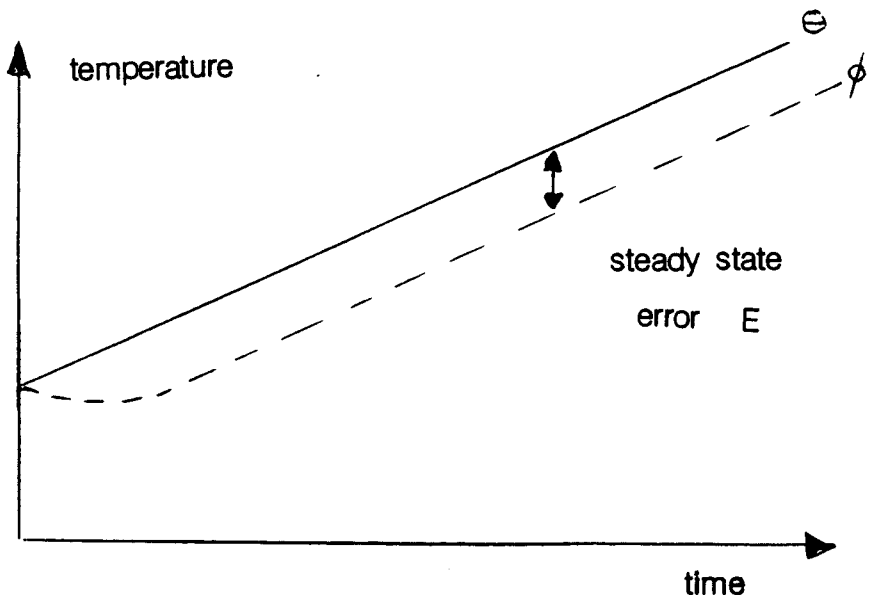

# APPENDIX VIII

Material properties and thermal capacitances.

## COEFFICIENTS OF LINEAR EXPANSION

($\times 10^6/^\circ C$)

| | |
|---|---|
| Stainless steel | 16 |
| Glass (pyrex) | 3 |
| Silica (fused) | 0.5 |
| Duralumin | 23 |

## DENSITIES

(grams $cm^{-3}$)

| | |
|---|---|
| Air (Dry at 1 atmosphere) | 0.0012 |
| Stainless steel | 7.8 |
| Glass (pyrex) | 2.23 |
| Silica (fused) | 2.2 |
| Duralumin | 2.8 |

## THERMAL CONDUCTIVITIES

($Wm^{-1}\ k^{-1}$)

| | |
|---|---|
| Air | 0.024 |
| Stainless steel | 24.5 |
| Glass (pyrex) | 1.1 |
| Silica (fused) | 1.33 |
| Aluminium | 236 |
| Copper | 403 |
| Water | 0.56 |

## SPECIFIC HEATS

($Jg^{-1}$ $^{\circ}C^{-1}$)

| | |
|---|---|
| Air | 1.006 |
| Stainless steel | 0.51 |
| Glass (pyrex) | 0.78 |
| Silica (fused) | 0.84 |
| Aluminium | 0.9 |

## THERMAL CAPACITIES (Density × specific heat)

($J\ cm^{-3}$ $^{\circ}C^{-1}$)

| | |
|---|---|
| Air | 0.0012 |
| Stainless steel | 3.98 |
| Glass (pyrex) | 1.74 |
| Silica (fused) | 1.85 |
| Aluminium | 2.52 |

## VOLUMES IN DUAL COMPARTMENT AIR REFRACTOMETER CELL

(Related to a cell 31.6 cms long)

| | |
|---|---|
| Air in inner chamber | 15.8 ccs |
| Material in inner tube | 8.9 ccs |
| Air in outer chamber | 118 ccs |
| Material in outer tube | 12.2 ccs |

THERMAL CAPACITIES IN DUAL COMPARTMENT AIR REFRACTOMETER CELL

($J\ ^{\circ}C^{-1}$)

| | |
|---|---|
| Air in inner chamber | 0.019 |
| Air in outer chamber | 0.142 |
| Inner tube glass (pyrex) | 15.5 |
| Outer tube glass (pyrex) | 21.2 |
| Inner tube stainless steel | 35.4 |
| Outer tube stainless steel | 48.6 |

# A P P E N D I X IX

## CARBON DIOXIDE CALCULATIONS

Inhaled air contains 79% nitrogen and 21% oxygen whilst exhaled air contains 79% nitrogen, 17% oxygen and 4% carbon dioxide. An average breathing rate is 0.5 litres of air every 4 seconds, a single human being generating 18 litres of carbon dioxide every hour. A typical laboratory has a volume of 90,000 litres of air and the 0.02% per hour of induced carbon dioxide is equivalent to a rate of rise in the refractive index of the atmosphere of 2 parts in $10^8$. This is confirmed experimentally by the measured values in the figure. (The Southampton laboratory had a volume of 180,000 litres due to the exceptionally high ceiling) requiring a carbon dioxide correction of 1 part in $10^8$ per hour in the measured refractive index value for one person in the laboratory.

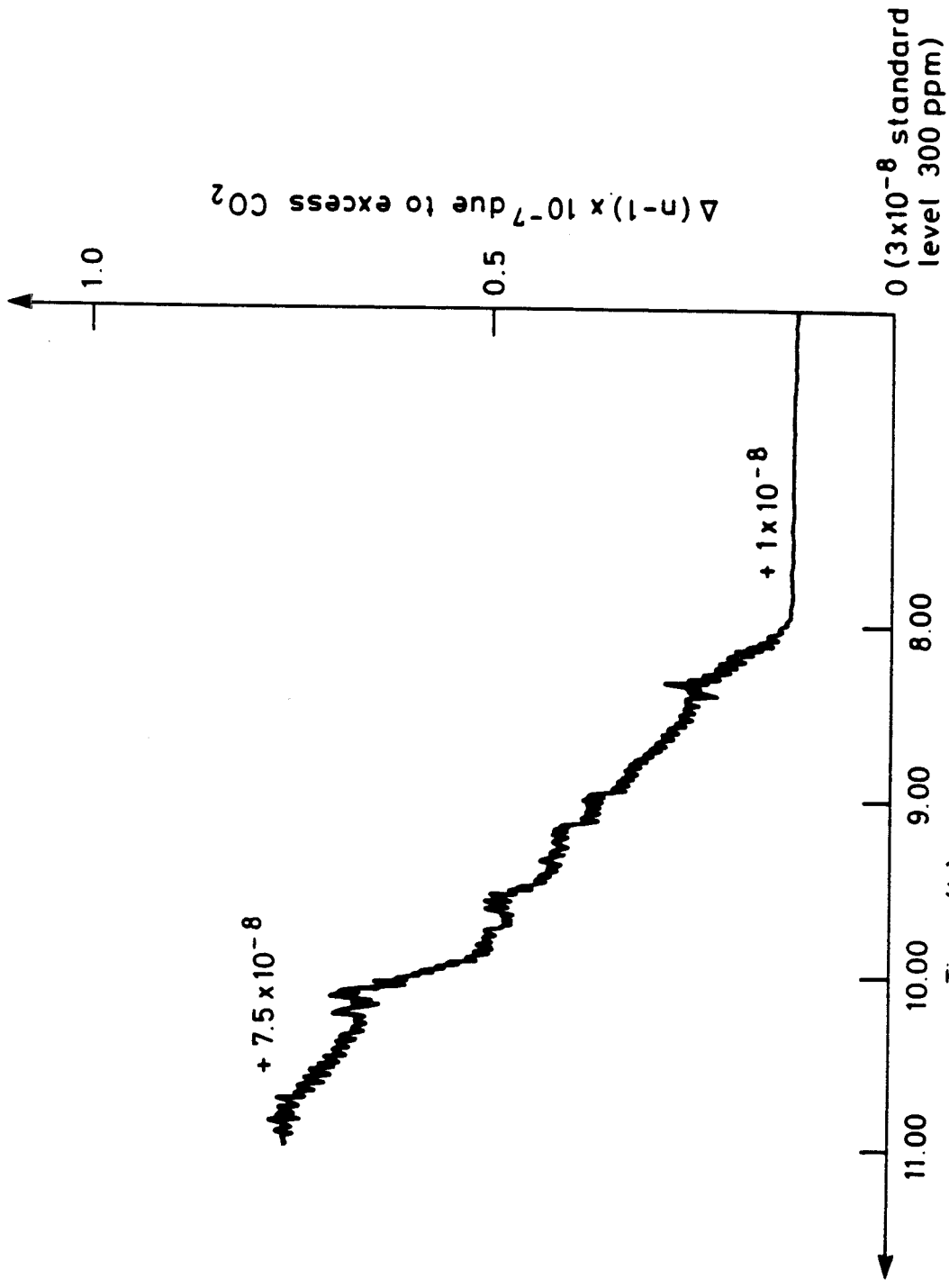


Typicol build-up of $Co_2$ levels in an average sized laboratory (one person)
(Appendix IX)

# OPTICAL PATH LENGTH CHANGES INDUCED IN CELL WINDOWS AND SOLID ETALONS BY EVACUATION

K P Birch, M J Downs and D H Ferriss

## ABSTRACT

When optical components are subjected to pressure variations, anomalous path differences may be induced where the dimensional change in the component is not compensated for by a corresponding change in the refractive index of the material. Examples of these effects are discussed with particular emphasis on interference gas refractometer cell windows and solid etalons.

Interference refractometers are widely used for the measurement of the absolute refractive indices of gases by evacuating a cell of known length and measuring the optical path length difference introduced into the system when the cell is filled with the gas under examination (Schellekens et al 1986, Downs and Birch 1983). These interferometers normally use a 'common path' design that makes them insensitive to mechanical changes, thus enabling a sub-nanometric measurement sensitivity of optical path difference to be achieved ($\lambda/2000$). In order to maintain the measurement accuracy at this sensitivity it is necessary to correct for the path length changes that are induced in the optical windows during the measurement process. These changes are predominantly the result of vacuum on one side of each window being replaced by atmospheric pressure, which causes a change in shape of the window. The exact form of this distortion is dependent upon the dimensions and mechanical properties of the windows, and their mounting arrangement.

To investigate these effects, both theoretical and experimental approaches have been used. The theoretical approach employed the use of a finite element analysis computer program (PAFEC) to determine the shape changes induced in optical windows, and the differentiated form of the Lorenz-Lorentz equation to determine the corresponding optical path length changes.

The PAFEC program calculated the thickening and bending of a 30 mm diameter silica window mounted on different diameter tubes, each with a wall thickness of 1 mm. For the purposes of the calculation it was assumed that the effect of the supports was totally to constrain the axial displacement over the contact region between the window and support; radial relative displacement was allowed. The results of the calculations are shown in Table 1. The table shows that whilst the bending of the window is highly dependent upon the mounting location of the window, the thickening term is relatively insensitive to the mounting location. The thickening is proportional to the window thickness, unless the diameter of the support is comparable to, or SMALLER than, the thickness of the window. The calculations also show that the thickening of the window is insensitive to the material Poisson's Ratio and inversely proportional to the Young's Modulus. It should be noted that whilst the bending of the thinnest window (2.5 mm) was 1.6 $\mu$m, this would only introduce an error in the measurement to the refractive index of a gas of 1.6 parts in $10^9$ for a 32 cm long cell.

An example of the results from the PAFEC programme is shown in Figure 1 for the case of a 30 mm diameter, 5 mm thick fused silica window mounted on a 17 mm outside diameter tube. The regular rectangular grid shows the undeformed window whilst the dotted grid shows the deformed configuration produced after the atmospheric pressure is removed from the window area enclosed by the tube. The change in dimensions shown in the figure have been exaggerated by PAFEC for clarity.

In order to translate the window deformations calculated using PAFEC, into optical path differences, the Lorenz-Lorentz equation:

$$\frac{(n^2 - 1)}{(n^2 + 2)} \frac{1}{\rho} = R$$

can be differentiated to produce:

$$\frac{d\rho}{\rho} = \frac{6n^2}{(n^2-1)(n^2+2)} \frac{dn}{n} \qquad (1)$$

where $\rho$ is the density, n is the refractive index and R is the specific refraction[1] of the medium. By substituting

$$\frac{d\rho}{\rho} = -\frac{dt}{t}$$

where t is the window thickness, into equation (1) the relationship between the change in window thickness and the corresponding change in the refractive index of the window is derived.

In a typical 'double-pass' refractometer, the light beam passes twice through each of the cell windows. When this initially evacuated cell is filled with air at atmospheric pressure, it can be shown that the measured optical path difference will be in error by an amount dl given by:

$$dl = \frac{2}{3} \frac{dt}{n} (n^4 - 5n^2 + 6n - 2) \qquad (2)$$

where dt is the contraction of the window as the air is admitted and n is the refractive index of the window material. This error is due to the change in thickness of the cell window and to the increase in the length of the air path in the cell due to the dimension changes of the windows. The equation confirms the trivial case, dl = 0 when n = 1.0. However, in the case of a cell using fused silica windows (n = 1.45) of 5 mm thickness supported on a diameter larger than the window thickness, dl = + 0.9 nm. For a similar size of window made from SF 57 low stress glass (n = 1.84), dl = + 3.2 nm. In the determination of the refractive index of gases, these windows would introduce errors of 3 parts in $10^9$ and 1 part in $10^8$ respectively for a 32 cm long cell and the errors would be proportionally larger either for thicker windows or for shorter cells.

The calculations indicate that the choice of a low index material for the refractometer cell windows would minimise this source of error. In order to confirm this conclusion experimentally, a 30 mm long cylindrical refractometer cell was made with 12.5 mm thick silica windows supported on two tubes of outside diameters 12 mm and 24 mm as shown in Figure 2. The cell, which had two separate chambers, was initially evacuated. Dried laboratory air was then leaked into the outer chamber and the refractive index of the air was measured from the total change in the optical path length in the outer arm of the refractometer.

This refractive index was compared with that calculated by Edlen's equation (1966) from the direct measurement of the atmospheric pressure and the temperature of the air contained in the cell. Since the total measurement uncertainty with the short cell was $\pm 1 \times 10^{-7}$ in terms of refractive index, which includes the uncertainty associated with Edlen's equation for dry air, any

significant difference between the measured and calculated air refractive indices would be due to a change in the optical path described by equation (2). Ten sets of measurements were made and all the differences were found to be within $\pm 1 \times 10^{-7}$ (corresponding to $\pm$ 3.2 nm), indicating that $dl < \pm$ 3.2 nm. This is consistent with the value of $dl = +$ 1.6 nm derived from equation (2) and the mechanical dimension changes calculated using PAFEC and the Young's Modulus for fused silica of 73 GPa.

Further experimental confirmation was obtained by comparing the measured change in optical path length through a solid etalon as the pressure on one of the optical faces was changed from vacuum to atmospheric pressure with the change derived directly from the differentiated Lorenz-Lorentz equation. The experimental arrangement which is shown in Figure 3, used a 12 mm solid BK7 glass etalon with a Young's Modulus of 81 GPa mounted on the end of a vacuum chamber. The chamber was evacuated and then filled with air, during which process the change in optical path length through the etalon was determined by examining the transmittance characteristics with a photodetector. The transmittance characteristic of the etalon was calibrated using a cosine term generated by rotating the etalon on the divided circle. The measured change of $-$ 10 $\pm$ 3 nm agreed with the $-$ 8 nm value calculated from a modified version of equation (2) for a solid etalon (with one side evacuable) given by:

$$dl = \frac{dt}{6n}(n^4 - 5n^2 - 2) \qquad (3)$$

There are other applications in which a solid etalon may be used alternately in a vacuum and in the atmosphere, eg in earth/space applications. Under these conditions the entire medium surrounding the etalon is changing pressure and it is possible to derive a third expression for the change in optical path length through the etalon given by:

$$dl = \frac{dt}{2n}(n^4 - n^2 - 2) \qquad (4)$$

The equation shows the important condition that when $n = \sqrt{2}$, $dl = 0$. This implies that for this unique value of n, the optical path in the etalon is constant and independent of the thickening produced by pressure variations. Further PAFEC calculations showed that in this case the change in thickness is inversely proportional to both the Poisson's ratio and Young's modulus of the material.

In conclusion, the error contributions that window deformations make to the absolute measurement of the refractive indices of gases have been discussed. The bending of the window has been shown to produce a second order error compared with the main error arising from the thickening of the window.

Equations have been presented for calculating the effect that window thickening has on both the measurement of gaseous refractive indices using a 'double-passed' refractometer cell, and on the change in optical path for solid etalons. The results derived for these equations have also been confirmed experimentally using a short refractometer cell and a solid etalon. They also indicate that the use of the equations in conjunction with the calculations of the mechanical deformation should enable suitably accurate values for the optical path changes induced in a particular system to be theoretically calculated. The results show that the errors generated by these effects in refractometers can be minimised by making the cell windows as thin as possible and selecting a material with a low refractive index.

## REFERENCES IN ALPHABETICAL ORDER

M J DOWNS and K P BIRCH, Bi-directional Fringe Counting Interference Refractometer, Prec Eng 5, 105 (1983).

B EDLEN, The Refractive Index of Air, Metrologia 2, 71 (1966).

P SCHELLEKENS, G WILKENNING, G REINBOTH, M J DOWNS, K P BIRCH and J SPRONCK, Measurements of the refractive index of air using interference refractometers, Metrologia 22, 279 (1986).

**TABLE 1**

**Results for 30 mm diameter silica window**

| WINDOW THICKNESS mm | TUBE 8 mm I/D 10 mm O/D | | TUBE 16 mm I/D 18 mm O/D | | TUBE 28 mm I/D 30 mm O/D | |
|---|---|---|---|---|---|---|
| | THICKENING nm | BENDING nm | THICKENING nm | BENDING nm | THICKENING nm | BENDING nm |
| 10 | 5.14 | 2.33 | 7.07 | 12.6 | 6.97 | 74.1 |
| 5 | 3.54 | 5.65 | 3.37 | 44.6 | 3.30 | 351 |
| 2.5 | 1.67 | 19.9 | 1.65 | 192 | 1.70 | 1590 |

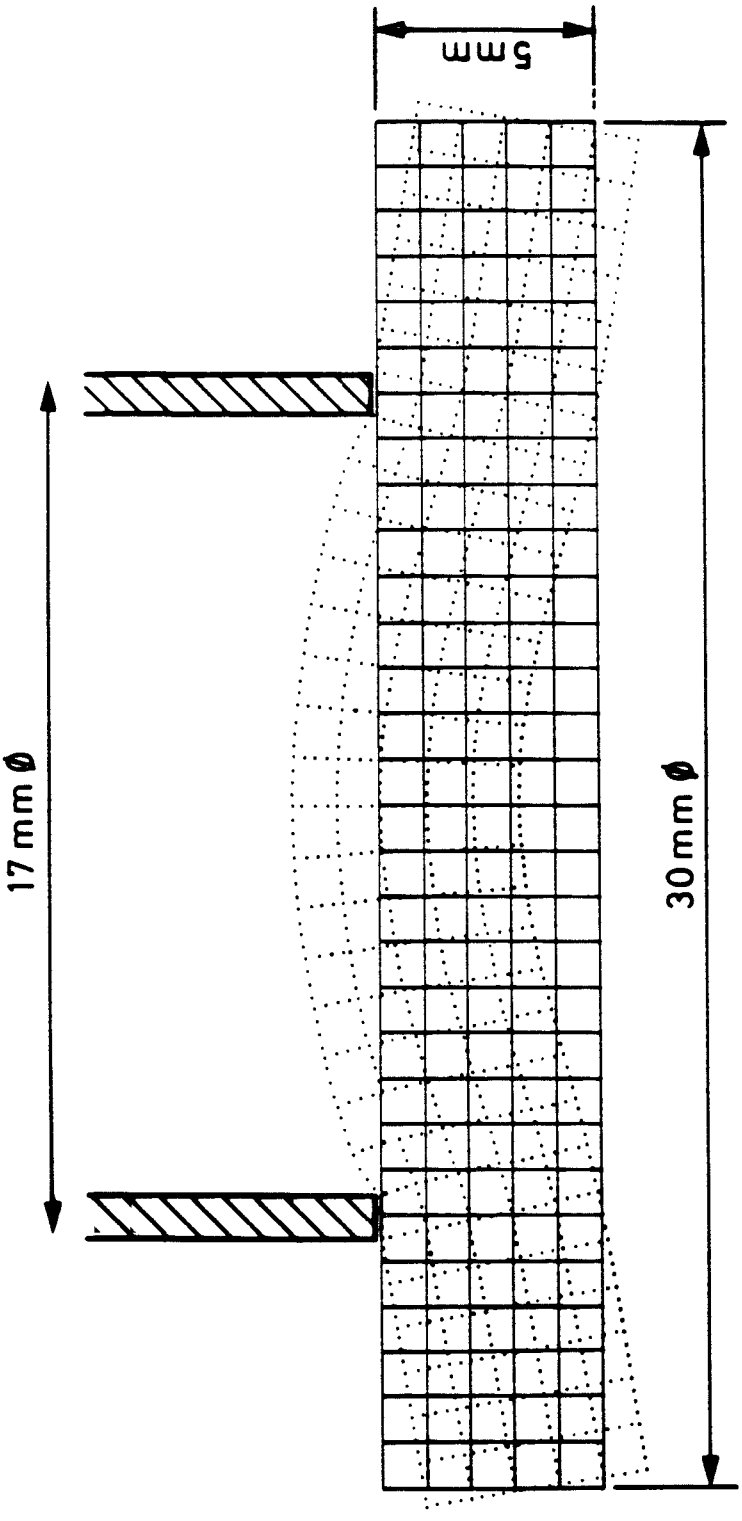


Fig 1 Window deformation calculated using PAFEC

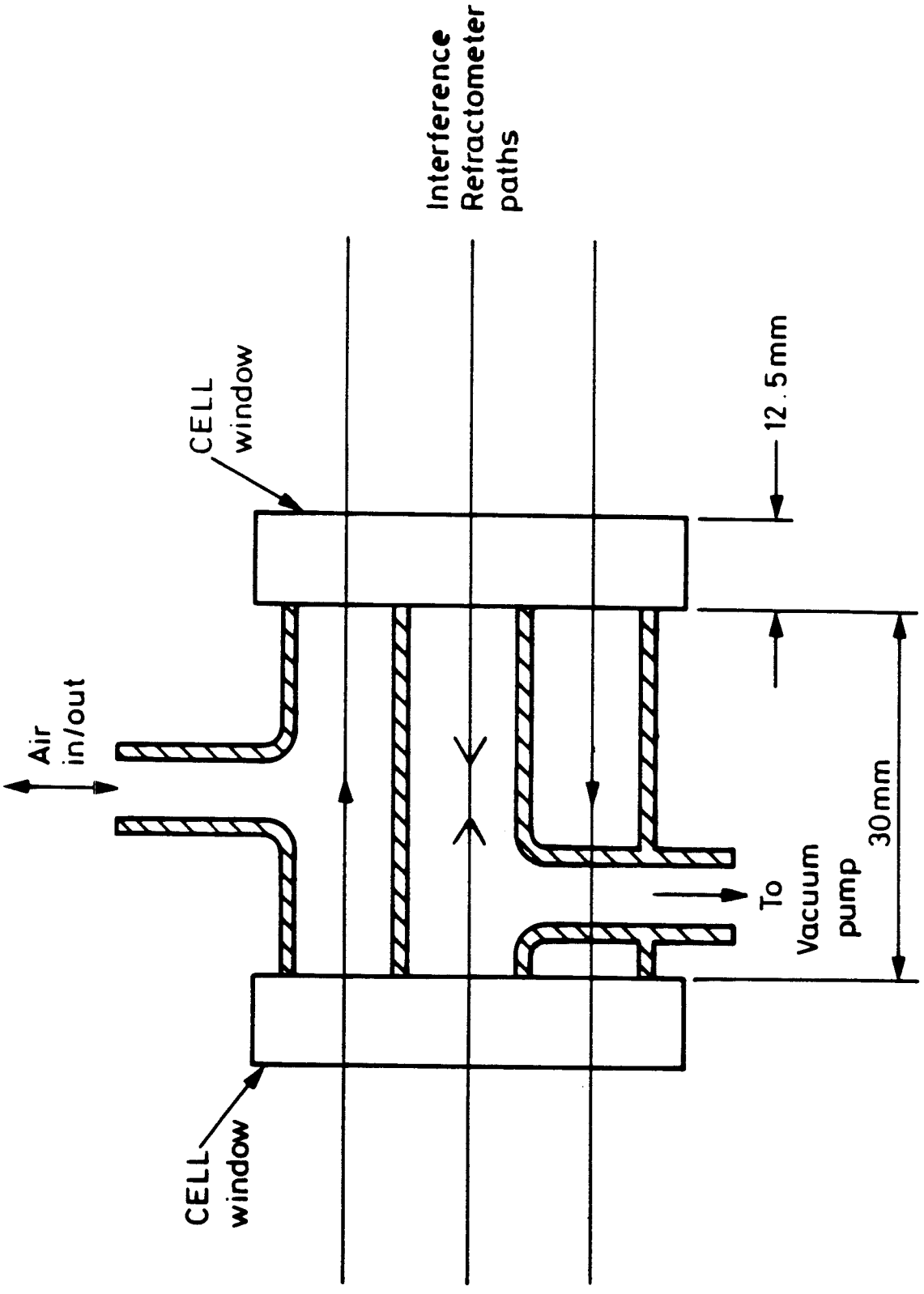


Fig 2 Short cell configuration

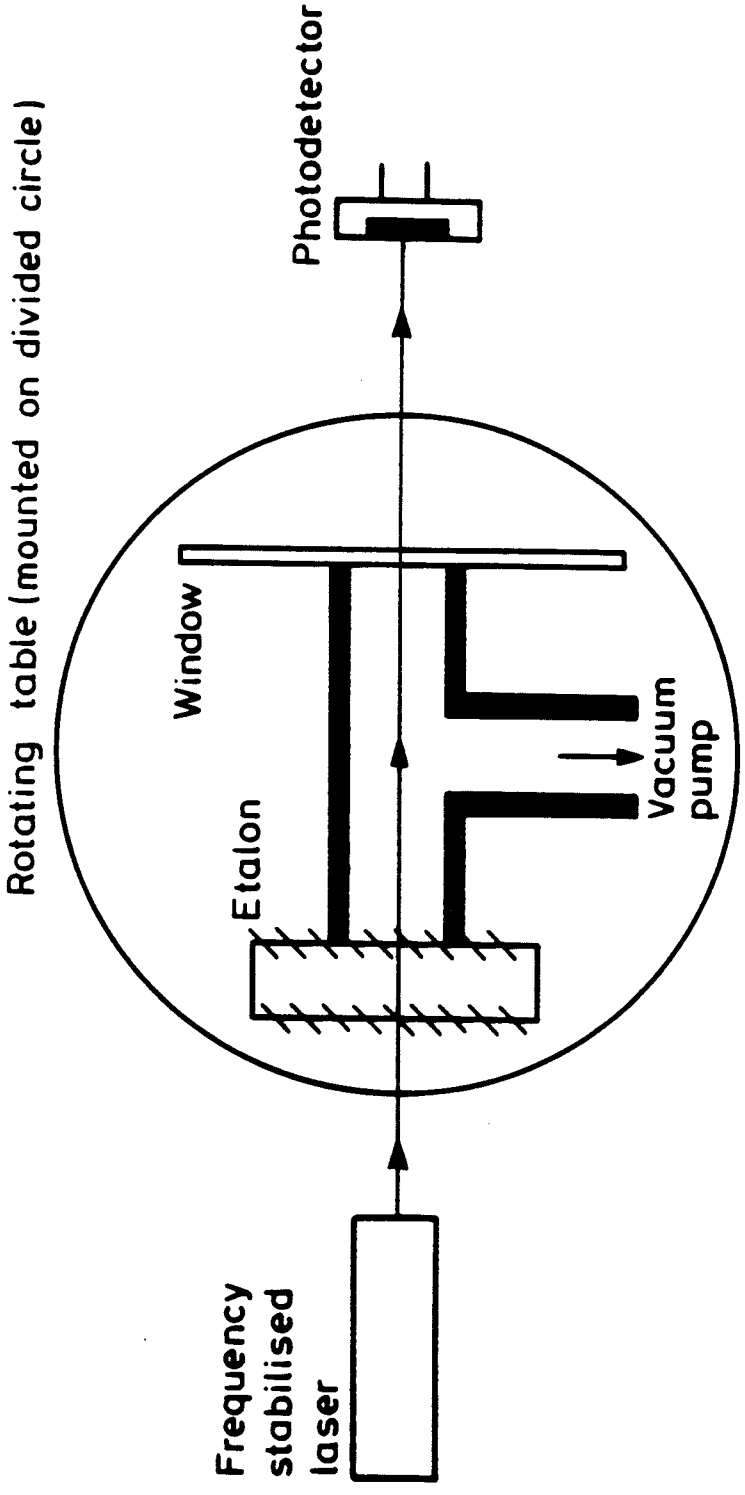


Fig 3 Test configuration for mechanically induced path changes in cell windows

# THE MEASUREMENT OF HUMIDITY VARIATIONS IN GASES RESULTING FROM THE ADSORPTION OF WATER ON TO SURFACES

K P Birch, M J Downs and R E Ward

## ABSTRACT

Water vapour adsorption onto solid surfaces can cause measurement anomalies in a number of applications. In the particular case of interference gas refractometry this produces a reduction in the humidity of the moist gas contained within the sample cell leading to errors in the measurement of the refractive index. A technique is described for investigating these anomalies for a variety of material surfaces and results from fused silica and stainless steel are discussed.

---

The adsorption of water vapour on to solid surfaces has been well studied (Bowden and Throssell 1951, Kell et al 1969, Kochsiek 1977, Wechter and Kramer 1985) and its effects are important in a variety of applications. For example, in the precise measurement of the refractive indices of moist gases, where a relatively small volume of gas is contained in a cell with a large surface area, the relative humidity of the gas is extremely sensitive to even low levels of water adsorption on this surface. If adsorption occurs, the measurement of the refractive index is then made on a gas with a modified humidity and this can lead to anomalous results if the relative humidity of the gas is measured external to the cell.

Water vapour adsorption on to an optically cleaned and polished silica surface was initially investigated using total internal reflection ellipsometry, the optical configuration of which is shown in figure 1. An evacuated cell was flushed with laboratory air that had a relative humidity of about 50% and this resulted in a measured adsorption equivalent to a third of one molecular layer on the silica surface. As this level of adsorption would only cause a relatively small humidity change, even in a cell constructed with narrow bore tubing, this material was chosen to act as an effective reference standard. The NPL interference refractometer (Downs and Birch 1983) which, when used with narrow bore cells, has a measurement sensitivity equivalent to better than two molecular layers of

water vapour being adsorbed on to the silica surface, was then used to study the adsorption of water from air on to unpolished stainless steel surfaces in the configuration shown in figure 2.

The outer and inner optical paths through the refractometer cell are seen to be predominantly enclosed by two 7 mm internal diameter unpolished stainless steel tubes and a silica tube respectively, all of the surfaces having been prepared by degreasing with a mixture of teepol and water followed by an alcohol rinse. This type of cell, which uses a common inlet and outlet manifold, is insensitive to changes in gas temperature, pressure and dry constituents but sensitive in this case to any changes in humidity induced by the adsorption of water vapour on the stainless steel surfaces enclosing the optical path.

Air specimens with a controlled humidity were flowed through the cell at 0.1 litre per minute for about one minute following which the flow was stopped. A progressive optical path difference between the inner and outer refractometer paths was observed during the first few minutes of contact between the stationary air and the stainless steel tubes, which indicated that adsorption was occurring during this period. This difference was seen to be approximately proportional to the relative humidity of the air and for fully saturated air at 20°C it was found to be equivalent to a 15% reduction in the relative humidity or a change of 15 parts in $10^8$ in terms of air refractive index. This corresponds to the adsorption of 24 molecular layers of water vapour from 0.18 $cm^3$ of moist air in contact with 1 $cm^2$ absolutely smooth surface in the case of the refractometer cell constructed with the 7 mm inner diameter tubing. It was also found that when the air was flushed through the cell at higher flow rates than 0.1 litre per minute, the optical path difference disappeared. These results imply that there is a very weak bond existing between the adsorbed water vapour molecules and the stainless steel surface and that the number of adsorbed layers is dependent upon the relative humidity of the stationary air contained in the cell. Both of these effects are attributable to physisorption and are fully described in the literature by surface chemists (Brunauer et al 1938).

It was also found that by increasing the diameter of the refractometer cell tubes the water vapour adsorption was reduced. The number of adsorbed molecular layers of water vapour was found to be inversely proportional to the diameter of the tubes ie proportional to the surface area to volume ratio. The results obtained from these stainless steel surfaces are similar to those discussed by Kochsiek (1977) who investigated the changes induced in mass standards by

variations in the relative humidity of the ambient air. A possible explanation for these effects may be that a similar amount of water vapour adsorption is occurring on both the stainless steel and silica surfaces but the effect is being enhanced in the stainless steel case due to the rough surface finish producing a significantly larger adsorption area than that calculated assuming a smooth surface.

In conclusion, these results have identified a significant error source in the precise measurement of the refractive indices of moist gases when using stainless steel refractometer cells. The magnitude of this error could be as great as a few parts in $10^7$. From the work of Kochsiek (1977), similar effects are likely to be found for other metallic surfaces.

These results have further shown that, by measuring the optical path differences produced by humidity changes, this technique can measure the thickness of the absorbed water layer on a surface. A resolution of better than two molecular layers can be achieved by using a 32 cm long cell with an internal diameter of 7 mm. This sensitivity could be improved where narrower bore tubing is available.

The technique described allows a variety of material surfaces to be easily examined for molecular adsorption from any gas, whilst in addition allowing bonding and associated time effects to be investigated.

In the application of interference refractometry, the measurement accuracy of an instrument could be maintained either by fabricating the refractometer cell in a material with polished surfaces or alternatively, by applying a suitable correction for the effect of a particular surface finish.

REFERENCES IN ALPHABETICAL ORDER

F P BOWDEN and W R THROSSELL, Adsorption of Water Vapour on Solid Surfaces, Proc Roy Soc A209, 297 (1951).

S BRUNAUER, P H EMMETT and E TELLER, Adsorption of Gases in Multimolecular Layers, J Amer Chem Soc 60, 309 (1938).

M J DOWNS and K P BIRCH, Bi-directional Fringe Counting Interference Refractometer, Prec Eng 5, 105 (1983).

G S KELL, G E McLAURIN and E WHALLEY, PVT Properties of water. II. Virial Coefficients in the Range 150°-450°C without Independent Measurement of Vapor Volumes, J Chem Phys 48, 3805 (1968).

M KOCHSIEK, $H_2O$ Adsorption Layers on Surfaces of Mass Standards, PTB-Mitteilunger, Forshen und Prüfen, 87, 478 (1977).

S G WECHTER and F KRAMER Jr, Evaluation of Gas Phase Moisture Standards Prepared in Treated Aluminium Cylinders, presented at 21st National Symposium of the Analysis Instrument Division, Instrument Society of America (1985).

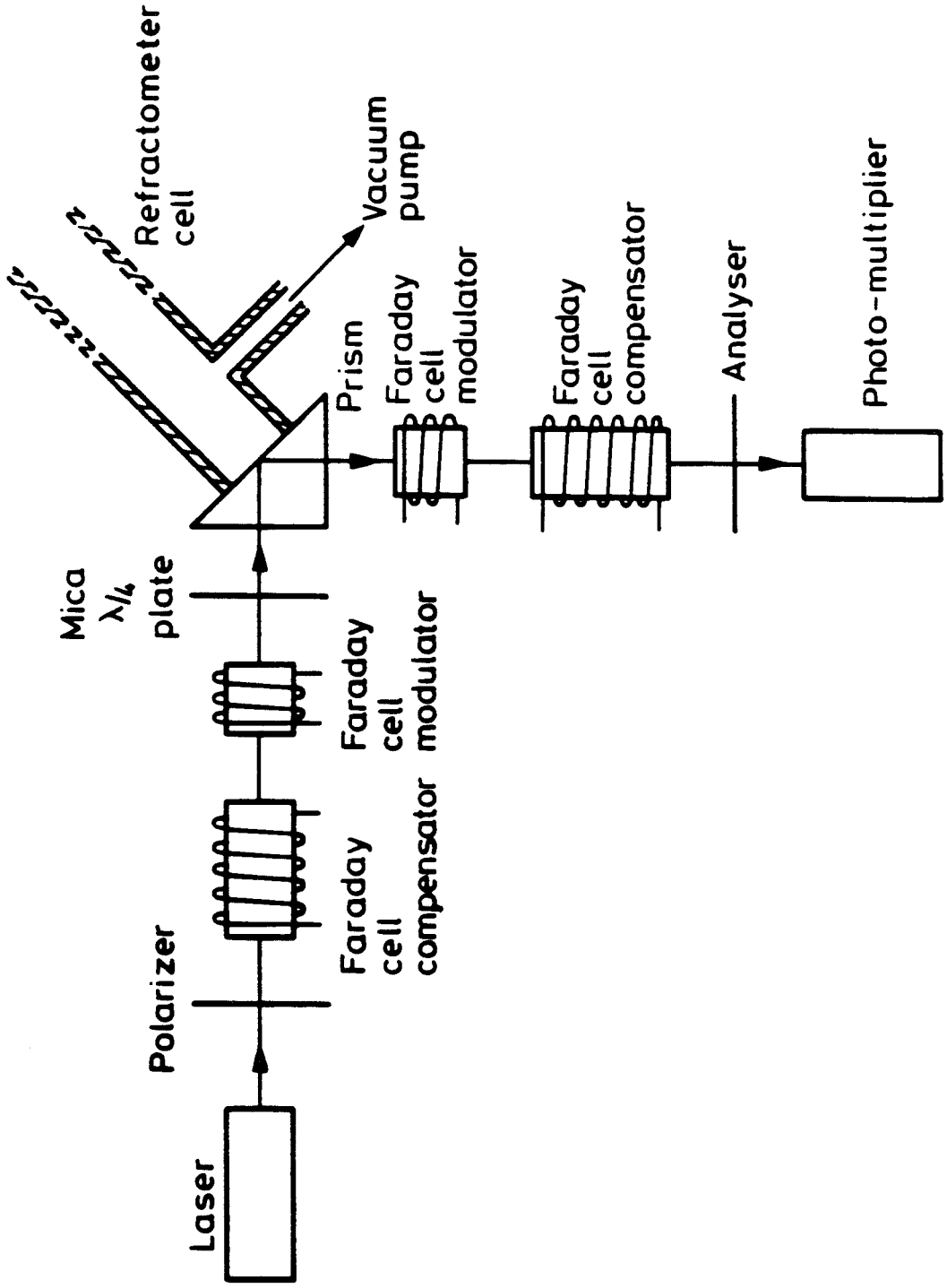


Fig 1 Measurement of absorbed water by ellipsometry

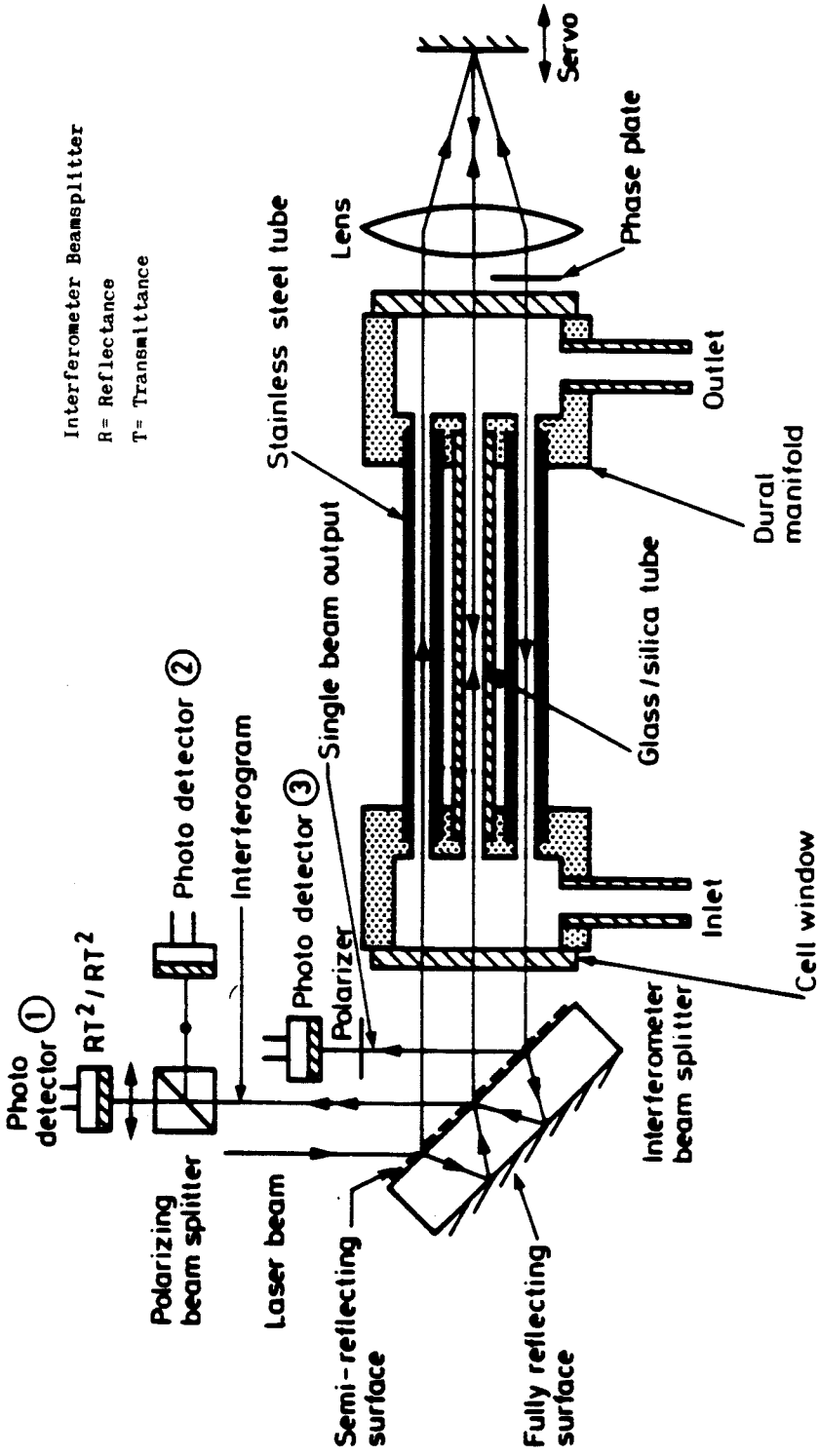


Fig 2 NPL Refractometer configuration for examining water vapour absorption effects

# THE RESULTS OF A COMPARISON BETWEEN CALCULATED AND MEASURED VALUES OF THE REFRACTIVE INDEX OF AIR

K P Birch and M J Downs

## ABSTRACT

When optical techniques are applied to high accuracy length measurement in the free atmosphere it is essential to apply a correction for the refractive index of the air. This can be obtained either by calculation using Edlen's equations or by direct measurement using a gas refractometer. An investigation of the accuracy achievable using Edlen's equation has been made using a high precision interference gas refractometer developed at the NPL. The results have shown that a correction to the water vapour term in Edlen's equation is required to achieve the highest accuracy.

---

Optical techniques are widely used for the measurement of length and, following the invention of lasers with their intense collimated beams and narrow bandwidths, a greatly extended range and accuracy is achievable using these systems.

In order to achieve the optimum performance from these instruments when they are used for measurement applications in the free atmosphere, it is essential to correct the wavelength of the radiation for the refractive index of the air. Two techniques are currently employed to obtain a refractive index value of the air for performing this correction. They are the calculation of a value using Edlen's equation (1966) by the use suitable sensors to take precision measurements of atmospheric pressure, temperature and humidity, and the direct measurement using an interference refractometer. The latter technique has the advantages that it is completely independent of variations in the consistuents of the air and that the only calibration required is the initial relatively crude measurement of the length of the refractometer cell.

A comparison of air refractivity values measured directly using the NPL refractometer (Downs and Birch 1983) fitted with a polished silica cell (Birch, Downs and Ward) with silica windows (Birch, Downs and Ferriss), and those

calculated using Edlen's equation has been carried out at the NPL. The sensors used for measuring the temperature, pressure and humidity were calibrated against the national standards maintained at the NPL. The measurements were made at 633 nm on a known standard composition of dry air, on which Edlen's equation is based, which was flushed into the refractometer cell from a gas cylinder.

The refractive indices of the dry air were determined over the temperature range 10 - 30°C and pressure range 20 to 115 kPa. The results showed that all the differences between the measured and calculated values were within the measurement uncertainty of $\pm$ 3.2 $\times$ $10^{-8}$. However, when a range of air specimens with varying humidities were examined the measured value was found to be greater than the calculated value by up to 13 parts in $10^8$ for fully saturated air at 20°C. The measurements imply an error in the water vapour term of Edlen's equation which was based on the work of Barrell and Sears (1939). Further confirmation of this error and its magnitude was obtained by using the NPL refractometer in a differential measurement mode which involved the use of the dual compartment cell shown in figure 1. In this case either dry or moist standard air specimens were flushed through one or both chambers of the cell in order to measure optical path differences in the refractometer as the relative humidity of the air was varied. This method of comparing optical path differences has the advantage of being insensitive to the temperature and pressure of the gas and to any dry air constituent variation. An additional advantage of the 'common-path' optical configuration of the NPL refractometer is that the 'zero-path' condition can be achieved with either moist or dry air in both arms of the interferometer, which allows the humidity of the specimen in either cell compartment to be varied confirming that no anomalous path differences exist between the two interferometer paths.

The error in Edlen's equation may be attributable to physisorption effects (Birch, Downs and Ward) in the original Barrell and Sears apparatus (1939) and therefore it is recommended that the following modification to Edlen's equation be used:

$$(n-1)_{tpf} - (n-1)_{tp} = -f(3.7209 - 0.03436\sigma^2)10^{-10} \qquad (1)$$

where $(n-1)_{tp}$ is the refractivity of dry air at t°C and at atmospheric pressure p Pa: $(n-1)_{tpf}$ is the refractivity of moist air under the same temperature and pressure conditions containing f Pa of water vapour; f is the partial pressure of water vapour in Pa and $\sigma$ is the vacuum wavenumber in $\mu m^{-1}$. The Edlen

equation with this modification is expected to have an uncertainty of ± 3.3 × $10^{-8}$ which is the limit at which the measurements were made.

Using refractometer cells constructed in polished silica tubing and fitted with silica windows, an agreement of approaching ± 3 parts in $10^8$ was achieved between directly measured refractive indices and those calculated from the modified Edlen equation after correcting for levels of carbon dioxide which exceed the 300 ppm assumed by the equation. However it should be noted that this accuracy in the calculated refractive index was limited by the precision with which the required atmospheric parameters could be measured. This contrasts with the ± 1 part in $10^8$ uncertainty for the directly measured refractive index.

In conclusion, where an uncertainty of < ± 1 part in $10^7$ is required in air refractive index, the modified Edlen equation may be used provided the only significant air contaminant is carbon dioxide for which corrections should be applied. Where an uncertainty of better than ± 1 part in $10^7$ is required the use of a suitable refractometer is to be recommended.

## ACKNOWLEDGEMENTS

The authors would like to thank both the Engineering Services and the Thin Film Unit of the NPL and in particular the assistance of Mr M Hammond and Miss S Lindberg for their practical help in this work.

REFERENCES IN ALPHABETICAL ORDER

H BARRELL and J E SEARS, The Refraction and Dispersion of Air for the Visible Spectrum, Phil Trans Roy Soc London Ser A238, 1 (1939).

K P BIRCH, M J DOWNS and D H FERRISS, Optical Path Length Changes Induced in Cell Windows and Solid Etalons by Evacuation, to be published.

K P BIRCH, M J DOWNS and R E WARD, The Measurement of Humidity variations in Gases Resulting from the Adsorption of Water onto Surfaces: to be published.

M J DOWNS and K P BIRCH, Bi-directional fringe counting interference refractometer, Prec. Eng. 5, 105 (1983).

B. EDLEN, The Refractive Index of Air, Metrologia 2, 71 (1966).

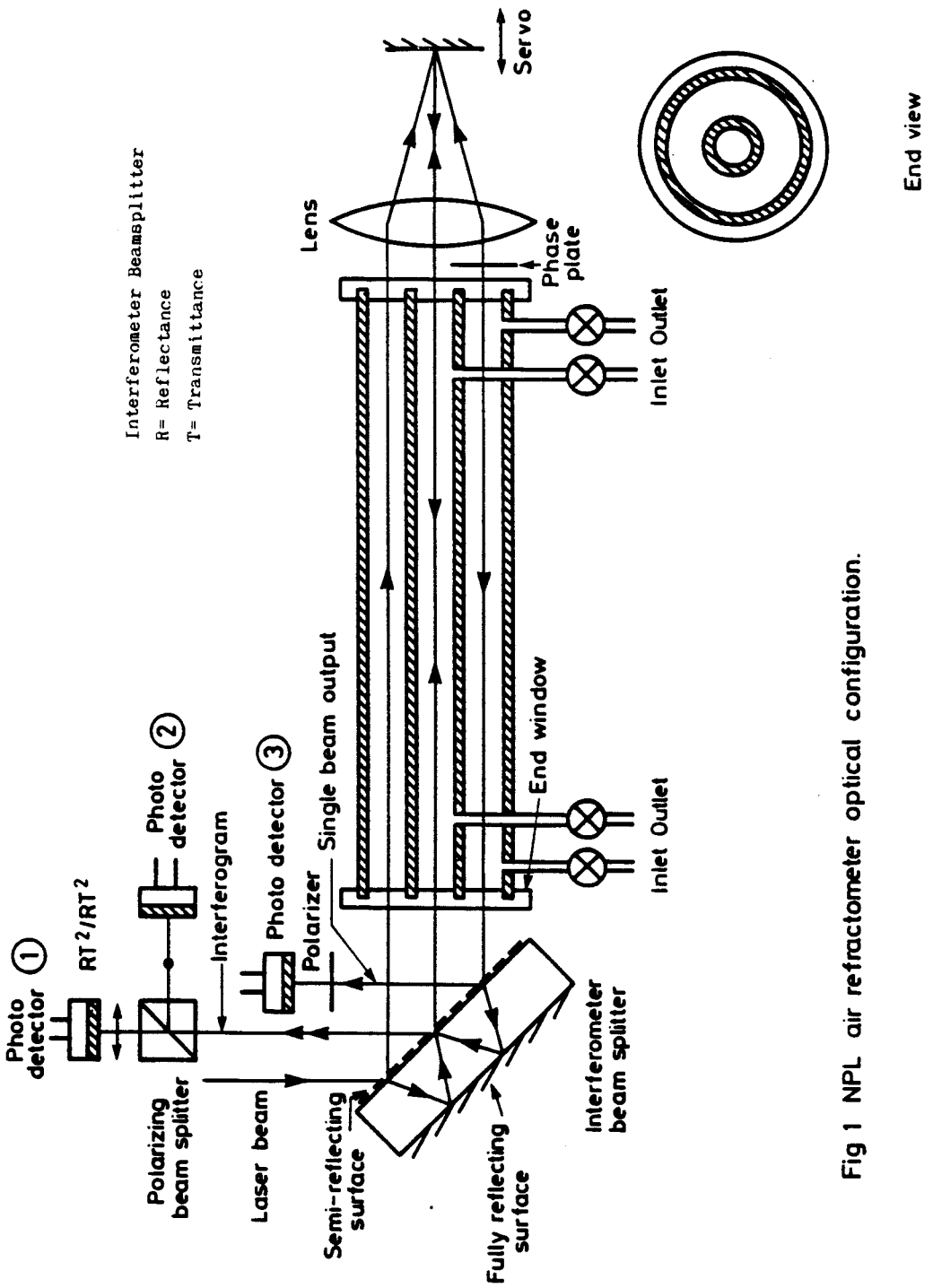


Fig 1 NPL air refractometer optical configuration.

## ACKNOWLEDGEMENTS

The work in this thesis has been carried out in the physics laboratories of the University of Southampton under the supervision of Dr H G Jerrard B Sc., Ph D., F inst P. The author's thanks go to Dr R J King for his support through the years, to Dr W R C Rowley for his advice and guidance, and to Dr Jerrard in particular, both for his encouragement to start the research in the first place and for his continual interest and support in the realisation of the completion of this thesis.

The author would also like to thank his other colleagues at the National Physical Laboratory including Miss S H Lindberg, Mr K P Birch, Mr R E Ward, and Mr M B McCarthy for practical help and useful discussions.